SYNTHESIS, PHOTOPHYSICAL AND PHOTOVOLTAIC PROPERTIES OF 11-FLUORODIBENZO[A,C]PHENAZINE BEARING DONOR–ACCEPTOR TYPE CONJUGATED POLYMERS

A THESIS SUBMITTED TO
THE GRADUATE SCHOOL OF NATURAL AND APPLIED SCIENCES
OF
MIDDLE EAST TECHNICAL UNIVERSITY

BY

ECE AKTAŞ

IN PARTIAL FULFILLMENT OF THE REQUIREMENTS
FOR
THE DEGREE OF MASTER OF SCIENCE
IN
CHEMISTRY

AUGUST 2016

Approval of the thesis:

SYNTHESIS, PHOTOPHYSICAL AND PHOTOVOLTAIC PROPERTIES OF 11-FLUORODIBENZO[A,C]PHENAZINE BEARING DONOR–ACCEPTOR TYPE CONJUGATED POLYMERS

submitted by **ECE AKTAŞ** in partial fulfillment of the requirements for the degree of **Master of Science in Chemistry Department, Middle East Technical University** by,

Prof. Dr. Gülbin Dural Ünver ____________________
Dean, Graduate School of **Natural and Applied Sciences**

Prof. Dr. Cihangir Tanyeli ____________________
Head of Department, **Chemistry Dept., METU**

Prof. Dr. Levent Toppare ____________________
Supervisor, **Chemistry Dept., METU**

Examining Committee Members:

Assoc. Prof. Dr. Ali Çırpan ____________________
Chemistry Dept., METU

Prof. Dr. Levent Toppare ____________________
Chemistry Dept., METU

Assoc. Prof. Dr. Ertugrul Şahmetlioğlu ____________________
Chemistry and Chemistry Processing Dept., Erciyes Uni.

Assoc. Prof. Dr. Yasemin Arslan Udum ____________________
Advanced Technologies Dept., Gazi Uni.

Assist. Prof. Dr. Görkem Günbaş ____________________
Chemistry Dept., METU

Date: 25.08.2016

I hereby declare that all information in this document has been obtained and presented in accordance with academic rules and ethical conduct. I also declare that, as required by these rules and conduct, I have fully cited and referenced all material and results that are not original to this work.

Name, Last name: Ece AKTAŞ

Signature:

ABSTRACT

SYNTHESIS, PHOTOPHYSICAL AND PHOTOVOLTAIC PROPERTIES OF 11- FLUORODIBENZO[A,C]PHENAZINE BEARING DONOR–ACCEPTOR TYPE CONJUGATED POLYMERS

AKTAŞ, Ece
M. S., Department of Chemistry
Supervisor: Prof. Dr. Levent Toppare
August 2016, 96 pages

In this study, dibenzo[a,c]phenazine moiety was modified with fluorine atom to decrease the HOMO level of acceptor unit. Benzodithiophene derivative and dibenzosilole derivative were used as donor unit in the polymer backbone. In addition, 3-hexyltihophene was used as the π-bridge molecule with their donor character in polymer backbone. Also, 3,4-ethylenedioxythiophene was used to obtain new monomer to compare oxidation potential with 3-hexylthiophene based monomer. In this manner, two new conjugated monomers (PTFBPz and PEFBPz) and two new conjugated polymers (PBDT-FBPz and PBDT-TFBPz) were synthesized via Stille cross-coupling. In addition, the new conjugated polymer (PSi-TFBPz) was synthesized via Suzuki cross-coupling reactions. The electrochromic studies of all homopolymers and copolymers were performed and HOMO-LUMO energy levels of them were calculated. The absorption properties of polymers were investigated in solution and thin film. The photovoltaic studies of three polymers were performed. All photovoltaic devices were constructed with the conventional device structure (ITO/PEDOT:PSS/polymer:PCBM71/LiF/Al). In addition, the photovoltaic device fabrication and current-voltage characteristics of these devices were studied in an oxygen and moisture free glove box system. The power conversion efficiency (PCE) of conjugated polymers were measured under standard AM 1.5 Global illumination (100mW/cm^2). The highest PCE values was found as 1.53% for **PBDT-TFBPz,** 1.12% for **PBDT-FBPz** and 0.58% for **PSi-TFBPz.**

Keywords: Dibenzo[a,c]phenazine, Benzodithiophene, Conjugated Polymers, Organic Solar Cells

ÖZ

11-FLUORODİBENZO[A,C]FENAZİN İÇEREN DONO-AKSEPTOR TÜRÜNDEKİ KONJUGE POLİMERLERİN SENTEZİ, FOTOFİZİKSEL VE FOTOVOLTAİK ÖZELLİKLERİ

AKTAŞ, Ece
Yüksek Lisans, Kimya Bölümü

Tez Yöneticisi: Prof. Dr. Levent Toppare

Ağustos 2016, 96 sayfa

Bu çalışmada, dibenzo[a,c]phenazine kısmı akseptör birimi olarak kullanıldı ve flor atomu sayesinde HOMO enerji seviyesi düşürüldü. Benzoditiyofen türevi ve dibenzolsilol türevi polimer zincirinde donor ünitesi olarak kullanıldı. Buna ek olarak, 3-hekziltiyofen molekülü donor karakteri ile polimer zincirinde π-köprüsü olarak kullanıldı. Ayrıca, 3,4-etilendioksitiyofen yeni monomer elde etmek ve oksidasyon potansiyelini 3-hekziltiyofen ile karşılaştırmak için kullanıldı. Böylelikle, Stille çapraz kenetleme reaksiyonu ile iki yeni konjuge monomer (PTFBPz ve PEFBPz) ve iki yeni konjuge polimer (PBDT-FBPz ve PBDT-TFBPz) sentezlendi. Buna ek olarak, Suzuki çapraz kenetleme reaksiyonu ile yeni konjuge polimer (PSi-TFBPz) sentezlendi. Bütün kopolimer ve homopolimerlerin elektrokromik çalışmaları tamamladı ve bunların HOMO-LUMO enerji seviyeleri hesaplandı. İnce film ve çözülmüş halde bulunan polimerlerin absorpsiyon özellikleri incelendi. Bütün organik fotovoltaik cihazlar klasik cihaz yapısına (ITO/PEDOT:PSS/polimer:PCBM/LiF/Al) göre yapılmıştır. Buna ek olarak, fotovoltaik cihaz üretimi ve bu cihazların akım-voltaj karakterizasyonları oksijensiz ve nemsiz ortam olan eldivenli kabin sisteminde çalışıldı. Polimerlerin güç dönüşüm verimleri (PCE) standart AM 1.5 küresel aydınlatma (100 mW/cm^2) altında ölçülmüştür. En yüksek PCE değerleri **PBDT-TFBPz** için %1.53, **PBDT-FBPz** için %1.12 ve **PSi-TFBPz** için %0.58 bulunmuştur.

Anahtar kelimeler: Dibenzo[a,c]fenazine, Benzoditiyofen, Konjüge Polimerler, Organik Güneş Pilleri

To My Family,

ACKNOWLEDGEMENTS

I would like to express my greatest appreciations to my supervisor Prof. Dr. Levent Toppare who made it possible to spend three years in Toppare Research Group at METU with all benefits where I could learn so much not only about science but also life in general and for his guidance, encouragement, advice, criticism and patience.

I would like to express my sincere gratitude to Assoc. Prof. Dr. Ertuğrul Şahmetlioğlu. He always gives advices for determining my carrier since I started my license in Chemistry. I would like to thank for his great support and beyond everything being a father for me.

I would like to thank Assoc. Prof. Dr. Ali Çırpan for his guidance and support.

There are no enough words to express my gratitude to Naime Akbaşoğlu Ünlü. She always tried to teach me anything that she knows about organic chemistry at every opportunity. I am grateful to her for anything I know. Also, I would like to thank to her for endless patience and support during my thesis study. She was always with me with a shoulder to hug in my good and bad times. I feel so lucky for having such lovely friend who will always support me expecting anything in return.

I would like to thank to Gönül Hızalan Özsoy for teaching me about organic photovoltaics and also everything. She became more than a lab boss from the moment I started to study in Toppare Research Group. Also, she is being a sister to me, giving a shoulder to cry and a hug for great moments.

I would like to thank to Hande Unay for her long-standing friendships, sisterhood and for being ready to listen to me timeless. I ensure you with no doubt, you will remain as a sister even years and life separate us.

I would like to thank to Şerife Özdemir Hacıoğlu for electrochemical, spectroelectrochemical characterizations and for their valuable discussions.

I would like to thank to Doğukan Hazar Apaydın, Ali Can Özelçağlayan and Nazlı Buket Zaifoğlu for their advices and their friendship. I also grateful for their

motivations to start my master at METU.

I would like to thank to Şevki Can Cevher and Çağla İstanbulluoğlu for their friendship, motivations and our joyful evening dinners also weekends. I am proud to be part of OSC laboratory member.

I owe great thanks to all Toppare and Çırpan Group Members specially Özge Azeri, İpek Önk, Cansel Temiz, Emre Ataoğlu, Nima Sohrabnia, Duygu Keleş, Özge Karagaçtı, Aslı Çetin and Fatma Demir for a wonderful research environment. They made laboratory joyful and I feel like being also a part of Cirpan Research Group.

I would like to thank TUBİTAK (115M036) (Turkish Scientific and Technical Research Council) for the financial support.

Last but not least, words fail to express my gratitude to my dear family. Without their love and understanding, I could not succeed anything.

TABLE OF CONTENTS

LIST OF TABLES

TABLES

LIST OF FIGURES

FIGURES

LIST OF ABBREVIATIONS

ACN Acetonitrile

Ag Silver

BHJ Bulk Heterojunction Solar Cell

CB Conduction Band

CE Counter Electrode

CIE La Commission Internationale de l’Eclairage

CP Conducting Polymer

CV Cyclic Voltammetry

DBP Dibenzo[a,c]phenazine

DCM Dichloromethane

DIO 1,8-diiodooctane

DMF Dimethylformamide

ECD Electrochromic device

EDOT 3,4-Ethylenedioxythiophene

E_g Band gap

FF Fill Factor

HOMO Highest Occupied Molecular Orbital

ITO Indium Tin Oxide

IPCE Incident Photon to Current Efficiency

J_{sc} Short circuit current density

L, a, b Luminance, hue, saturation

LBG Low Band Gap

LUMO Lowest Unoccupied Molecular Orbital

MEH-PPV Poly(2-methoxy-5-(2-ethylhexyloxy)-1,4-phenylenevinylene)

NBS N-bromosuccinimide

NMR Nuclear Magnetic Resonance Spectrometer

OLED Organic Light Emitting Diode

OSC Organic Solar Cell

OPV Organic Photovoltaic

PA Polyacetyene

PLED Polymer Light Emitting Diode

PPV Poly(p-phenylene vinylene)

PVDF Polyvinylidene fluoride

Pt Platinum

PTFE Polytetrafluorethylene

P3HT Poly(3-hexylthiophene)

TBAPF$_6$ Tetrabutylammonium hexafluorophosphate

THF Tetrahydrofuran

V$_{oc}$ Open circuit voltage

VB Valence Band

CHAPTER 1

1. INTRODUCTION

1.1. Organic Semiconducting Materials

Conducting polymers and their ability to be doped were discovered by Alan J. Heeger, Hideki Shirakawa and Alan MacDiarmid and their co-workers in 1976 [1]. They were awarded with the Nobel Prize in Chemistry in 2000 for this achievement. After this discovery, several researchers were focused on the field of conjugated polymers and their potential usage in different application areas. After the discovery of conductivity of polyacetyene (PA), conjugated polymers have become an alternative to inorganic counterparts due to low cost fabrication on large areas of flexible substrates and the opportunity of solution processing and easy controlling over electronic, organic and physical properties [2][3]. Conjugated polymers have been utilized in different applications due to their tunable properties like electrochromic device (ECDs) and polymeric light emitting diodes (PLEDs) [4][5]. The enormously rising demand for energy throughout the world has adopted great emphasis on searching renewable and clean energy resources. Photovoltaic technology seems to be the most significant long-lasting solution that can harvest energy directly from sunlight.

1.1.1. Band Gap Theory

The band gap of the molecule is defined as the energy difference between the Highest Occupied Molecular Orbital (HOMO) energy level and Lowest Unoccupied Molecular Orbital (LUMO) energy level. These levels can also be named conduction band (CB) and valence band (VB), respectively. In conductors such as metals, the band gap does not exist which is based on an overlap of VB and CB. Therefore, the electrons can be transferred between two levels by applying an electric field. On the other hand, in an insulator, these energy levels have a larger gap which prevents any kind of electrical conductivity. When semiconductors are compared with insulators and conductors, it can be said that semiconductors have a larger band gap than conductors whereas a smaller than insulators. Conjugated polymers are considered as semiconductors with a band gap between 1 eV to 4 eV [6]. Therefore via simple doping process, electrons can move from valence to conduction band to generate electrical current [7]. The optoelectronic and optical properties of conjugated polymers depend on the band gap value which can be controlled by structural modification [8].

1.1.2. Band Gap Engineering

The band gap of conjugated polymers depends on five main parameters , which are bond length alternation (E_{BLA}), planarity (E_{θ}), aromaticity (E_{Res}), intermolecular interactions (E_{int}) and substituents (E_{Sub}) [6].

Bond length alternation (BLA) is explained as the relation between aromatic and quinoid forms of a molecule. The aromatic form of a molecule can be turned into the quinoid form by π-electron delocalization that ensures the decrease of the BLA value. Thus, leading to conjugated polymers with lower band gap energies. In the literature, Meng *et al*. reported that poly-isothianapthenes (PITN) have a small band gap (1.0 eV) compare to polythiophenes (band gap of polythiophenes is 2.0 eV). In this work, the ground state of thiophene was in quinoid form since an aromatic benzene ring is fused to the thiophene [9].

The planarity can affect on the HOMO and LUMO energy levels of polymer due to a decrease in the energy difference which ensures to obtain a low length BLA. There is an inverse relation between the conjugation length of the main chain and the energy band gap. An increasing conjugation length causes a lower band gap [10].

The HOMO and LUMO levels of the polymers can also be modified by mesomeric or inductive effects of substituents, respectively. Electron withdrawing groups decrease the energetic location of the LUMO and electron donating group increase the energetic location of the HOMO [11].

Aromatic energy is described as the energy difference between a hypothetical and aromatic structure, including the isolated double bonds. It is another factor determining band gap of the polymers. Since most π-conjugated polymers have aromatic moieties that have an aromaticity energy, aromaticity causes a limitation of the π-electrons on the polymer ring and plays with the delocalization [11].

Intermolecular interaction in the solid state was enhanced due to a rigid and well-ordered crystalline structure. As a result of this, the band gap of a molecule appears to be lowered in the solid state compared to the solution phase. In addition, rigid structure of molecules increases the π-π stacking that leads to red shift on the ground state. For this reason lower band gap polymers are observed [12].

1.1.3. Donor Acceptor Approach

In organic semiconductor materials, the HOMO energy level corresponds to the top of the valence band and the LUMO energy level corresponds to the bottom of the conduction band. When the HOMO and LUMO are changed, it allows control of the energy gap of the materials and also its ionization potential and electron affinity. Several strategies have been employed to control these energy levels. Havinga *et al*. reported molecular orbital energy level of an acceptor (A) and donor (D) part that are alternatively used in conjugated polymers [13]. This is known as donor-acceptor (D-A) approach that can explain the lower the energy gap of the resulting molecule compared to that of D and A. As seen in Figure 1 LUMO energy level is correlated to the LUMO of the acceptor, and its HOMO is interrelated with the HOMO of the donor.

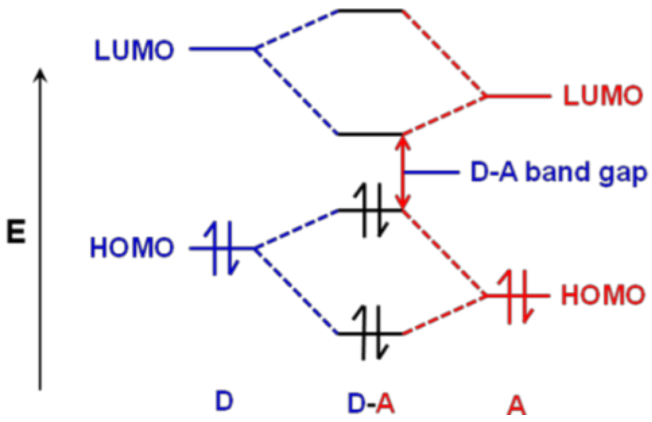

Figure 1. Molecular orbital energy diagram and that displaying interface among a conjugated donor-acceptor pair [14].

1.1.4. Doping Mechanism

Electrochemical and chemical doping are the two main routes to achieve doping process that ensure conductivity of the conjugated polymers. p-Doping causes positive charges to arise on the polymer where n-doping is used to implement negatively charged anions on the polymer backbone. Afterwards, these opposite charges are neutralized by dopants (Figure 2) [15]. Su *et al.* recommended that soliton is considered as a structural defect resulting from the formation of the free radicals on the backbone throughout the polymerization of PA. Soliton is an important part in the charge-transfer mechanism since formation energy of the soliton is lower than the energy of excitation [16].

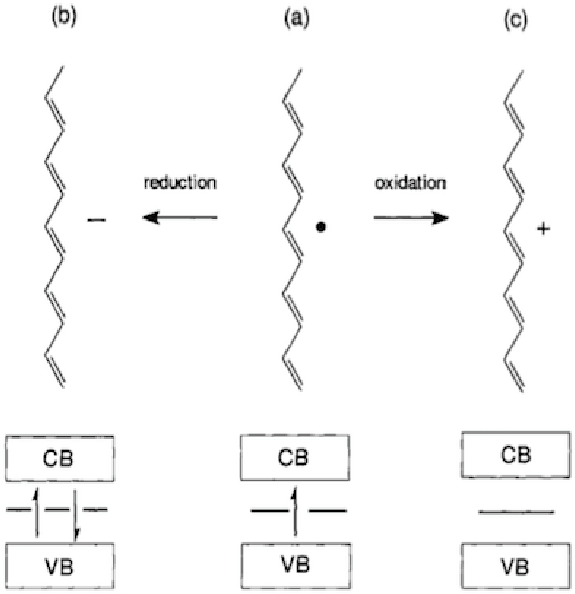

Figure 2. Illustration of the band structure for trans-polyacetylene chain (a) neutral, (b) negatively charged and (c) positively charged solitons [17].

The polymer can maintain its genuine structure without degradation in the doping process. This property of the polymer is very important for using it in electrochromic applications [18].

When comparing the heterocylic compounds to the PA band structures have a non-degenerate ground state energy. Polarons are radical ions produced via redox processes. Bipolarons are dianions and dications playing an important role in the electrical conductivity [19].

1.2. Electrochromism and Electrochromic Devices

The first reversibly electrochemically p-type and n-types doped of PA were studied by Macinnes *et al.* in 1981 [20]. Observation of reversible optical changes upon applied potential is called as electrochromism [21]. The band gaps of conducting polymers determine their colors and can be changed by doping process. For instance, if the polymers have a band gap which is greater than 3 eV, they are most likely to appear as colorless in their neutral states. These polymers can absorb light when doping process is applied in the visible region. When the band gaps of polymers are equal or smaller than 1.5 eV they can absorb light in the visible region in their neutral states. These polymers can become transparent upon doping [22]. Color changes for conjugated polymers are observed in the visible region hence, they can be used in special applications such as displays and windows [23][24]. Moreover, they have bleached and colored states that are used to construct transmissive/absorptive devices. Conjugated polymers are electrochromic materials with high optical contrast and rapid response times [25]. Optical contrast, switching speed, coloration efficiency and electrochromic stability are some parameters that define characteristics of the electrochromic polymers.

Optical contrast is the most significant factor in electrochromic materials. Percent transmittance change ($\Delta\%T$) is determined at a specific wavelength where the optical contrast is high. Electrochromic contrast is obtained by measuring the relative luminance modification, because it provides more realistic contrast values that offers a perspective on the transmissivity of a material [25].

Switching speed is also significant factor for switchable mirrors and dynamics display applications. It can be described as the time necessary for the bleaching/coloring processes of an electrochromic material. This parameter depends on some factors such as morphology of the thin film, thickness of the films, ion diffusion in thin films, the ionic conductivity of the electrolyte and amount of the applied potential [25].

Coloration Efficiency (CE) determines the amount of power necessary for observing the optical change. To calculate values of CE (cm^2/C), the amount of optical density change (ΔOD) and the transported charge per unit area (Q_d) must be identified in the following eauqtion;

$$\eta = (\Delta OD)/Q_d) = \log[T_b/T_c]/Q_d \qquad (1.1)$$

the CE is shown as η at a given λ and the colored and bleached transmittance values are shown as and T_c and T_b, respectively [25][26].

The stability of electrochromic materials generally depends on their electrochemical stability. This situation can be explained that the degradation of the active sites causes a loss in electrochromic contrast decreasing device efficiency. Side product during electron gain or loss processes, heat dissipation and irreversible redox reactions are some reasons for a decrease in stability [25][27].

1.3. Organic Photovoltaics

In recent years, renewable and non-polluting energy sources are gained prominence around worldwide. One of renewable energy; solar energy has the capacity to meet the world’s large and rising energy demand. Sun is an endless energy source for producing electrical energy. In principle, solar cells directly convert the solar energy to current which is one of the most effective technology to produce electrical energy [28]. The French physicist A. Edmund Becquerel discovered the photovoltaic effect in 1839 while examining an electrolytic cell made up of two metal electrodes. In this study, he discerned that some materials create little electric current under light [29]. However, theoretically photovoltaic effect was explained by Einstein in 1905. When photons are irradiated on a metal surface in the UV range, electrons can be free to escape from the metal surface thanks to excitation energy supplied by the incident light [30]. Light is made up of photons that also called as packet of energy that contingent upon the color or frequency of light. The solar spectrum involves all ultra violet to infrared wavelength ranges. In the visible light range, incident light energy is limited only 30% however in the infrared range energy can reach over 50%. In the UV-Vis range the photons have enough energy to eject electrons from semiconducting material that can be used for charge creation. On the contrary, the infrared waves have not enough energy to obtain electricity (Figure 3) [31].

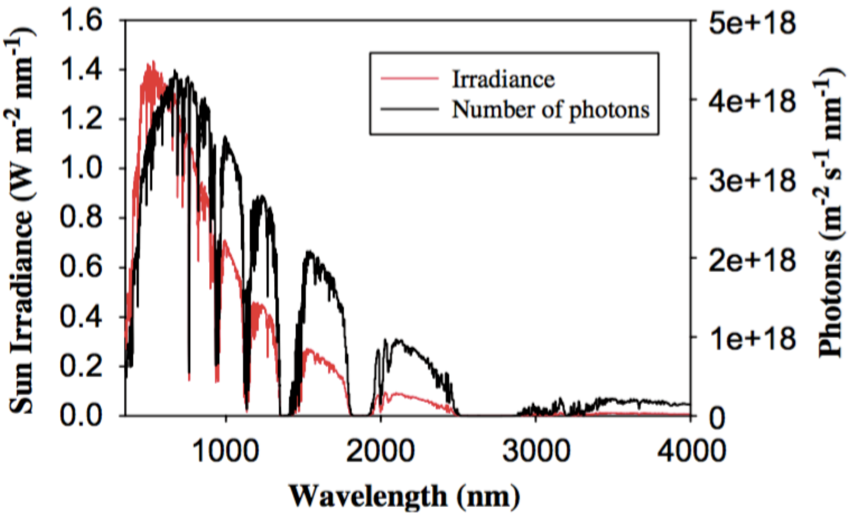

Figure 3. Sun irradiance shown in red and number of photons as in black as a function of wavelength [32].

1.3.3. The Materials of Organic Photovoltaics

The materials for organic photovoltaics are usually used either as vacuum-deposited small molecules or solution processable organic semiconducting molecules. These molecules having a conjugated system that absorb sunlight, produce photogenerated charge carriers and transport these charge carriers [33]. For fabrication of organic photovoltaics conjugated polymers (electron donor) and fullerene derivatives (electron acceptor) have commonly utilized [34]. Electrochemical, chemical and photochemical doping is applied to generate extrinsic charge carriers onto organic semiconductor materials [35].

The organic photovoltaic devices are constructed in a sandwich geometry (Figure 4). The conducting electrode is chosen as a transparent indium tin oxide (ITO) which is coated on glass or plastic. Nanotube network electrodes can be used as alternatives for ITO [36]. ITO coated glass or plastic can be designed to avoid short circuit via chemical etching. The chemical etching is mentioned in the experimental part of thesis.

Poly(3,4-ethylenedioxythiophene)-poly(styrenesulfonate) (PEDOT:PSS) is an acidic buffer solution. PEDOT:PSS is coated on ITO coated substrate by spin-coating or doctor blading [37]. PEDOT:PSS is used as the hole extraction/injection layer in organic photovoltaics. In addition it ensures greater surface for coating organic active layer [38].

PCBM (1-(3-methoxycarbonyl)propyl-1-phenyl[6,6]C_{61}) is commonly used as n-type material which can be reduced by six electrons. This derivative of buckminsterfullerene is soluble in common solvents [39]. PCBM71 is a fullerene derivative and has a much larger absorption of light than PCBM61 hence, it is commonly chosen as n-type material in organic photovoltaic applications [40].

A lower work function metals are utilized to complete the OPV device. Aluminum (Al), calcium (Ca) and lithium fluoride (LiF) are commonly used as metal electrodes. LiF is evaporated before aluminum to improve interfacial properties of OPVs [41]. In addition, the work function of metals are reduced significantly when LiF is evaporated under the metals [42].

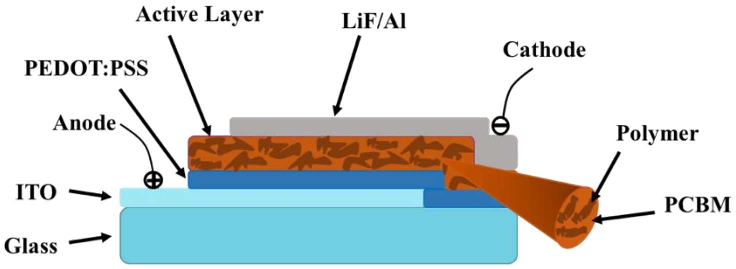

Figure 4. Illustration of traditional device structure of OPVs

1.3.4. Preparation techniques of Organic Photovoltaics

In organic photovoltaics, solution processing and vacuum evaporation techniques are commonly applied to achieve thin films in the construction. Vacuum evaporation has advantages. Its preparation is clean that prevents contamination and more homogenous thin films can be obtained compared to coating/printing techniques. Besides, oxygen and humidity can be eliminated under ultra high vacuum since these negatively affect the performance of OPVs [33][43]. On the other hand, coating/printing techniques are preferred for conjugated polymers since they can decompose under higher temperature and their high molecular weight for evaporation is not suitable for vacuum deposition [33].

1.3.5. Operating Principles of OPVs

The photovoltaic process of converting light into the electricity is composed of four serial steps; light absorption (η_{abs}), exciton dissociation efficiency (η_{diss}), charge transport efficiency (η_{tans}) and charge collection efficiency (η_{col}) [44];

$$\eta_{eff} = \eta_{abs} * \eta_{diss} * \eta_{tans} * \eta_{col} \qquad (1.2)$$

In the first step light absorption leads to exciton (electron-hole pair) formation. In organic semiconductor materials, the usual exciton diffusion length is about 10-20 nm [45]. When exciton did not reach the interface recombination of hole and electron takes place causing photocurrent loss. Photosensitive conducting polymers are excited by sun light and electrons in HOMO energy level are moved to LUMO energy level of donor unit. Then, free electrons are moved to LUMO energy level of acceptor and free holes are moved from HOMO energy level of donor to electrode to produce a potential difference (Figure 5).

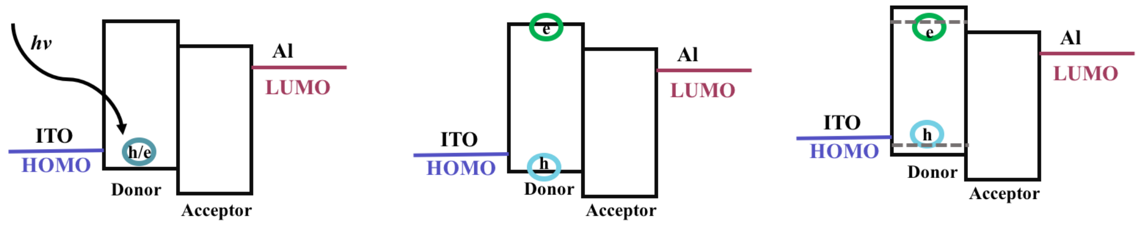

Light Absorption Excitation Exciton Formation

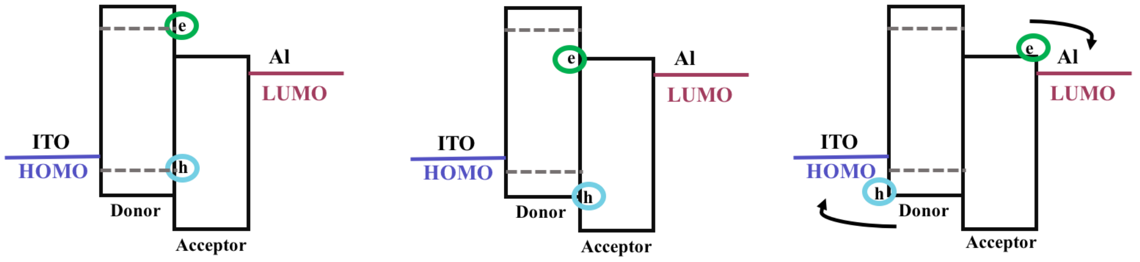

Exciton Diffusion Exciton Dissociation Charge Transport and Collection

Figure 5. Working principle of Organic Photovoltaics (OPVs)

1.3.6. Organic Photovoltaic Device Architectures

1.3.6.1. Single Layer Organic Photovoltaics

In 1994, R. N. Marks *et al.* created single layer device structure of OPV cells that is composed of organic photosensitive semiconductor between transparent electrode as ITO and a low work function cathode as shown in Figure 6. Poly(p-phenylene vinylene) (PPV) was used as the organic semiconducting material with a thickness about 50-320 nm. This single layer device had around 0.1% quantum efficiency under 0.1 mW/cm^2 light intensity [46]. This low result was due to low mobility of charges. As a result, in semiconducting organics the photogenerated charges need additional time to be collected from electrodes. Therefore, the efficiency of OPVs decrease due to slow charge transport and recombination processes [47].

1.3.6.2. Bilayer Organic Photovoltaic

The bilayer organic photovoltaic cells different from single layer organic photovoltaics have additional electron transporting layer as shown in Figure 6. In 1985, C. W. Tang firstly reported this structure utilizing indium tin oxide (ITO)/copper phthalocyanine (CuPc)/perylene tetracarboxylic derivative(PV)/silver (Ag) [34]. The power conversion efficiency was reported as 1 % under AM 2.0 G illumination. Electron transport layer increased PCE ten-fold due to improved exciton separation efficiency. However, the PCE for an inorganic based photovoltaic was still higher than its organic bilayer counterpart, since the essentially short exciton diffusion length of excitons are around 10-20 nm in organic semiconductor layers [48]. The buckminsterfullerene (C_{60}) was used to overcome this drawback in the bilayer organic photovoltaic cells where the exciton diffusion length is nearly 20 nm. In 2003, P. Peumans *et al.* reported a PCE of 3.6 %. This device involved C_{60} as the electron transport layer and perylene tetracarboxylic derivative as the donor unit [49]. In 1993, a semiconducting conjugated polymer was firstly used by Sariciftci *et al.* to construct a bilayer OPV cell. They used poly[2-methoxy-5-(2-ethylhexyloxy)-1,4-phenylenevinylene] (MEH-PPV) as the hole transport material and C_{60} as the electron transport material in this device. MEH-PPV was used to produce the excitons at the interface[50]. In 1996, Halls *et al.* reported 9 % quantum efficiency under an intensity of 0.25 mW/cm^2. They optimized the thicknesses of poly(p-phenylene vinylene) (PPV) as 65 nm and C_{60} as 40 nm in the bilayer OPV device [51].

1.3.6.3. Bulk Heterojunction Organic Photovoltaic

Bulk heterojunction OPV cells have an active layer consist of donor and acceptor units. These devices have an advantage of having larger interface area between donor and acceptor as shown in Figure 6. This concept overcomes the problem of low exciton diffusion distances and also lowers recombination of excitons. The working principle of bulk heterojunction organic photovoltaics is mentioned in the operating principles of OPVs section.

In 2005, Li *et al.* constructed polymer based bulk heterojunction OPVs. Poly(3-hexylthiophene) (P3HT) was used as the hole transporting polymer and a soluble C_{60} derivative was used as the electron transporting layer in the active layer. The best performance of 4.4 % was reported for optimized blend OPV cells with solvent annealing. This PCE result was the best result for polymer based bulk heterojunction OPVs in 2005. Thin film morphologies of P3HT-PCBM were improved to form fibril-like crystalline P3HT and aggregates of PCBM by solvent annealing. Thus, increase in the hole mobility and enhanced absorption efficiencies of fibril-like P3HT were observed [52].

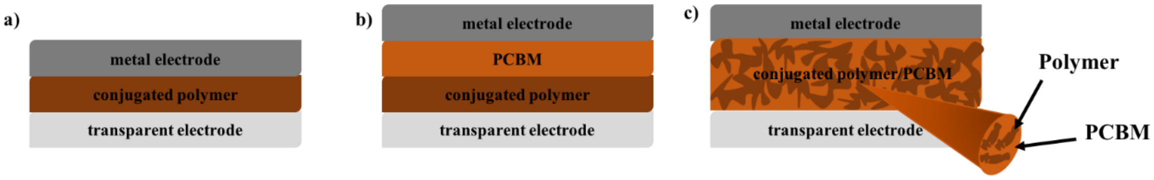

Figure 6. The Device Structures of a) Single layer; b) Bilayer; c) Bulk heterojunction Organic Solar Cells

1.3.6.4. Inverted Organic Solar Cell

The BHJ model is commonly constructed as traditional device architecture. ITO is used as the hole collecting transparent metal oxide and it is usually coated with the PEDOT:PSS as the hole extraction layer (HEL). In addition, metal electrodes (LiF, Ca, Al etc.) are evaporated on top of active layer as the electron collection electrode. These metals are chosen for their work functions. ITO can be etched over time upon exposure to the acidic PEDOT:PSS buffer layer [53]. For this reason, new hole-transporting materials are synthesized to replace PEDOT:PSS layer. However, high power conversion efficiency could not be achieved due to their high resistance [54].

The metal electrodes can be evaporated under high vacuum which increases fabrication cost. Moreover, device degradation may occur due to oxidation of these electrodes [55]. To improve device stability of organic photovoltaics, the electron extraction buffer layers (EEL) such as ZnO or TiO_2 can be added under the active layer instead of PEDOT:PSS. These layers decrease oxygen diffusion between metal electrodes and active layer. Nevertheless, the metal electrodes are evaporated under high vacuum to complete device [56]. The contact between the PEDOT:PSS and ITO is evaded in the inverted device architecture. By this way, high work function metal electrodes such as Au, Ag or Cu should be used at the top of interface. In this manner, the construction of BHJ based organic photovoltaic device is reversed as shown in Figure 7. These high work function metal electrodes are used as hole collecting layers. In addition, they are less air sensitive thus, life time of device is increased by using these metal electrodes [57]. Inverted device architectures are investigated by researchers to improve stability, processing of the different interface layer and increase the efficiency of device.

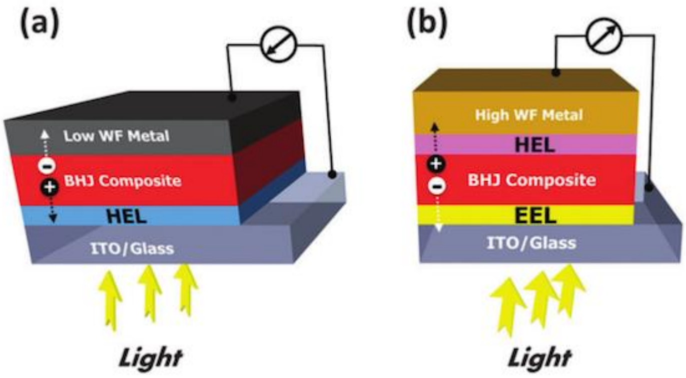

Figure 7. The organic photovoltaic device structure based on a) traditional device structure b) inverted device structure bottom-illumination [58].

1.3.7. Characterization of an Organic Photovoltaic Devices

The current-voltage characteristics and the fill factor of an organic photovoltaic devices are critical parameters for solar cell efficiency. The open circuit voltage (V_{oc}), the short circuit current density (J_{sc}) and the fill factor must be determined to calculate efficiency of an organic photovoltaic device. The open circuit voltage is the potential when no current is flowing through the photovoltaic and the short circuit current is the one when the voltage is the zero. The fill factor (FF) can be described as the ratio among the potential power and the maximum power delivered to an external circuit [59]. The photovoltaic power conversion efficiency (PCE) is calculated by the next formula;

$$e = \frac{P_{max}}{P_{in}} \qquad P_{max} = V_{oc} * J_{sc} * FF \qquad FF = \frac{V_{max} * J_{max}}{V_{oc} * J_{sc}} \tag{1.3}$$

In the power conversion efficiency formula, P_{in} symbolizes the incident light power density and it is standardized at 1000 W/m^2 with a spectral intensity division similar to that of sun on the earth's surface at an incident angle of 48.2°, which is named as Air Mass 1.5 spectrum. The intensity of the sun light is decreased by scattering and reflection and also absorbed by gas clouds, water vapour and dusts [60]. In Figure 8, the different AM sun light spectra were described. I_{mpp} and V_{mpp} symbolize the maximum power point of current and voltage, respectively.

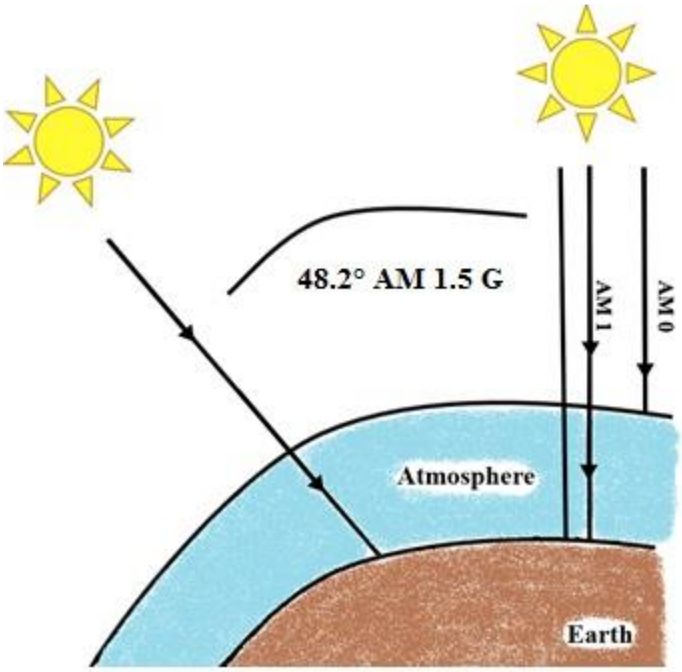

Figure 8. Schematic description of the different AM sun light spectra.

1.3.7.1.Critical Parameters for Solar Cell Efficiency

1.3.5.1.1. Open Circuit Voltage (V_{oc})

Several studies were performed to discover the factors affecting V_{oc} in terms of energy levels of donor and acceptor and work function of electrodes. Scharber *et al.* studied the effect of HOMO energy levels of 26 conjugated polymers on V_{oc} and found a linear relation among them [61] . Effect of LUMO energy level of acceptor and studies showed that the open circuit voltage (V_{oc}) is not only affected by HOMO energy level of the donor but also affected by LUMO energy level of the acceptor. V_{oc} is defined as the energy difference between HOMO level of the donor and the LUMO level of the acceptor in organic solar cells [62]. High-lying LUMO and low-lying HOMO energy level is a critical factor for obtaining high V_{oc} [63].

Adjusting the work function of the electrodes can also affect the open circuit voltage [64]. For example , LiF is used as a modifier for the cathode and is located among the active layer and the metal electrode, which ensures to obtain high open circuit voltage [65]. Besides, modification of indium tin oxide (ITO) is commonly done by plasma etching to control the work function of ITO [66].

1.3.5.1.2. Short Circuit Current Density (J_{sc})

The short-circuit current density (J_{sc}) is defined as the produced current through the solar cell when the voltage is zero. It is designated by the charge carrier mobility and the results of the photoinduced charge carrier density in the organic semiconductors. In the following equation;

$$\mathbf{J_{sc}} = \boldsymbol{ne\mu E} \tag{1.4}$$

n symbolizes the density of charge carriers, *e* represents the elementary charge, μ presents the mobility and *E* symbolize the electric field. In the bulk heterojunction mixture, the photo induced charge generation is supposed to have the 100 % efficiency [43]. Herein *n* is the amount of absorbed photons per unit volume.

Mobility is one of the parameter that affects the J_{sc} and is strongly affected by morphology of active layer. The morphology of active layer is hinge on film preparation and can be changed by some parameters such as deposition method, solvent type and the solvent evaporation time [67].

1.3.5.1.3. Fill Factor (FF)

The fill factor (FF) of the device is also another critical parameter for efficiency and determined with the following formula;

$$\mathbf{FF = P_m / J_{sc} * V_{oc} \qquad FF = I_{max} * V_{max} / J_{sc} * V_{oc}} \tag{1.5}$$

The FF ratio is illustrated in Figure 9. It symbolizes how ‘easy’ or ‘difficult’ the photogenerated carriers can be extracted out of a photovoltaic device. Therefore, when the current-voltage curve is a rectangle, the maximum value (100%) is achieved for FF. The maximum value of FF actually is not reached. In organic solar cells, the fill factor generally is in between only 50% and 70% [68].

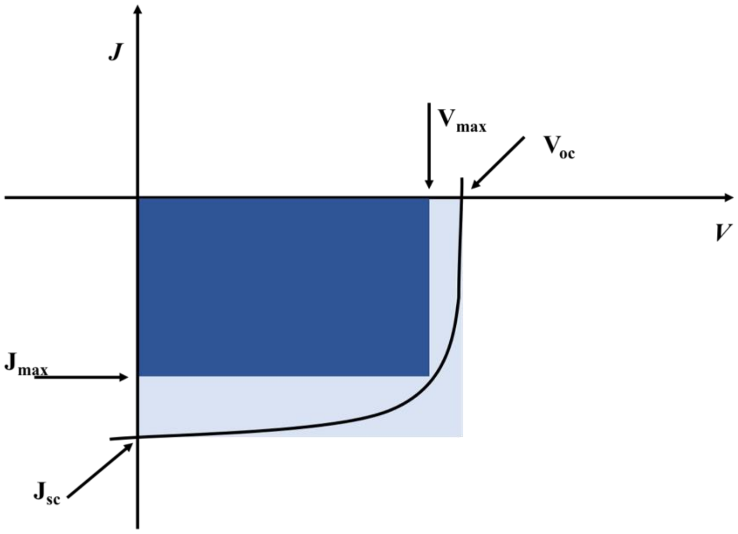

Figure 9. Current–voltage (J-V) curve on an organic photovoltaic device under illumination. The short circuit current (J_{sc}), current at maximum power output (J_{max}), the open circuit voltage (V_{oc}) and voltage at maximum power output (V_{max}) are illustrated.

1.3.8. Organic Photovoltaic Device Stability

Degradation and photooxidation can occur in the presence of water and oxygen especially under light illumination. Therefore it is crucial to avoid humidity and air to ensure long lifetimes for devices [69]. To construct OPV devices, aluminum (Al) and calcium (Ca) are used as low work function metal electrodes. These metal electrodes can easily be oxidized by oxygen which decreases electrical conductivity.

Formation of metal oxide layer causes transport barrier thus lowers the performance of the device [70]. On the other hand, the oxygen doping of polymer causes traps for electrons and decreases the fill factor (FF) and the open circuit voltage of OPV [71].

The presence of hygroscopic sides on PEDOT:PSS buffer layer can diffuse into active layer which results unnecessary aggregation of fullerenes derivatives. Thus affects the donor-acceptor interfaces that render exciton dissociation [72].

The durability of bulk heterojunction solar cells was remarkably increased since last ten years. The first devices were stored in an inert atmosphere. Nowadays, organic photovoltaics especially on flexible substrates have a life time of few years [73].

1.4. Light Emitting Diodes (LEDs)

A light emitting diodes is a remarkable electronic device that is capable of emitting light when required voltage is applied. The first commercial light emitting diodes (LEDs) were constructed and discovered in 1962 by Holonyak which were based on Ga/As/P (Galium, Arsenic and Phosphorous) inorganic semiconductors. These films had fascinating luminescent and conducting properties as well as long life times, low-cost technology and eco-friendly. On the other hand, organic light emitting diodes (OLEDs) has several advantages over inorganic counterparts therefore, OLEDs were developed for the flexible devices [74]. Figure 10 shows the types of OLEDs that were designed to obtain high efficiency. Multilayer device configuration can decrease exciton recombination in the charge transport thus, it is generally preferred for device fabrication [75].


A. Single Layer Device

B. Two-Layer Device


C. Three-Layer Device

D. Multilayer Device

Figure 10. Several kinds of OLED structures

Principally, the OLEDs are based upon electroluminescence occurring due to radiative recombination of holes and electrons in an organic semiconductor by an external electrical field. A Light is emitted through fluorescence and/or phosphorescence processes. The probability of existence of excitons on a singlet state is 25 % however on a triplet state is 75 %. This means that, to obtain high quantum yield phosphorescence is favorable and these processes were proven in '*Jablonski Diagram*' as given in Figure 11 [76][77].

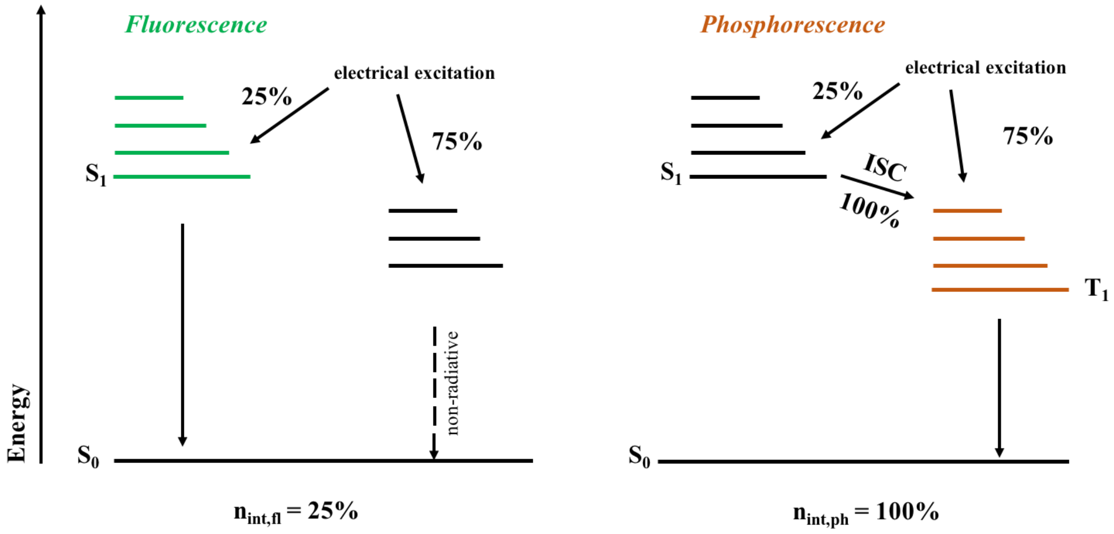

Figure 11. Presentation of *Jablonski Diagram* that briefly explanation of fluorescent and phosphorescent processes [77]

The traditional OLED consists of two organic layer, the first layer is used to ensure hole transport and the second one is used as the electron transport and light emitting layer. These layers are embedded between two electrodes. Holes are transported by a highly transparent low work function ITO layer to active layer. The electrons are transported by a low work function and high reflective metal i.e. aluminum (Al), calcium (Ca) to active layer.

The highly transparent ITO can be arranged by chemical etching. Poly(ethylenedioxythiophene) doped with polystyrene-sulfonic acid (PEDOT:PSS) is coated usually on the top of the ITO that increases the surface quality of the ITO electrode. Also, the work function of a transparent ITO surface can be controlled by electrochemical/chemical redox reactions of that layer [78]. The OLED has four fundamental steps to generate light under applied electric field. In the first step, electron leaves from the cathode and hole leaves from the anode. In the second step, the charge carriers move into the semiconductor organic layer and herein an exciton forms by columbic attraction. The exciton leads to the formation of a photon among the LUMO and HOMO levels of the organic light emitting molecules. When the electrical power was applied to the electrodes, light is produced by radiative decay in the final step (Figure 12) [77].

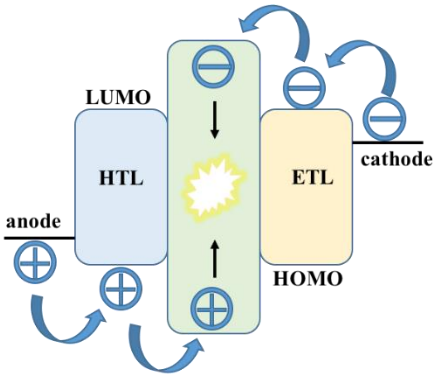

Figure 12. Working principle of an Organic Light Emitting Diodes

1.5. Palladium Mediated Cross-Coupling Reactions

Metal-catalyzed cross-coupling reactions have been commonly used to synthesize conjugated polymers. These kinds of reactions can be performed with palladium catalyst i.e. Suzuki coupling [79], Stille coupling [80], Sonogashira coupling [81] and Butcwald-Hartwing coupling [82][83] with copper i.e. Glaser coupling [84] and Ullmann reactions [85] and with nickel i.e. Negishi coupling [86] and Yamamoto coupling [87]. The best methods of polycondensation was observed with palladium catalysis. Stille coupling, Suzuki coupling and Sonogashira coupling were commonly used in this field. In 2010, A. Suzuki, E. Negishi and R. Heck were awarded with the Nobel Prize in chemistry due to the importance of Pd-catalyzed cross-coupling reactions. In this thesis, two cross-coupling reactions were used and described.

1.5.3. Suzuki Coupling

Suzuki cross-coupling is performed in the presence of a base and palladium catalyst and utilized for formation of carbon-carbon (C-C) bond. In this coupling reaction, the aromatic organoboron compounds are present as the active material to react with aromatic halides (Figure 13). Organoboranes, boronic esters or potassium trifluoroborates can be used instead of boronic acid. In addition, triflates can be used instead of the halides as the coupling partners. The boron atom is commonly activated with a base and this activation is not needed for other coupling reactions. When the boron atom is activated, the polarization of the organic ligand is increased in the reaction medium. After all that, the trans metallation is started and a proposed mechanism of Suzuki coupling is illustrated in Figure 14.

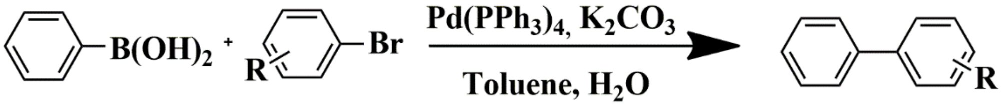

Figure 13. General illustration of phenylene derivatives via Suzuki coupling reaction

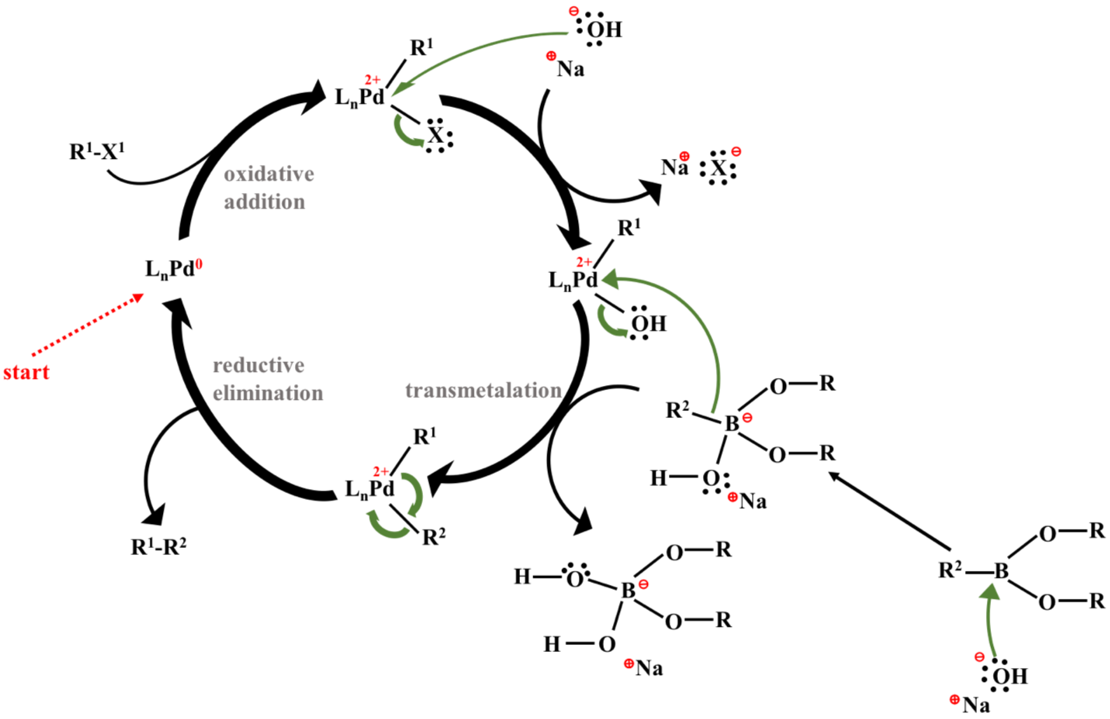

Figure 14. A suggested Suzuki Cross-Coupling mechanism [79]

The coupling mechanism starts with oxidative addition of the organohalide to the Pd(0) to occur a Pd(II) complex. A molecule of alkoxide base exchanges the halide on the palladium complex while another reacts with the organoborane to form a borate regent creating its nucleophilic R group. Trans metallation is started with the borate then its R group replaces the halide anion on the palladium complex. The final product is achieved after reductive elimination. The palladium catalyst is regenerated and this cycle can continue again [79].

1.5.4. Stille Coupling

Stille cross-coupling is the organic reaction to form carbon-carbon (C-C) bond using palladium catalyst and proposed mechanism is shown in Figure 15.

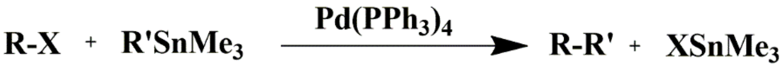

$$R\text{-}X + R'SnMe_3 \xrightarrow{Pd(PPh_3)_4} R\text{-}R' + XSnMe_3$$

Figure 15. General mechanism of Stille cross-coupling reaction

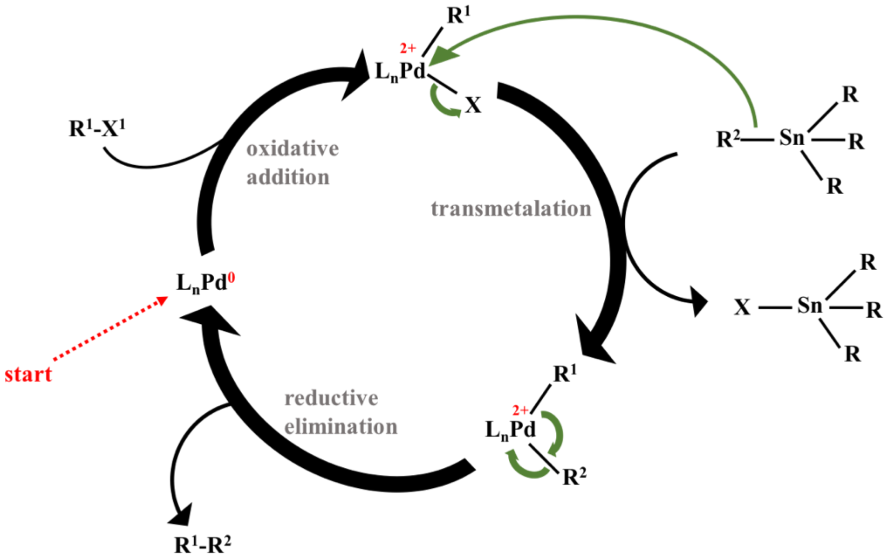

Figure 16. A suggested Stille Cross-Coupling mechanism [88]

Stille cross-coupling has similar steps with Suzuki cross-coupling that is defined above. These steps consists of oxidative addition , trans metalation, and reductive elimination (Figure 16) [89].

1.6. Moieties in Donor-Acceptor Approach Based Copolymers

1.6.3. Dibenzo[a,c]phenazine Moiety

Dibenzo[a,c]phenazine (DBP) derivatives were used as the acceptor moiety for the development of D-A type conjugated polymers. Summary of structures of polymers are shown in Figure 17.

Benzopyrazine is a heterocyclic compound which consists of a pyrazine and a benzene ring in its structure [90]. Pyrazine ring consists of two imine nitrogens having electron withdrawing property and is almost stable in quinoid form [91][92]. The DBP unit is also functionalized with linear or alkoxy chains, fluorine to control optical, electrochemical and physical properties in recent studies.

Wang *et al.* synthesized four conjugated D-π-A copolymers based on 11,12-difluorodibenzo[a,c]phenazine as an acceptor unit, benzodithiophene (BDT) with an alkoxy side chain or thiophene conjugated side chain as a donor unit and thiophene as π-bridge. The optimum performance of the devices was recorded at a 1:1 weight ratio of polymer:PCBM, with a PCE of 1.21%, a Voc of 0.79 V, a Jsc of 4.57 mA/cm^2 and a FF of 34% [93].

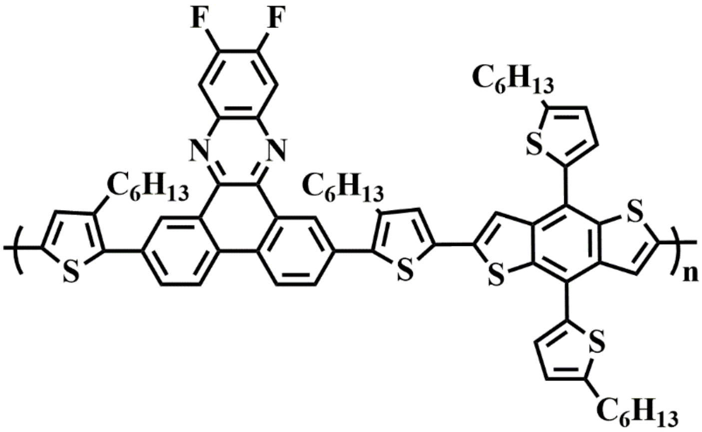

Wang *et al.*, 2013

Figure 17. Molecular structures of Dibenzo[a,c]phenazine derivative used in OPVs.

1.6.4. Benzodithiophene (BDT) based Polymers

In recent years, benzodithiophene unit was used in more than 500 studies. Benzo[2,1-b:3,4-b']dithiophene derivatives were chosen as donor moieties in the organic photovoltaics. It is consisted of a fused benzene with two flanking thiophene units which leads to high hole mobility, proper side chain patterns for improved solubility and exceedingly extended π–conjugated structures (Figure 18) [94][95].

In 2009, Liang *et al.* developed a novel conjugated copolymer based on benzoditiophene units as the donor unit and ester substituted thieno[3,4-b]thiophene as the acceptor unit and used as the active layer of organic photovoltaics. The polymer was mixed with fullerene derivatives which revealed a high fill factor of over 65 % and a high PCE of 5.6 % without any treatment [96]. In 2010, Liang *et al.* designed and synthesized a new copolymer consisted of benzodithiophene as the donor unit in copolymer backbone. In this study also ester substituted thieno[3,4-b]thiophene was used as the acceptor unit. A fluorine atom was also incorporated in acceptor unit to decrease the HOMO level of copolymer which offers higher V_{oc}. As a result, the power conversion efficiency was increased up to 7.40 % with an additive treatment [97].

In 2016, Li *et al.* have designed and synthesized two novel copolymers. BDT was modified by two 4-alkyl-3,5-difluorophenyl side chains and used as the donor moiety. In addition, benzooxadiazole and benzothiadiazole were used the acceptors and thiophene was used the π-bridge. The maximum power conversion efficiency was 8.24 % when benzothiadiazole and benzodithiophene and thiophene were combined as D-A-D configuration without any treatment [98].

Zhang *et al.* have synthesized and designed two new conjugated polymers which consist benzodithiophene and benzothiadiazole units in 2013. BDT was modified by adding alkylphenyl substituent into the benzodithiophene backbone for promising high efficiency in OSCs [99]. In this study, they investigated the amount of 1,8-diiodooctane (DIO) in the device efficiency. They achieved higher power conversion efficiency of 8 % and higher fill factor 70.9 % with 0.5 % DIO. 1,8-Diiodooctane has a high boiling point and used as an additive in organic photovoltaics. It enhances efficiently the crystallinity of the polymer and ensures to produce multi-length scale morphology that raises charge transport and exciton dissociation. Therefore, the high efficiency of the conjugated polymers are achieved by using this method [100].

In 2015, Liu *et al.* have synthesized four copolymer based on quinoxaline derivatives as the acceptor unit and benzodithiophene moiety as the donor and applied in polymer solar cells. The photophysical properties of donor and acceptor units are improved by having fluorine atom as the substituent. Fluorinated copolymer revealed the lowest HOMO and LUMO among four polymers which led to V_{oc} of 0.90 V with a power conversion efficiency of 8.55 % with a 5 % additive treatment [101].

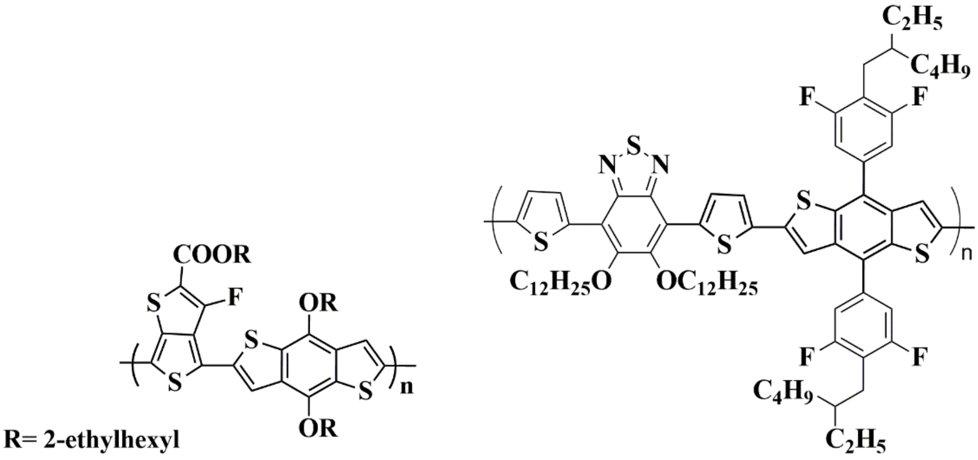

Liang *et al.*, 2010　　Li *et al.*, 2016

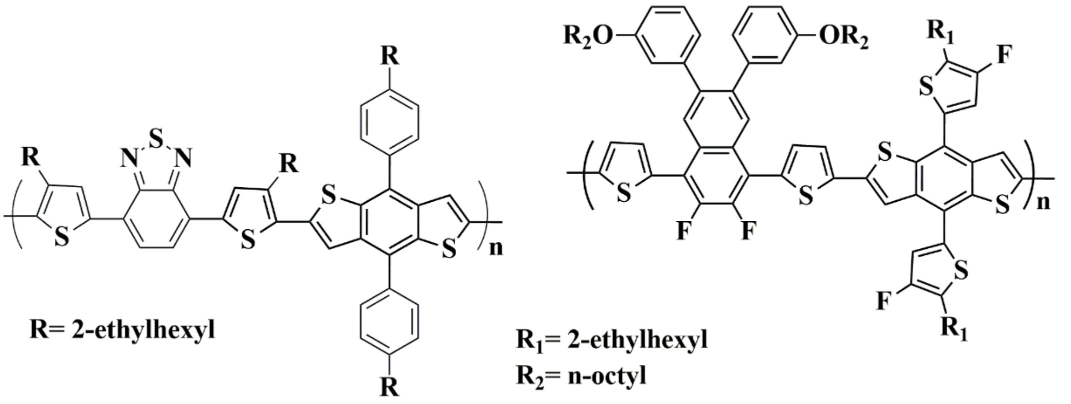

Lİ *et al.*, 2013　　Liu *et al.*, 2015

Figure 18. Molecular structures of benzodithiophene derivatives used in OPVs.

1.6.5. Dibenzosilole based Copolymers

Lately, silole based donor units are widely used since silole atom can be connected to alkyl units. By this means, the silicon atom provides improved hyper conjugation and it stabilizes partially the negative carbon atom. Moreover, the lowest LUMO energy level can be achieved by overlapping between π* orbital of the butadiene moiety and σ* orbital of the exocyclic silicon-carbon bonds. Silicon atom stabilized the HOMO energy level of butadiene ensuring ambient stability (Figure 19) [102].

In 2014, Li *et al.* synthesized three novel semiconducting polymers by Suzuki coupling. The newly developed fluorine atom based monomer achieved low HOMO and LUMO energy levels. Also, they attached alkoxy chain on acceptor unit to increase solubility of copolymers without interfering the dense packing of polymers in the solid state. The highest PCE and V_{oc} were obtained as 6.41 % and 0.98 % with additive treatment, respectively. This score is the best result in PCSs based on benzothiadiazole and silafluorene containing polymers [103].

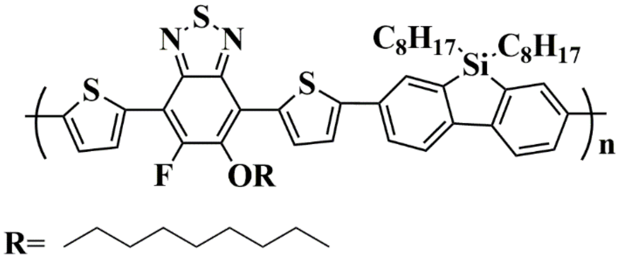

Li *et al.*, 2014

Figure 19. Molecular structure of silafluorene derivatives used in OPVs.

1.6.6. Thiophene Moiety effects as π-Bridge Group

Conjugate based bridges enhance interactions between acceptor and donor units and remarkably affect polymer's electronic structure. Accordingly, these bridges significantly change optical, electrochemical and photovoltaic properties of the polymers. For obtaining novel polymers that have high efficiency in organic photovoltaics understanding the role of π bridges on the photovoltaic and the physicochemical properties is important [104]. Thiophene is mostly used as a π bridge for increasing π-conjugation of polymer backbone and reducing steric hindrance in copolymers. These properties of thiophene decrease the band gap of copolymers due to the quinoidal character of the bridging group along the polymer backbone [105][106]. Sun. *et al.* used alkyl substituted thiophene units as the π-bridge to enhance solubility of copolymer in common solvents [107]. Also, when the copolymers have π-conjugation as thiophene, the thin film properties of polymers are becoming better that improve fill factor (FF) and obtain high power conversion efficiency in organic photovoltaics. Thiophene bridged conjugated copolymers slightly having deeper HOMO level that leads to obtain higher open circuit voltage (V_{oc}) [108].

1.6.7. Fluorine atom effect on Polymers

Fluorine has a specific character among halogens since it has the sterically second smallest van der Waal's radius (1.35 Å vs 1.20 Å for hydrogen) and the highest electronegativity. Furthermore, a fluorine-carbon bond is stronger than a hydrogen-carbon bond (485 kJ/mol vs 414 kJ/mol). For this reason, when the organic compounds contain a fluorine atom, they gain exclusive physical and chemical properties [109]. This atom is used as an electron-withdrawing group in high-efficiency organic photovoltaic polymers [110]. Also, it can be introduced onto the conjugated polymer backbone without any harmful steric effects (Figure 20).

Price *et al.* designed and synthesized two almost identical conjugated polymers that had a medium band gap of 2.0 eV. One of them had two fluorine atoms instead of hydrogen. They demonstrated that fluorine atom affect on the HOMO level as detractive and on the hole mobility of the polymer as increaser that improve the organic photovoltaic performance [111].

Wang *et al.* have designed and synthesized thieno[3,2-b]thiophene as π-bridge in conjugated D-π-A alternating copolymers. Benzo[1,2-b:4,5-b']dithiophene was used as donor unit and benzothiadiazole as the acceptor unit. One of the acceptor is modified by two fluorine atoms to obtain high open-circuit voltage and hole mobility. Fluorine atoms did not increase the power conversion efficiency since it decreased solubility of the polymer [112].

Stuart *et al.* have revealed that the critical device parameters (V_{oc}, $J_{sc,}$ and FF) of polymer based bulk heterojunction solar cells were improved by adding fluorine atoms onto the conjugated polymer backbone. When the number of fluorine atoms increased on the conjugated backbone, the HOMO levels of conjugated polymers were decreased and FF and J_{sc} of the BHJ solar cells were enhanced. In addition, the morphology of active layer was improved by having fluorine substituents. The power conversion efficiency was increased from 4 % to 7.16% whereby having two F atoms as substituents [113].

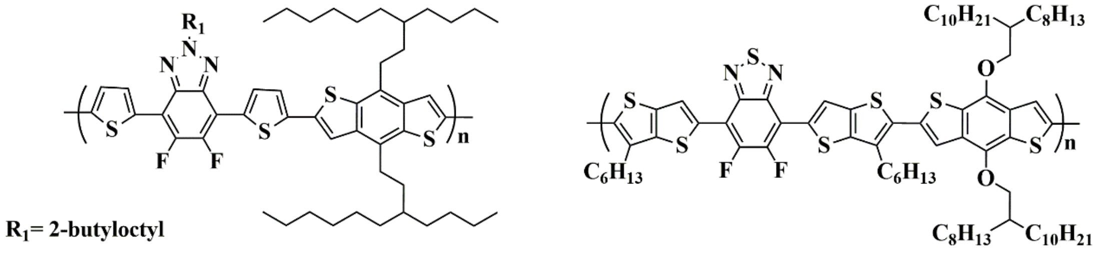

Price *et al.,* 2011 Wang *et al.,* 2014

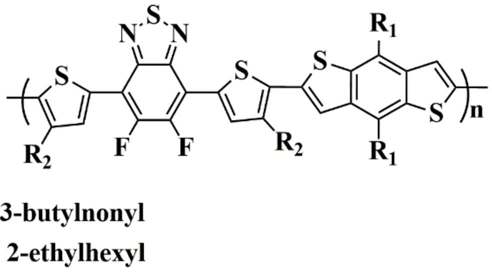

Stuart *et al.,* 2013

Figure 20. Molecular structures of conjugated polymer derivatives effected with fluorine atom used in OPVs

1.7. Aim of the Work

In recent years, D-A approach is commonly used method to achieve low band gap conjugated polymers. This approach ensures to obtain high power conversion efficiency for organic photovoltaics as mentioned in introduction part of this thesis. For this aim, a fluorinated dibenzo[a,c]phenazine derivative is chosen as an acceptor unit to observe how fluorine atom affects on HOMO-LUMO level of conjugated polymers when compared with literature examples. 3-hexylthiophene is used as a donor unit to increase solubility of monomer and 3,4-ethylenedioxythiophene is chosen as a donor unit to decrease oxidation potential of homopolymer.

Fluorinated dibenzo[a,c]phenazine, 3-hexylthiophene, benzodithiophene and silafluorene bearing conjugated polymers were designed and synthesized via both Stille and Suzuki cross-coupling reactions. Silafluorene derivative is used as a donor unit in copolymer backbone to decrease HOMO energy level that ensures to obtain higher open circuit voltage in organic photovoltaic applications. Benzodithiophene derivative is chosen as donor units in two copolymers backbone. It leads to improve solubility of copolymers and ensures to obtain high hole mobility in organic photovoltaic applications. In addition, 3-hexylthiophene is used as π-bridge in two copolymers backbone to increase absorbance that ensure to obtain low band gap polymers due to planar structure. These copolymers are used as the donor units and PCBM71 is used as the acceptor in the active layer of organic photovoltaic devices.

In this manner, two new fluorine atom consisted homopolymers and three new copolymers were synthesized and they showed in the experimental part of this thesis.

CHAPTER 2

2. EXPERIMENTAL

2.1. Materials and Methods

9,10-Phenanthrenequinone, 3-hexylthiophene, thiophene, 3,4-ethylenedioxythiophene, 4-fluoro-2-nitroaniline N-bromosuccinimide (NBS), n-butyllithium (n-BuLi), tributyltin chloride, bis(triphenylphosphine)palladium(II) dichloride, tris(dibenzylideneacetone) dipalladium(0), tri(o-tolyl)-phosphine, 2,6-bis(trimethylstannyl)-4,8-bis(2-ethylhexyloxy)benzo[1,2-b:4,5-b0]dithiophene and 9,9-Dioctyl-9H-9-silafluorene-2,7-bis(boronic acid pinacol ester) were purchased from Sigma-Aldrich Chemical Co. Ltd. Indium Tin Oxide (ITO) coated glass sheets was purchased from Visiontek Systems Ltd. Tetrahydrofuran (THF) was dried over metallic sodium/ benzophenone ketyl and freshly distilled prior to use while other solvents were used as standard without any drying procedure.

2.2. Equipment

^{1}H and ^{13}C spectra were recorded on a Bruker Spectrospin Avance DPX-400 Spectrometer. The internal reference was trimethylsilane (TMS) to report chemical shifts in ppm. Merck Silica Gel 60 was used to obtain pure materials as the stationary phase and organic solvents were used as the mobile phase in the purification system.

Electrochemical studies of the π-conjugated monomers and polymers were examined by GAMRY Reference 600 potentiostat with three-electrode system; ITO-coated glass slide was used as working electrode (WE), silver wire was calibrated to Fc/Fc^+ redox couple to use as the reference electrode (RE) and a platinum wire as counter electrode (CE) in a cell. The electrochromic measurements of the polymer film were carried out by Varian Carry 5000 UV-Vis spectrophotometer. Solartron 1285 potentiostat/galvanostat was used to control applied potential. A Konica Minolta CS-100 spectrophotometer was used to achieve colorimetry measurements.

The organic solar cells were constructed in a MBraun glove-box system (0.1 ppm < O_2, 0.1 ppm < H_2O). The current density voltage (J-V) characteristics were measured using a Keithley 2400 source meter under AM 1.5 G illumination at 100 mW/cm^2 using a Xe lamp-based Newport solar simulator. Incident-photon-to-current efficiency (IPCE) of solar cells was determined using an Oriel Quantum Efficiency Measurement Kit. A calibrated monosilicon diode exhibiting a response at 300-900 nm was used as a reference.

2.3. Syntheses of *π*-Conjugated D-A Type Monomers and Copolymers

Tributyl(4-hexylthiophen-2-yl)stannane **(1)**, tributyl(thiophen-2-yl)stannane **(2)** and tributyl(2,3-dihydrothieno[3,4-b][1,4]dioxin-7-yl)stannane **(3)** were synthesized according to literature procedures [114]. Phenanthrene-9,10-dione was brominated with N-bromosuccinimide (NBS) [115]. 4-Fluoro-2-nitroaniline was reduced to 4-fluorobenzene-1,2-diamine **(5)** and reacted with 2,7-dibromophenanthrene-9,10-dione (4) to synthesize 2,7-dibromo-11-fluorodibenzo[a,c]phenazine **(6)** [116]. Compound 6 was coupled with tributyl(4-hexylthiophen-2-yl)stannane via Stille cross-coupling to afford 11-fluoro-2,7-bis(4-hexylthiophen-2-yl)dibenzo[a,c]phenazine **(7)**. Bromination of compound 7 was performed in the presence NBS and $CHCl_3$ to synthesize 2,7-bis(5-bromo-4-hexylthiophen-2-yl)-11-fluorodibenzo[a,c]phenazine **(8)**. Then, compound 8 was used for the syntheses of polymers (PBDT-TFBPz and PSi-TFBPz). PBDT-TFBPz was synthesized via Stille cross-coupling and copolymerization of 8 with 2,6-bis(trimethylstannyl)-4,8-bis(2-ethylhexyloxy)benzo[1,2-b:4,5-b0]dithiophene was achieved in the presence of tris(dibenzylideneacetone)dipalladium(0) and tri(o-tolyl)-phosphine in THF solvent.

Also, PBDT-FBPz was synthesized via Stille coupling and copolymerization of 6 with 2,6-bis(trimethylstannyl)-4,8-bis(2-ethylhexyloxy)benzo[1,2-b:4,5-b0]dithiophene in the presence of tris(dibenzylideneacetone)dipalladium(0) and tri(o-tolyl)-phosphine in THF solvent. Furthermore, compound 6 was coupled with tributyl(2,3-dihydrothieno[3,4-b][1,4]dioxin-7-yl)stannane via Stille cross-coupling to afford 2,7-bis(2,3-dihydrothieno[3,4-b][1,4]dioxin-5-yl)-11-fluorodibenzo[a,c]phenazine **(9).** Moreover, PSi-TFBPz was synthesized via Suzuki cross-coupling and copolymerization of 6 and 9,9-Dioctyl-9*H*-9-silafluorene-2,7-bis(boronic acid pinacol ester) in the presence of bis(triphenylphosphine)palladium(II) dichloride, K_2CO_3 solution (2M, 0.5 mL), tetrahexyl ammonium iodide in THF-water solvent system. The PBDT-TFBPz, PSi-TFBPz and all monomer structure were characterized with NMR spectroscopy. Low solubility of PBDT-FBPz was an obstacle to investigate its chemical structure by NMR, however it was enough to find its molecular weight by GPC.

2.3.1. Tributyl(4-hexylthiophen-2-yl)stannane (1)

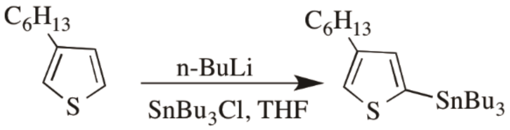

Figure 21. Synthesis of tributyl(4-hexylthiophen-2-yl)stannane

3-Hexylthiophene (1.0g, 5.9 mmol) was dissolved in freshly dried THF in a 50 mL two-neck round bottom flask and the solution was cooled to -78˚C under inert atmosphere. Then, 2.5 M n-BuLi in hexane (2.6 mL, 6.6 mmol) was added drop wise to the reaction mixture. The mixture was stirred at the same temperature (-78˚C) for one hour. Stannyltributyltin chloride (1.80 mL, 6.6 mmol) was added slowly at -78˚C. The reaction was continued for one hour at -78˚C and warmed to room temperature and stirred overnight. The solvent was removed under reduced pressure. The crude product was poured into the saturated aqueous sodium hydrogen carbonate ($NaHCO_3$). Organic layer was separated and the aqueous layer was extracted with dichloromethane several times. The combined organic phase was dried over $MgSO_4$ and the solvent was removed at under reduced pressure to obtain as a colorless oil (2.18 g, yield 81%). ^{1}H NMR (400 MHz, $CDCl_3$) δ 7.11 (s, 1H), 6.90 (s, 1H), 2.60 (t, *J* = 7.7 Hz, 2H), 1.51 – 1.48 (m, 8H), 1.25 – 1.20 (m, 12H), 1.03 – 0.90 (m, 6H), 0.91 – 0.77 (m, 12H).

2.3.2. Tributyl(thiophen-2-yl)stannane (2)

Figure 22. Synthesis of tributyl(thiophen-2-yl)stannane

A sample of thiophene (2.0 g, 23.8 mmol) was dissolved in freshly dried tetrahydrofuran (THF) and the reaction mixture was cooled to -78˚C under argon atmosphere. Then, 1.6 M n-BuLi in hexane (10 mL, 26.1 mmol) was added drop wise to the reaction mixture. After end of the addition n-BuLi, the mixture was stirred at the same temperature (-78˚C) for one hour. The same addition procedure was applied for stannyltributyltin chloride (6.45 mL, 23.8 mmol) when the reaction mixture temperature was at -78˚C. At the same temperature, the reaction was continued for one hour and after all addition process the mixture stirred overnight at room temperature. The solvent was removed under reduced pressure. The residue was poured into the saturated aqueous sodium hydrogen carbonate ($NaHCO_3$) and aqueous phase was extracted with dichloromethane (3x100 mL). The combined organic phase was dried over $MgSO_4$ and the solvent was removed under reduced pressure. The crude product was purified by flash column chromatography with hexane to obtain gold yellow oil (6.43 g, yield 75%). ^{1}H NMR (400 MHz, $CDCl_3$) δ 7.56 (d, *J* = 4.7 Hz, 1H), 7.18 (dd, *J* = 4.7, 2.9 Hz, 1H), 7.12 (d, *J* = 2.9 Hz 1H), 1.49 (m, 6H), 1.25 (m, 6H), 1.02 (m, 6H), 0.83 (t, *J* = 7.3 Hz, 9H). ^{13}C NMR (101 MHz, $CDCl_3$) δ 136.1, 135.1, 130.5, 127.8, 29.3, 29.0, 27.2, 13.7, 10.8, 8.7.

2.3.3. Tributyl(2,3-dihydrothieno[3,4-b][1,4]dioxin-7-yl)stannane (3)

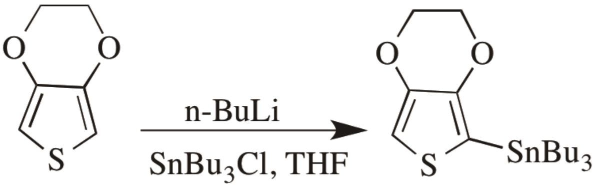

Figure 23. Synthesis of tributyl(2,3-dihydrothieno[3,4-b][1,4]dioxin-7-yl)stannane

In a 50 mL two-neck round bottom flask, a sample of 3,4-ethylenedioxythiophene (2.0 g, 14.0 mmol) was dissolved in freshly distilled anhydrous THF. The reaction medium temperature was adjusted to -78˚C and 2.5 M n-BuLi in hexane (1.43 mL, 15.4 mmol) were added drop wise then at the same temperature the reaction mixture was stirred for one hour under inert atmosphere. After one hour, the tributylstannyl chloride (3.79 mL, 14.0 mmol) was added slowly to the reaction solution and it was maintained at the same temperature for one hour. Then temperature of the reaction medium was increased to room temperature. The reaction was continued overnight afterwards the solvent of reaction was removed under reduced pressure. Thereafter the residue was transferred into saturated aqueous ammonium chloride and extracted with dichloromethane. The organic phase was washed with saturated brine several times and dried over $MgSO_4$. The solvent of extraction was removed under reduced pressure to obtain tributyl(2,3-dihydrothieno[3,4-*b*][1,4]dioxin-7-yl)stannane (4.8 g, 80%) as a yellow liquid. ^{1}H NMR (400 MHz, $CDCl_3$) δ 6.48 (s, 1H), 4.08 (s, 4H), 1.54 – 1.41 (m, 6H), 1.31 – 1.19 (m, 6H), 1.02 (t, 6H), 0.81 (t, *J* = 7.3 Hz, 9H). ^{13}C NMR (101 MHz, $CDCl_3$) δ 147.71, 142.48, 105.83, 99.65, 64.70, 64.62, 28.98, 27.19, 13.70, 10.52.

2.3.4. 2,7-dibromophenanthrene-9,10-dione (4)

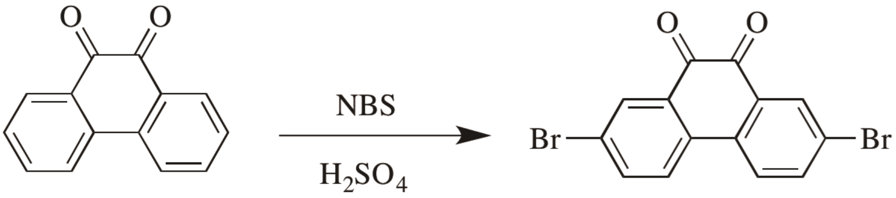

Figure 24. Synthesis of 2,7-dibromophenanthrene-9,10-dione

In a 100 mL two-neck round bottom flask, a phenanthrene-9,10-dione (1.0 g, 4.8 mmol) was dissolved in H_2SO_4 (98%) and the flask was surrounded with Al foil paper since NBS is photosensitive. N-bromosuccinimide (2.08 g, 12.0 mmol) was added at room temperature for 24 h. The acidic reaction mixture was poured into cool water. The orange product was filtered and washed with cool water to remove acid. After that, it was recrystallized from DMSO to obtain orange solid product (1.29 g, 73%). ^{1}H NMR (400 MHz, $CDCl_3$) δ 8.24 (s, 2H), 7.78 (s, 4H).

2.3.5. 4-Fluorobenzene-1,2-diamine (5)

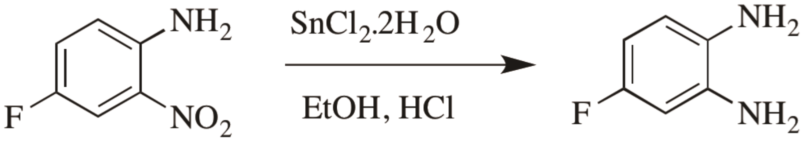

Figure 25. Synthesis of 4-fluorobenzene-1,2-diamine

To a solution of 4-fluoro-2-nitroaniline (3.0 g, 19.20 mmol) in ethanol and concentrated hydrochloric acid (37%). Tin(II)chloride dihydrate ($SnCl_2.2H_2O$) (14.5

g, 76.8 mmol) was added in several portions. The mixture was refluxed for 1 hour and stirred overnight at room temperature. Then, pH value of the mixture was adjusted to 8-9 by adding aqueous potassium hydroxide (KOH) and then the mixture was extracted with ethyl acetate three times. The combined organic phases were dried over anhydrous magnesium sulfate ($MgSO_4$). The solvent was removed by rotary evaporation. Further purification was performed column chromatography using ethyl acetate as eluent to give dark green-brown solid product (1.81g, 75%). This material was air and light sensitive. ^{1}H NMR (400 MHz, $CDCl_3$) δ 6.55 (dd, *J* = 8.4, 5.5 Hz, 1H), 6.42 – 6.25 (m, 2H), 3.29 (d, *J* = 119.4 Hz, 4H).

2.3.6. 2,7-Dibromo-11-fluorodibenzo[a,c]phenazine (6)

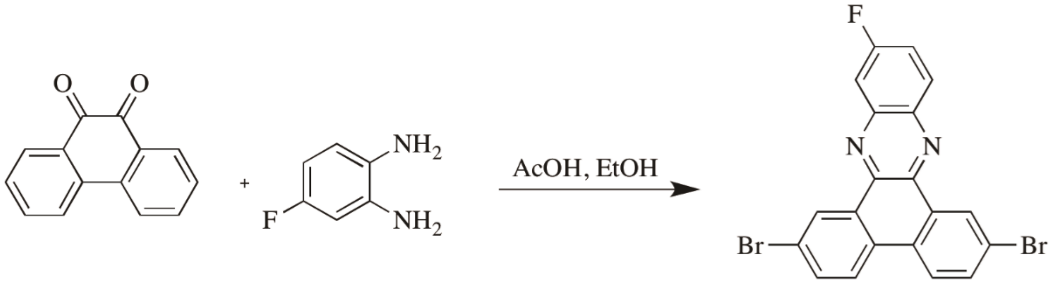

Figure 26. Synthesis of 2,7-dibromo-11-fluorodibenzo[a,c]phenazine

2,7-Dibromophenanthrene-9,10-dione (1.20 g, 3.27 mmol) and 4-fluorobenzene-1,2-diamine (1.65 g, 13.1 mmol) were dissolved in ethanol and acetic acid was added to the reaction solution. The mixture was refluxed for 1 hour then the reaction was maintained at room temperature for overnight. The mixture was poured into water and the yellow solid was filtered. The product has low solubility; it was washed with chloroform to remove impurities. 2,7-Dibromo-11-fluorodibenzo[a,c]phenazine was obtained as a yellow solid (0.54 g, 36%)**.** ^{1}H NMR (400 MHz, $CDCl_3$) δ 9.41 (dd, *J* = 2.17, 5.97 Hz, 2H), 8.28 (t, *J* = 8.13 Hz 3H), 7.84 (m, 3H), 7.63 (m, 1H).

2.3.7. 11-Fluoro-2,7-bis(4-hexylthiophen-2-yl)dibenzo[a,c]phenazine (7)

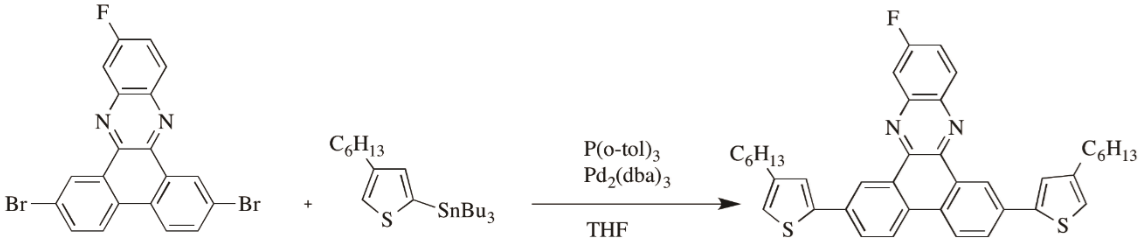

Figure 27. Synthesis of 11-fluoro-2,7-bis(4-hexylthiophen-2-yl)dibenzo[a,c]phenazine

2,7-Dibromo-11-fluorodibenzo[a,c]phenazine (500 mg, 1.09 mmol) and tributyl(4-hexylthiophen-2-yl)stannane(1.5 g, 3.30 mmol) were dissolved in anhydrous THF. The solution was degassed with argon for 30 minutes after which tris(dibenzylideneacetone) dipalladium(0) (50 mg, 5.5 μmol) and tri(o-tolyl)-phosphine (134 mg, 43.6 μmol) were added to the reaction mixture quickly to avoid exposure to oxygen. Reaction temperature was brought to 78˚C and the reaction was stirred overnight. The mixture was extracted with chloroform several times and solvent was removed by rotary evaporation. The yellow-orange solid was recrystallized from ethanol and pure 11-fluoro-2,7-bis(4-hexylthiophen-2-yl)dibenzo[a,c]phenazine(560 mg, 81%) was obtained. ^{1}H NMR (400 MHz, $CDCl_3$) δ 9.17 (dd, *J* = 11.9, 6.0 Hz, 2H), 8.20 – 8.08 (m, 3H), 7.82 – 7.68 (m, 3H), 7.55 – 7.46 (m, 1H), 7.31 (s, 2H), 6.91 (s, 2H), 2.63 (t, *J* = 7.7 Hz, 4H), 1.67 (dt, *J* = 15.0, 7.5 Hz, 6H), 1.41 – 1.26 (m, 13H), 0.87 (t, *J* = 6.9 Hz, 6H). ^{13}C NMR (101 MHz, $CDCl_3$) δ 144.45, 143.40, 143.35, 142.42, 142.33, 142.17, 141.15, 139.04, 133.48, 131.45, 131.43, 131.33, 130.26, 129.90, 129.71, 129.51, 127.17, 126.89, 125.12, 125.06, 122.91, 122.12, 122.08, 121.77, 120.34, 120.08, 120.03, 119.94, 31.80, 30.76, 30.51, 29.20, 22.72, 14.16.

2.3.8. 2,7-Bis(5-bromo-4-hexylthiophen-2-yl)-11-fluorodibenzo[a,c]phenazine (8)

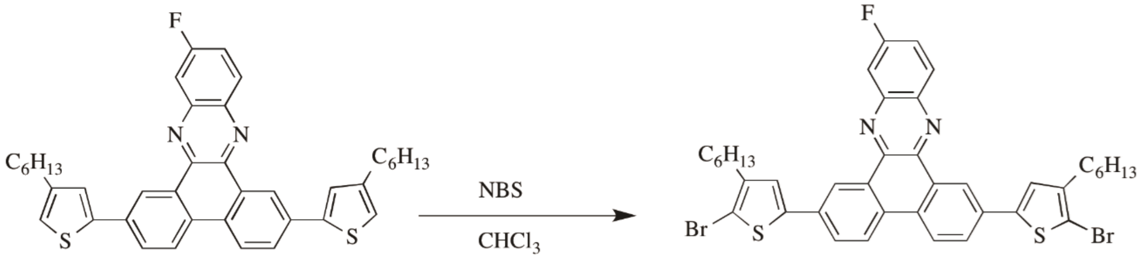

Figure 28. Synthesis of 2,7-bis(5-bromo-4-hexylthiophen-2-yl)-11-fluorodibenzo[a,c]phenazine

In a 50 mL two-neck round bottom flask, 11-fluoro-2,7-bis(4-hexylthiophen-2-yl)dibenzo[a,c]phenazine (500 mg, 1.04 mmol) was dissolved in chloroform and NBS (366 mg, 2.06 mmol) was added slowly at room temperature and the mixture was stirred for 12 hours. The mixture was extracted with chloroform with previous reaction extraction procedure. After then, the solvent was evaporated under pressure. The dark yellow product was recrystallized from ethanol to obtain pure product. 2,7-Bis(5-bromo-4-hexylthiophen-2-yl)-11-fluorodibenzo[a,c]phenazine (375 mg, 60%) was obtained as a dark yellow solid. ^{1}H NMR (400 MHz, $CDCl_3$) δ 9.30 (d, J = 5.4 Hz, 2H), 8.38 – 8.24 (m, 3H), 7.94 – 7.72 (m, 3H), 7.63 – 7.56 (m, 1H), 7.23 (s, 2H), 2.59 (t, 4H), 1.64 (m, 4H), 1.43 – 1.07 (m, 12H), 0.84 (t, J = 20.8 Hz, 6H).

2.3.9. 2,7-Bis(2,3-dihydrothieno[3,4-b][1,4]dioxin-5-yl)-11-fluorodibenzo[a,c]phenazine (9)

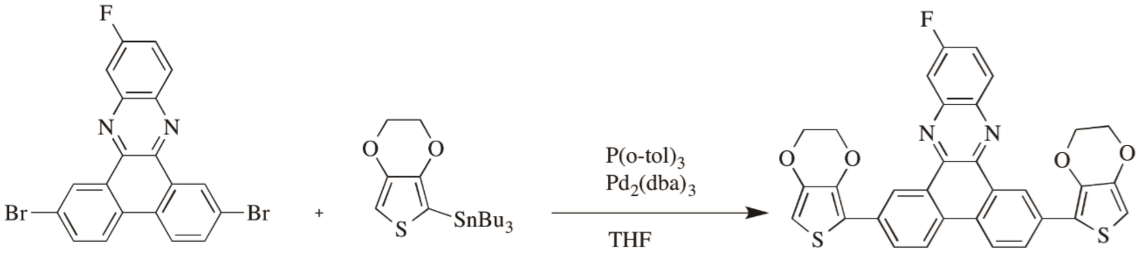

Figure 29. Synthesis of 2,7-bis(2,3-dihydrothieno[3,4-b][1,4]dioxin-5-yl)-11-fluorodibenzo[a,c]phenazine

2,7-Dibromo-11-fluorodibenzo[a,c]phenazine(240 mg, 0.520 mmol) and tributyl(2,3-dihydrothieno[3,4-b][1,4]dioxin-7-yl)stannane (910 mg, 2.10 mmol) were dissolved in dry THF under argon atmosphere. The solution was degassed with argon for 30 minutes after which tris(dibenzylideneacetone) dipalladium(0) (24 mg, 2.60 µmol) and tri(o-tolyl)-phosphine (64 mg, 21.0 µmol) were added and the reaction was heated to 78˚C and stirred for 16 hours. After that, the mixture was extracted with chloroform and brine for several times and organic solvent was removed by rotary evaporation. The orange solid was recrystallized by ethanol and pure 2,7-bis(2,3-dihydrothieno[3,4-b][1,4]dioxin-5-yl)-11-fluorodibenzo[a,c]phenazine was obtained after filtration. ^{1}H NMR (400 MHz, $CDCl_3$) δ 9.45 (dd, *J* = 10.9, 2.1 Hz, 2H), 8.39 – 8.18 (m, 3H), 8.04 (dd, *J* = 8.5, 2.0 Hz, 2H), 7.86 (dd, *J* = 9.5, 2.8 Hz, 1H), 7.59 – 7.50 (m, 1H), 6.34 (s, 2H), 4.46 – 4.19 (m, 8H).

2.4. Synthesis of Polymers

2.4.1. Synthesis of P1 (PBDT-FBPz)

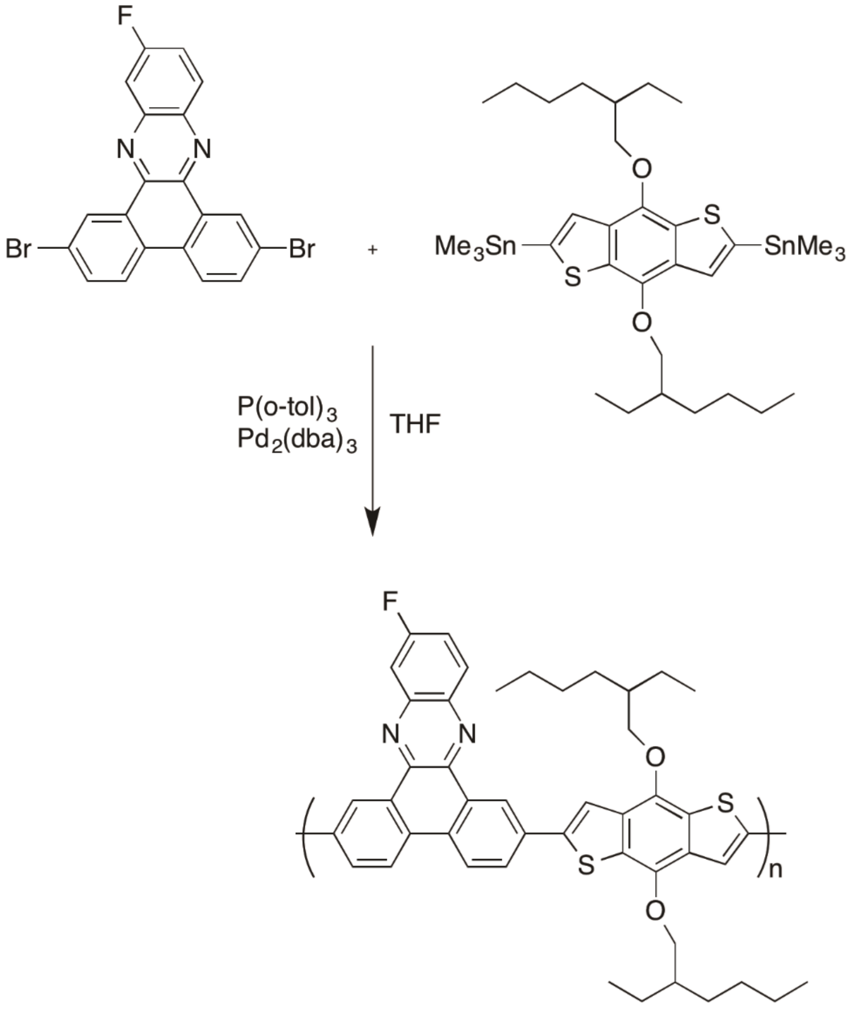

Figure 30. Synthesis of **PBDT-FBPz**

2,7-Dibromo-11-fluorodibenzo[a,c]phenazine (100 mg, 0.210 mmol) and 2,6-bis(trimethylstannyl)-4,8-bis(2-ethylhexyloxy)benzo[1,2-b:4,5-b0]dithiophene (178 mg, 0.230 mmol) were dissolved in dry THF and the solution was degassed with argon for 30 minutes after which tris(dibenzylideneacetone) dipalladium(0) (10 mg, 1.1

μmol) and tri(o-tolyl)-phosphine (26.6 mg, 84.0 μmol) were added and the reaction temperature was heated to reflux for 24 hours. 2-Bromothiophene (71.4 mg, 0.430 mmol) was added as first end-capper with a small amount catalyst after 24 hours. Afterwards, Tributyl(thiophen-2-yl)stannane (326 mg, 0.870 mmol) was added as second end-capper with a small amount catalyst after 30 hours. The solvent of polymerization was removed under reduced pressure and the polymer was precipitated in methanol. To obtain pure polymer, Soxhlet extraction was carried out with acetone and hexane. The polymer was then dissolved in chloroform and re-precipitated in methanol. When **PBDT-FBPz** dried under vacuum, it was obtained as an orange solid with a yield of 50 % (90 mg). GPC: number average molecular weight (Mn): 9400, weight average molecular weight (Mw): 13200, polydispersity index (PDI): 1.4.

2.4.2. Synthesis of P2 (PBDT-TFBPz)

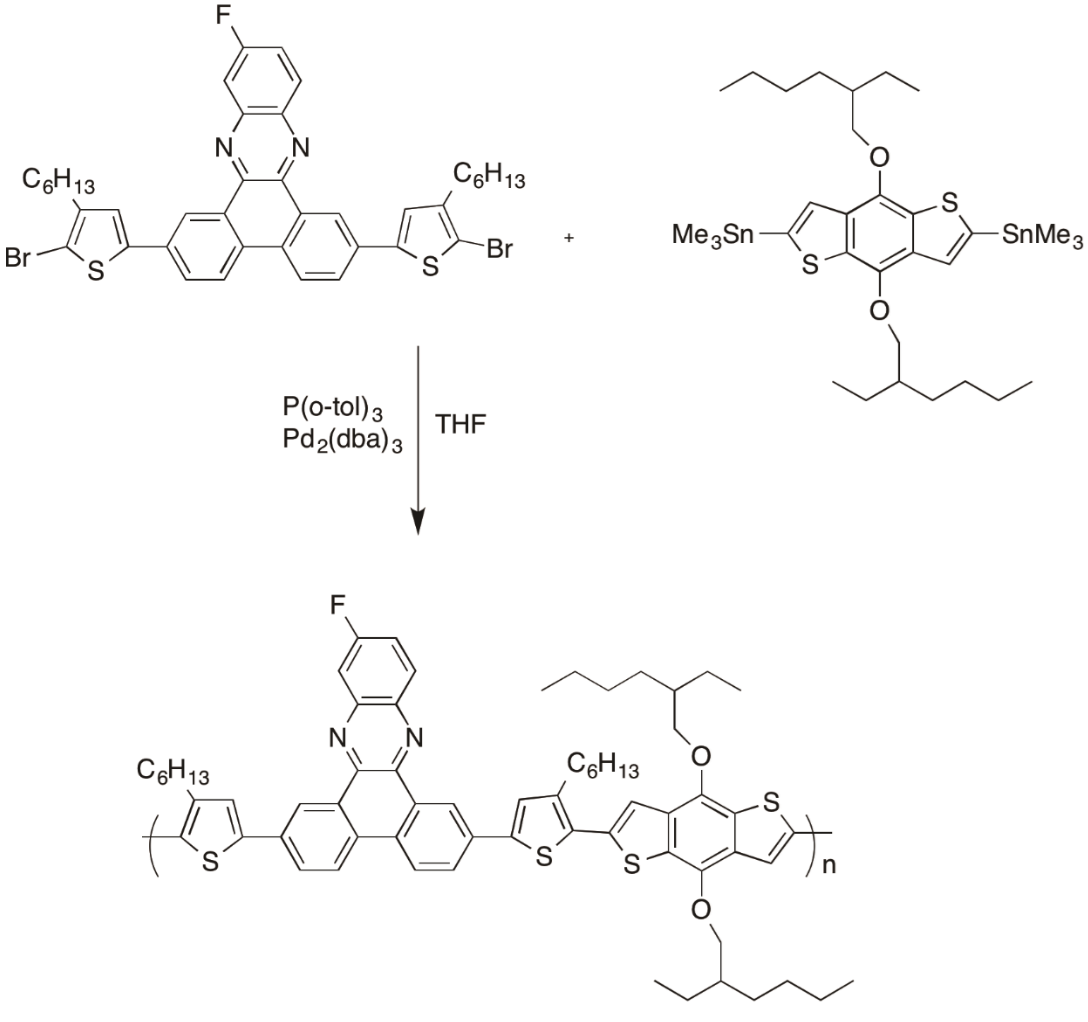

Figure 31. Synthesis of **PBDT-TFBPz**

The same procedure with synthesis of **PBDT-FBPz** was applied to synthesize the **PBDT-TFBPz**. 2,7-Bis(5-bromo-4-hexylthiophen-2-yl)-11-fluorodibenzo[a,c]phenazine (250 mg, 0.31 mmol) and 2,6-bis(trimethylstannyl)-4,8-bis(2-ethylhexyloxy)benzo[1,2-b:4,5-b0]dithiophene (247 mg, 0.320 mmol) were dissolved in anhydrous THF and the mixture was purged with argon to remove oxygen in medium. Tris(dibenzylideneacetone) dipalladium(0) (14.2 mg, 1.6 μmol) and tri(o-tolyl)-phosphine (37.8 mg, 12.4 μmol) were added to reaction mixture and the mixture was heated to 78˚C for 24 hours. 2-Bromothiophene (100 mg, 0.620 mmol) and tributyl(thiophen-2-yl)stannane (462 mg, 1.240 mmol) were added to reaction medium as the end-cappers. The solvent was removed under reduced pressure and polymer was then precipitated in methanol and extracted sequentially with acetone, and hexane. Afterwards the polymer was precipitated in the ethanol to afford a dark-orange solid with a yield of 5% (7 mg). GPC: number average molecular weight (Mn): 21700, molecular average molecular weight (Mw): 22500 polydispersity index (PDI): 1.1.

2.4.3. Synthesis of P3 (PSi-TFBPz)

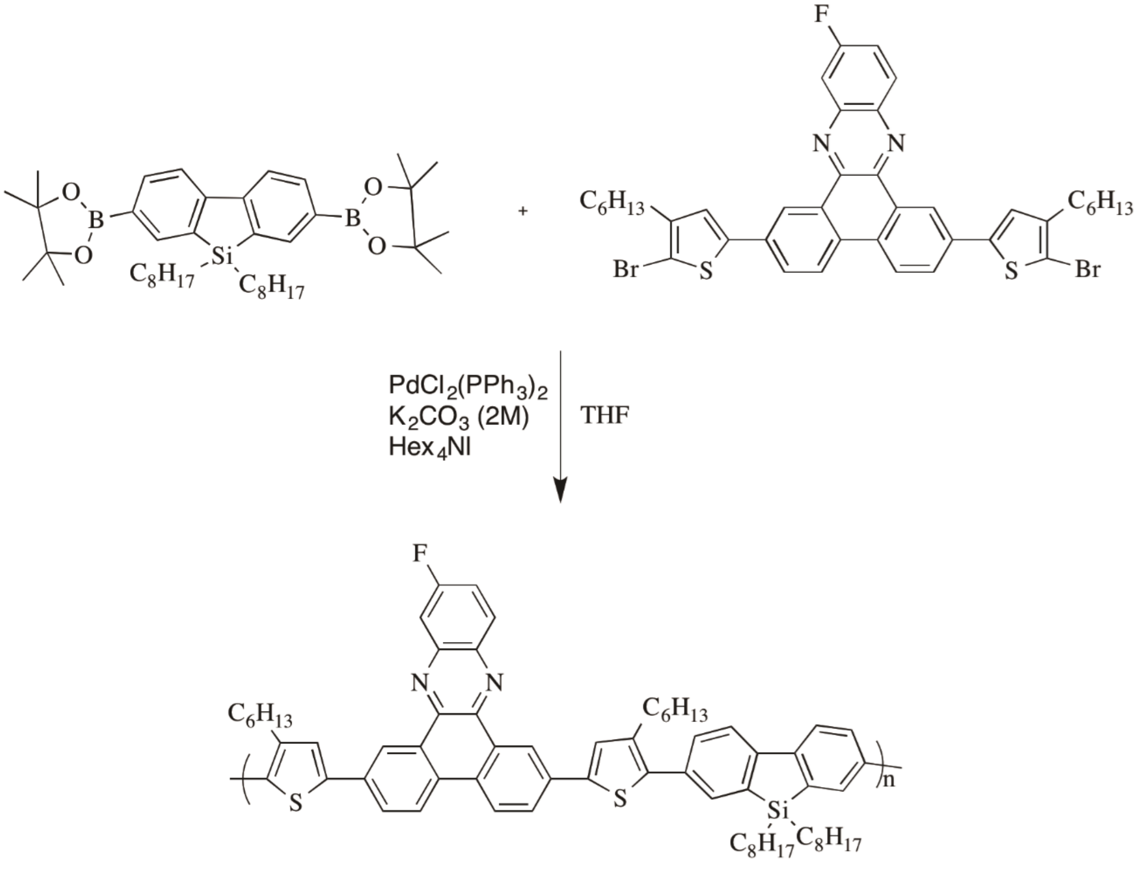

Figure 32. Synthesis of **PSi-TFBPz**

In a 100 mL two-neck round bottom flask, 2,7-bis(5-bromo-4-hexylthiophen-2-yl)-11-fluorodibenzo[a,c]phenazine (100 mg, 0.130 mmol), 9,9-Dioctyl-9*H*-9-silafluorene-2,7-bis(boronic acid pinacol ester) (92.2 mg, 0.140 mmol) and a catalytic amount of tetrahexyl ammonium iodide (25 mg) were added and the medium was purged with argon for 30 minutes. Then, K_2CO_3 solution (2M, 0.5 mL), tetrahydrofuran (THF) were then added to the reaction followed by argon purging for an additional 30 minutes. After that, bis(triphenylphosphine)palladium(II) dichloride (4.5 mg, 6.3 μmol) was added to the reaction mixture and the mixture was heated to 78 ˚C. The polymerization reaction was continued at this temperature under argon atmosphere for 24 hours. Bromobenzene (103 mg, 0.656 mmol) and extra catalyst (3.50 mg) were then added and the mixture was stirred for three hours, then phenyl boronic acid (160 mg, 1.31 mmol) was added and the mixture was stirred at 78˚C overnight. The polymer was precipitated in methanol. Afterwards, the polymer was filtered and extracted with acetone, and hexane to remove oligomers and small molecules in a Soxhlet extractor. The polymer was collected with chloroform and the solvent was evaporated. The residue was precipitated in methanol and a red solid polymer with a yield of 15% (35mg) was obtained. GPC: number average molecular weight (Mn): 7600, molecular average molecular weight (Mw): 20000, polydispersity index (PDI): 2.6.

2.5. Electrochemical studies of Homopolymers and Copolymers

A three-electrode cell was used with a potentiostat to determine the electrochemical properties of the conjugated polymers (Figure 33). In this system, a reference electrode (RE) was used to control the potential against the working electrode (WE). Platinum and ITO were used as the counter and working electrodes, respectively. The redox behavior of the conducting polymers was determined by using the cyclic voltammetry technique. The redox behavior of the conducting polymers was determined using the cyclic voltammetry technique. The reduction and oxidation tendencies of the conducting polymers were determined. In the end of this process, graphs of potential versus current were achieved to measure the LUMO and HOMO energy levels of conjugated polymers. These levels were used to determine the electronic band gap (E_g^{el}) of polymers. For electrochemical studies polymers were dissolved in chloroform and were sprayed onto ITO coated substrate with a omni spray gun. Afterwards, the ITO is dipped in the $TBAPF_6$/ACN/DCM (tetrabutylammonium hexafluorophosphate/acetonitrile/dichloromethane) electrolyte-solvents couple.

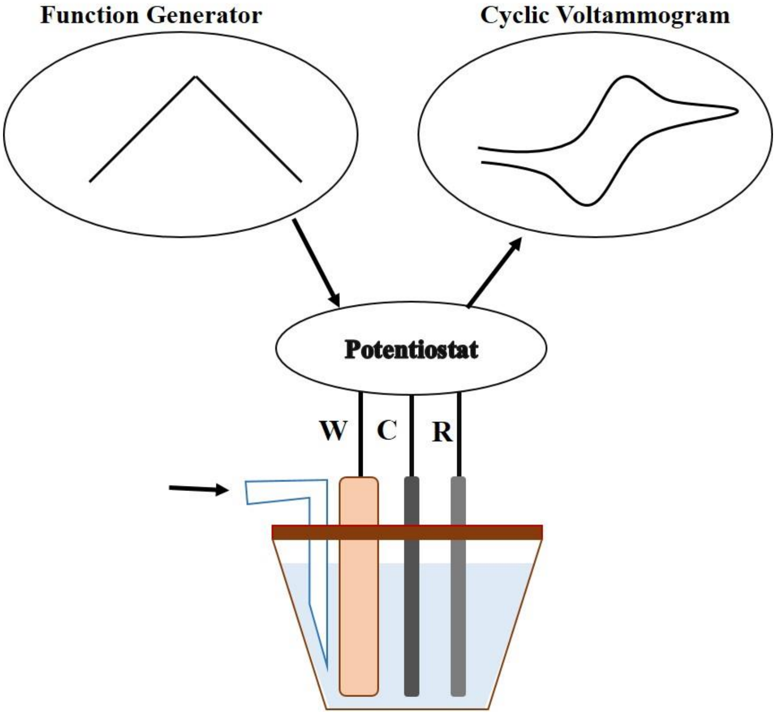

Figure 33. Schematic representation of cyclic voltammetry (CV)

2.6. Spectroelectrochemical and Kinetic Studies of Homopolymers and Copolymers

In spectroelectrochemical studies, a three-electrode system was used to analyze absorption spectra of conjugated polymers. The neutral states of polymers and also the polaron and bipolaron bands were determined with spectroelectrochemical studies.

The optical band gaps (E_g^{op}) of conducting polymers were calculated using the λ_{onset} of neutral state of the polymer.

The switching time and optical transmittance are important parameters for electrochromic applications as mentioned in introduction part. Optical contrast and switching time of the conjugated polymers were determined both in their neutral and doped (polaron and bipolaron) states by the square wave potential as a function of time. Optical contrast values were calculated from the difference of percent transmittance values between neutral and oxidized states and switching time could be defined as the time required for one full switch between two extreme states.

For further characterizations, colorimetry studies were achieved according to the CIE (Commission Internationale de l’Eclairage) standards. In CIE coordinates, L symbolizes the luminescence (brightness) of a color, a symbolizes the color between red/magenta and green, b symbolizes the color between yellow and blue. A Konica Minolta CS-100 was used to measure these coordinates.

2.7. Organic Solar Cell Applications of Copolymers

The traditional bulk heterojunction type was constructed to investigate photovoltaic properties of copolymers. ITO was used as the anode after chemical etching with acidic solution (HCl, 49% and HNO_3, 1%) at 100ºC for 3.5 minutes. Then, etched ITO was dipped in K_2CO_3 solution for neutralization for one minute. ITO was washed by toluene, a detergent solution, acetone and isopropyl alcohol in an ultrasonic bath for 15 minutes for each step. The detergent was purchased from Hellmanex which is special for cleaning optical materials. The cleaning of ITO was finished with nitrogen gun to remove alcohol from ITO surface. The plasma etching was used for chemical cleaning and reducing the surface tension of ITO [66]. At the end of the cleaning process, the PEDOT:PSS (Heraeus Clevios P VP AI 4083) was coated by using spin coater with 3000 rpm for one minute. PEDOT:PSS was filtered with 0.45 μm polyvinylidene fluoride (PVDF) membranes. The PEDOT:PSS coated substrates were dried at 130ºC for 15 minutes to remove water from surface on a hot plate. The thickness of PEDOT:PSS was around 40 nm. The substrates were transposed to a N_2-filled glove box after drying. All polymer:PCBM71 mixtures were dissolved in 1,2-dichlorobenzene (DCB) and filtered with 0.22 μm polytetrafluorethylene (PTFE) membranes to remove insoluble remnants. In the glove box, the active layer of OPVs were coated on the PEDOT:PSS layer at different ratios. LiF (0.6 nm) and Al (100 nm) were evaporated under $1x10^{-6}$mbar pressure with thermal deposition, respectively on the photoactive layers with an average deposition rate of 0.1 A/s. The effective layer of photovoltaic device area was 0.06 cm^2. The current density voltage (J-V) characteristics were measured using a Keithley 2400 source meter under AM 1.5 G illumination at 100 mW/cm^2 using a Xe lamp-based Newport solar simulator. Incident-photon-to-current efficiency (IPCE) of solar cells was determined using an Oriel Quantum Efficiency Measurement Kit. A calibrated monosilicon diode exhibiting a response at 300-900 nm was used as the reference.

CHAPTER 3

3. RESULTS and DISCUSSION

3.1. Photophysical and Photovoltaic Properties of 11-Fluorodibenzo[a,c]phenazine Bearing Donor-Acceptor Type Homopolymers and Copolymers

3.1.1. Electrochemical Properties of Homopolymers

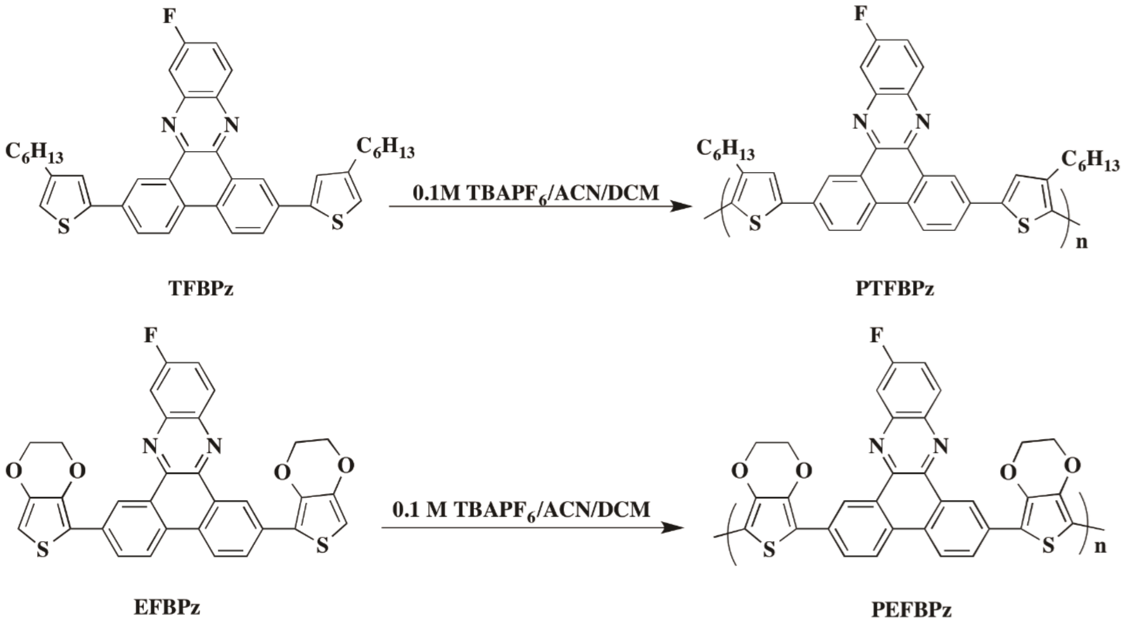

Figure 34. Electropolymerization conditions of **PTFBPz** and **PEFBPz**

Cyclic voltammetry is a versatile instrument and used to define oxidation and redox behaviors and HOMO and LUMO energy levels of the π-conjugated polymers and their band gap energies. All electrochemical polymerization reactions were examined in acetonitrile(ACN)/ dichloromethane (DCM)/ (50/50, v/v) solution containing 0.1 M tetrabutylammonium hexafluorophosphate ($TBAPF_6$) as the supporting electrolyte with 0.01 M monomer at a scan rate of 100 mV/s (Figure 34). The solvent system was determined as a mixture of ACN and DCM (50/50, v/v) since monomers had poor solubility in ACN. For TFBPz and EFBPz oxidation peaks were observed at 1.27 V and 0.94 V, respectively. Cyclic Voltammetry (CV) was used to investigate the polymers' p-doping and n-doping characteristics to determine highest occupied molecular orbital (HOMO) and lowest unoccupied molecular orbital (LUMO) energy levels from reduction and oxidation onset potentials using equations;

$$\mathrm{HOMO} = -\,(4.75 + E_{ox}^{onset}) \qquad (3.1)$$

$$\mathrm{LUMO} = -\,(4.75 + E_{red}^{onset})$$

$$E_g^{el} = \mathrm{HOMO} - \mathrm{LUMO}$$

In a monomer free solution, polymers revealed both p-dopable and n-dopable ability (Figure 35). PTFBPz has a redox couple at 1.20 V and 0.98 V representing p-doping and p-dedoping processes. A reversible redox couple for PTFBPz was determined at -1.43 V and -1.07 V for n-doping and n-dedoping processes. PEFBPz showed redox potentials at 0.72 V and 0.68 V for p-type doping/dedoping processes. The reversible redox couple for n-type doping/dedoping was determined at -1.55 V and -1.32 V (Figure 34). The HOMO energy levels were determined as -5.78 eV and -4.93 eV, the LUMO energy levels were -3.95 eV and -3.92 eV for PTFBPz and PEFBPz, respectively (Table 1). Electronic band gaps of homopolymers were 1.83 eV for PTFBPz and 1.01 eV for PEFBPz. To obtain lower both HOMO and LUMO energy levels of the conjugated polymers, fluorine atom was chosen as substituent on the polymer backbone [117]. Recently, Unver *et al.* reported electrochromic properties of an unsubstituted dibenzo[a,c]phenazine bearing conjugated polymer, which had same donor unit in the polymer backbone [116]. Herein, the fluorine atom was selected as the substituent on acceptor unit. The HOMO and LUMO energy level of polymers were found to be lower than those reported in earlier studies (Table 1).

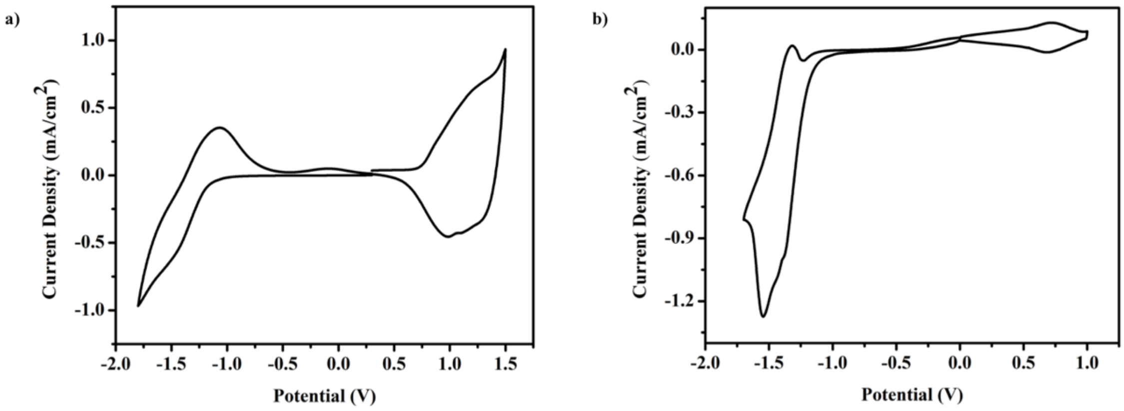

Figure 35. Single scan cyclic voltammograms of a) **PTFBPz** and b) **PEFBPz** in 0.1M TBAPF$_6$/ACN electrolyte/solvent couple on ITO

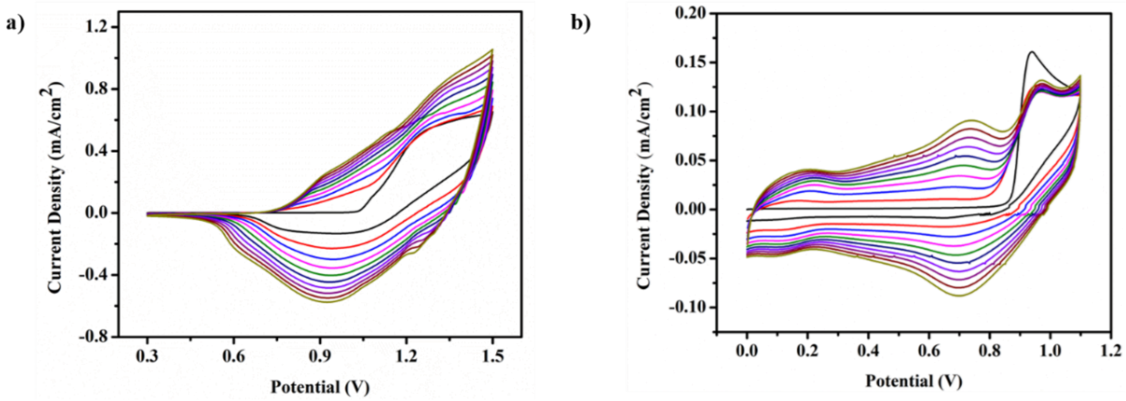

Figure 36. Electropolymerization of a) **PTFBPz** and b) **PEFBPz** in 0.1M TBAPF$_6$/ACN/ DCM electrolyte/solvent couple on ITO at a scan rate of 100 mV/s

Table 1. Electronic properties of homopolymers

Homopolymers	**E_m^{ox}**	**$E_{p\text{-}doping}^{p}$ (V)**	**$E_{p\text{-}dedoping}^{p}$ (V)**	**$E_{n\text{-}doping}^{p}$ (V)**	**$E_{n\text{-}dedoping}^{p}$ (V)**	**HOMO (eV)**	**LUMO (eV)**	**E_g^{el} (eV)**	**λ_{max} (nm)**	**E_g^{op} (eV)**
PTFBPz	1.27	1.20	0.98	-1.43	-1.07	-5.78	-3.95	1.83	353/370	2.40
PEFBPz	0.94	0.72	0.68	-1.55	-1.32	-4.93	-3.92	1.01	443	1.86

3.1.2. Scan Rate Studies

The scan rate studies give information about the electrochemical processes whether doping/dedoping processes are diffusion controlled or not. The linear association between current density and scan rate demonstrated that the polymers films were well adhered and doping/dedoping processes are non-diffusion controlled (Figure 37) and (Figure 38).

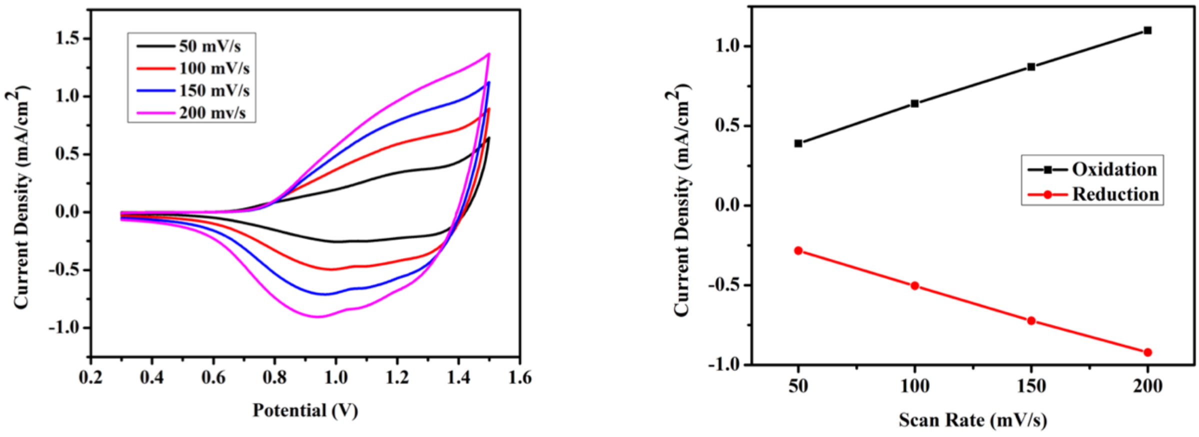

Figure 37. Scan rate study of PTFBPz

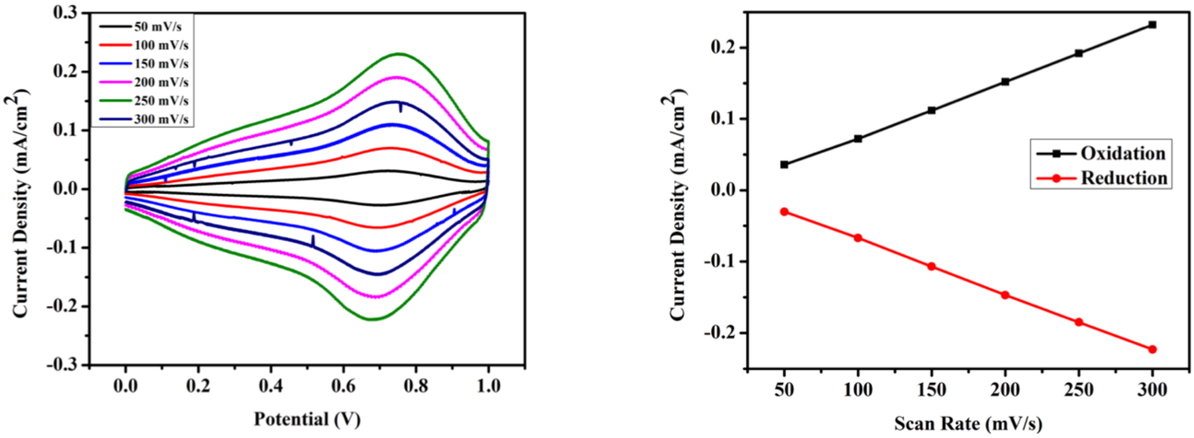

Figure 38. Scan rate study of PEFBPz

3.1.3. Spectroelectrochemical Properties of Homopolymers

The spectroelectrochemical properties of homopolymers were carried out to investigate the electronic structure and optical changes upon doping processes. The homopolymers films were deposited on ITO-coated glass slides and the optical changes were examined in a monomer-free 0.1 M TBAPF$_6$/ACN solution via applying increased potential from 0.0 V to +1.5 V for PTFBPz, 0.0 V to +1.0 V for PEFBPz. Spectroelectrochemistry and related color changes for PTFBPz and PEFBPz at their reduced and oxidized states are illustrated in Figure 39.

Neutral state absorption maxima (λ_{max}) of PTFBPz and PEFBPz were recorded at 353/370 nm and 443 nm, respectively. Their optical band gaps were calculated from onset of λ_{max} as 2.20 eV for PTFBPz and 1.86 eV for PEFBPz. In neutral state, PTFBPz has yellow color (L: 79, a: -9 b: 42), PEFBPz has light purple color (L: 76, a: 1, b: 4). The colors of polymers changed upon applied potential; PTFBPz was observed as green (L: 60, a: -20, b: 3) at 1.15 V, turquoise (L: 32 a: -12, b: -6) at 1.25 V and blue (L: 47, a: -10, b: -12) at 1.45 V. The colors of PEFBPz were observed as orange (L: 78, a: -3, b: 4) at -1.6 V and blue (L: 76, a: -2, b: -6) at 0.75 V (Table 2).

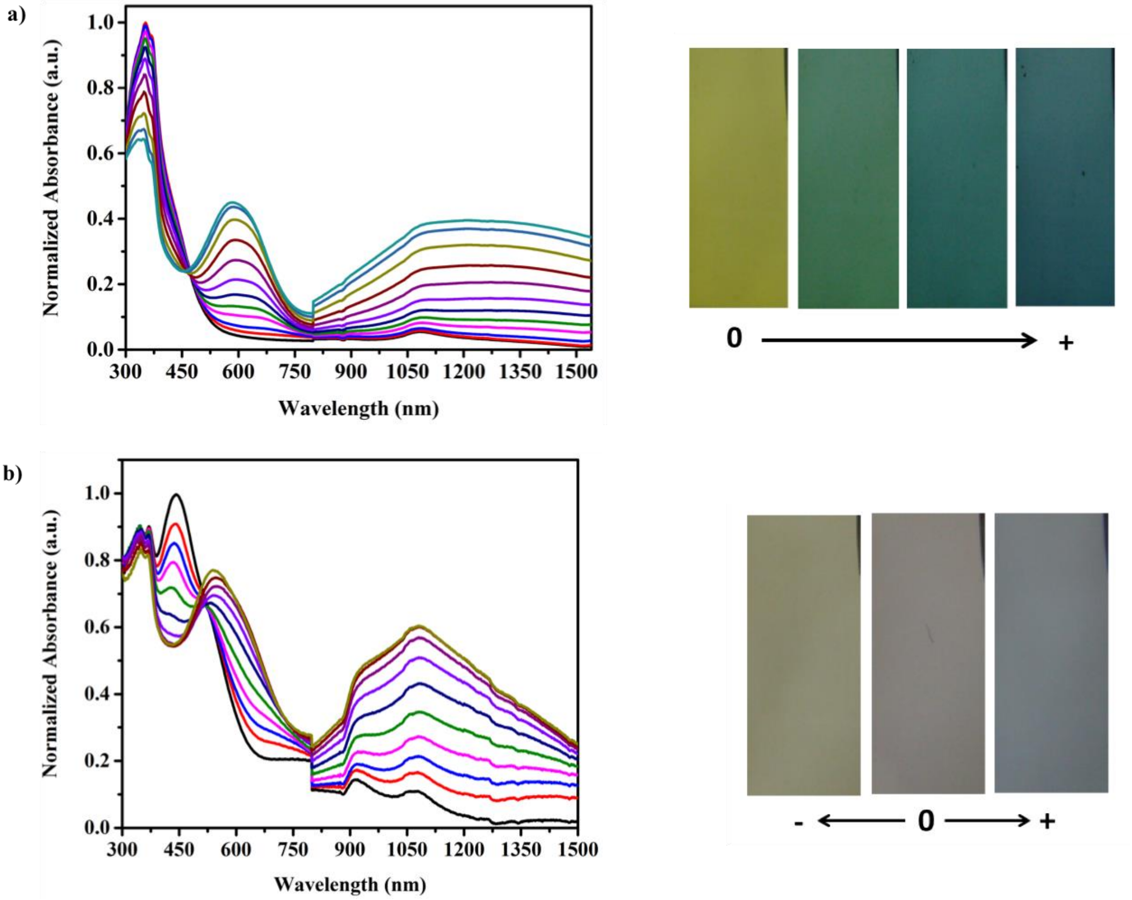

Figure 39. Spectroelectrochemistry and colors of (a) **PTFBPz** and (b) **PEFBPz** films on an ITO-coated glass slide in monomer-free, 0.1 M $TBAPF_6$/ACN electrolyte-solvent couple upon oxidative doping at potentials between 0.0/+1.50 V, 0.0 /+1.0 V, respectively

Table 2. Colorimetry results of the homopolymers

Homopolymer	Applied potential (V)	L	a	b
PTFBPz	0.00	79	-9	42
	1.15	60	-20	3
	1.25	32	-12	-6
	1.45	47	-10	-12
PEFBPz	-1.60	78	-3	16
	0.00	76	1	4
	0.75	76	-2	-6

3.1.3. Electrochromic Switching Studies of Homopolymers

The electrochromic switching characters of the homopolymer films were determined in the NIR and visible regions. Human eye is sensitive up to 95% of the full contrast. In this manner, the time needed for copolymers to switch from their neutral states to fully oxidized states, i.e. switching time, was defined at 95% of contrast value. During this experiment, the potential was set to an initial potential for 5 seconds and changed to a different one for 5 seconds before being switched back to the initial potential. The percent transmittance (%T) was detected with a UV-Vis-NIR spectrophotometer at their pre-determined maximum absorption wavelengths (Figure 40). The results of kinetic studies of homopolymers are summarized in Table 3, optical contrasts were calculated as 48% at 600 nm and 85% at 1100 nm while switching times were detected as 1.6 and 2.9 seconds for PTFBPz, respectively. Optical contrasts of PEFBPz was detected as 24 % at 1120 nm with a fast switching time of 0.5 seconds.

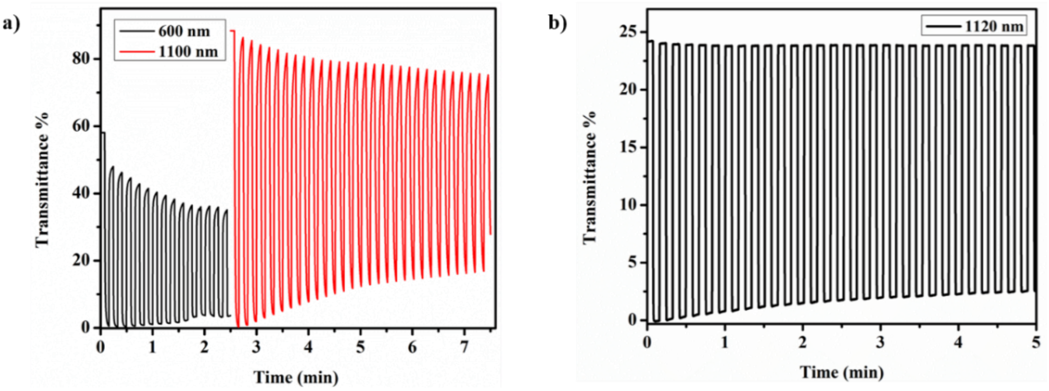

Figure 40. Percent transmittance changes and switching times at the maximum wavelengths of a) **PTFBPz** and b) **PEFBPz** in 0.1 M TBAPF$_6$/ACN solution system

Table 3. Optical contrast ratios and switching times of the **PTFBPz** and **PEFBPz**

Homopolymers	Wavelength (nm)	Optical Contrast (%)	Switching time (s)
PTFBPz	**600**	48	1.6
	1100	85	2.9
PEFBPz	**1120**	24	0.5

3.2. Electrochemical Properties of Copolymers

3.2.1. Electrochemical Properties of PBDT-FBPz

Redox potentials of PBDT-FBPz were observed at 0.95 V and 0.80 V as the p-doping and p-dedoping processes from cyclic voltammetry studies (Figure 41). The PBDT-FBPz showed only p-dopable characteristic, thus HOMO level of PBDT-FBPz was calculated from onset of the corresponding oxidation potential as -5.41 eV. The optical band gap was used to calculate the LUMO level of PBDT-FBPz as -3.07 eV. Neutral maximum absorption bands (λ_{max}) of PBDT-FBPz were at 380 and 395 nm and the optical band gap was calculated from onset of 395 nm as 2.34 eV.

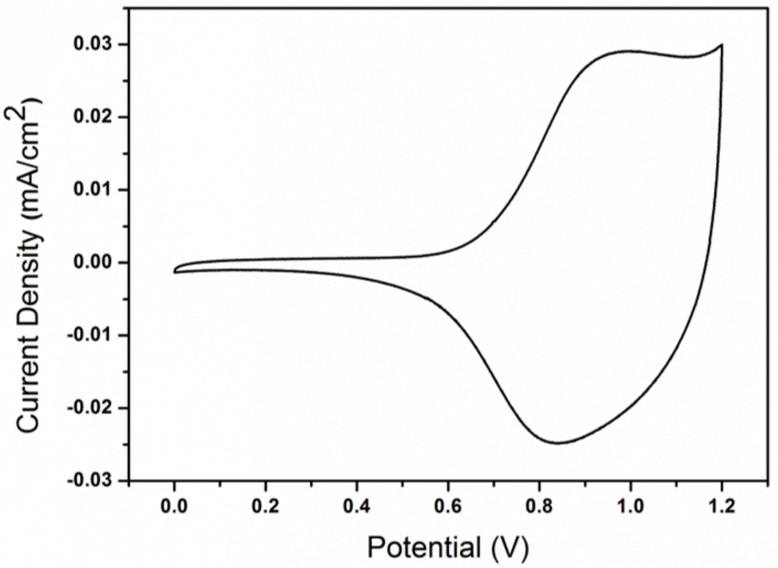

Figure 41. Single scan cyclic voltammogram of **PBDT-FBPz** on ITO between 0.0-1.20 V in 0.1 M $TBAPF_6$/ACN solution at a scan rate 100 mV/s

The scan rate dependence studies were carried out whether doping/dedoping processes are diffusion controlled or not. Since current and scan rate has a linear relation, these processess are found to be non-diffusion controlled (Figure 42).

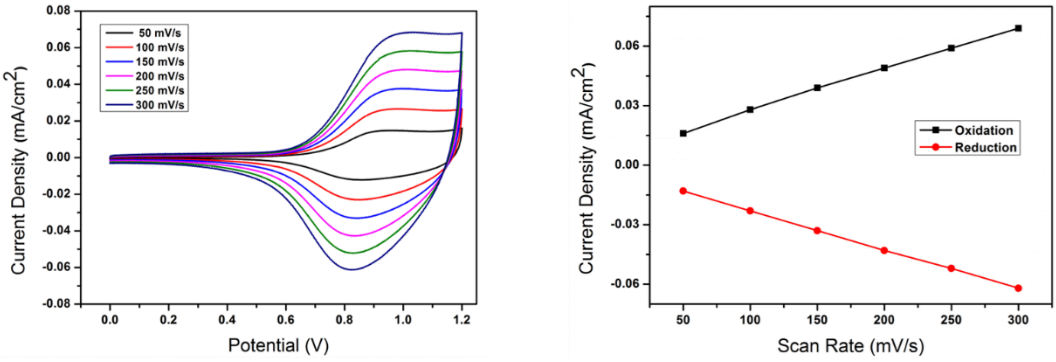

Figure 42. Cyclic voltammograms of **PBDT-FBPz** in 0.1 M TBAPF$_6$/ACN electrolyte/solvent couple at different scan rates

3.2.2. Electrochemical Properties of PBDT-TFBPz

PBDT-TFBPz revealed both p-type doping and n-type doping ability. Redox potentials of PBDT-TFBPz were determined at 1.04/1.23 V and 0.55/0.83 V in the p-doping and p-dedoping processes, respectively (Figure 43). PBDT-TFBPz showed a reversible redox couple at -1.46 V and -1.31 V in the n-doping and n-dedoping processes. The HOMO and the LUMO energy levels were calculated as -5.74 eV and -3.94 eV, respectively. The electronic band gap of PBDT-TFBPz was 1.80 eV.

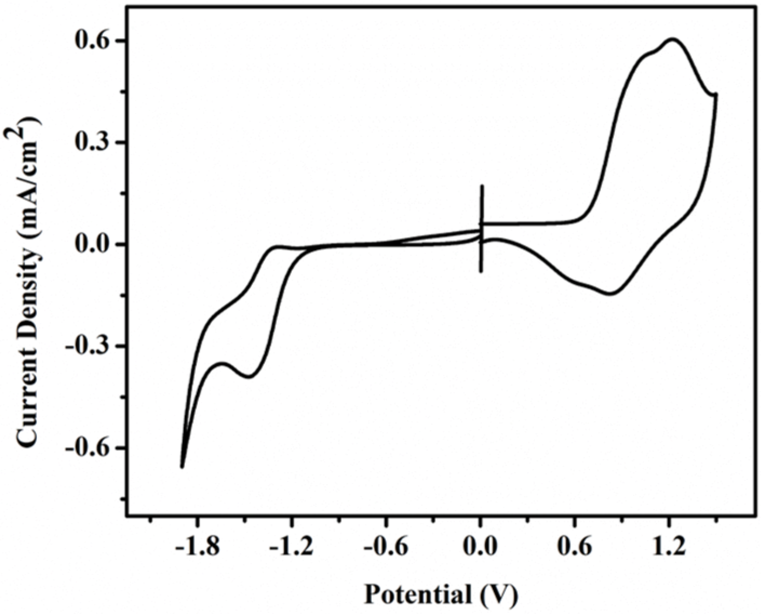

Figure 43. Single scan cyclic voltammogram of **PBDT-TFBPz** on ITO between 0.0-1.20 V in 0.1 M TBAPF$_6$/ACN solution at a scan rate 100 mV/s

3.2.3. Spectroelectrochemical and Kinetic Properties of PBDT-TFBPz

Spectroelectrochemical and kinetic properties of the PBDT-TFBPz were carried out in 0.1 M TBAPF$_6$/ACN electrolyte-solvent couple. Doping processes was studied to characterize optical changes via applying potentials ranging from 0.0 V to +1.2 V for polymer. Spectroelectrochemistry and related color changes of polymer at reduced and oxidized states are given in Figure 44. Compare to PBDT-FBPz, it has 3-hexylthiophene as the π–bridge enabling broad absorption spectra in UV-Vis range [118]. PBDT-TFBPz has an absorption maximum at 454 nm and the optical band gap was found from the onset of π-π* transition as 1.87 eV.

In neutral state, PBDT-TFBPz is orange (L: 71, a: 14, b: 28). The colors of polymer changed upon applied potential where PBDT-TFBPz was observed as green (L: 68, a: -6, b: 7) at -2.00 V, green (L: 68 a: -8, b: 11) at 1.10 V and gray (L: 67, a: -6, b: 6) at 1.40 V (Table 6).

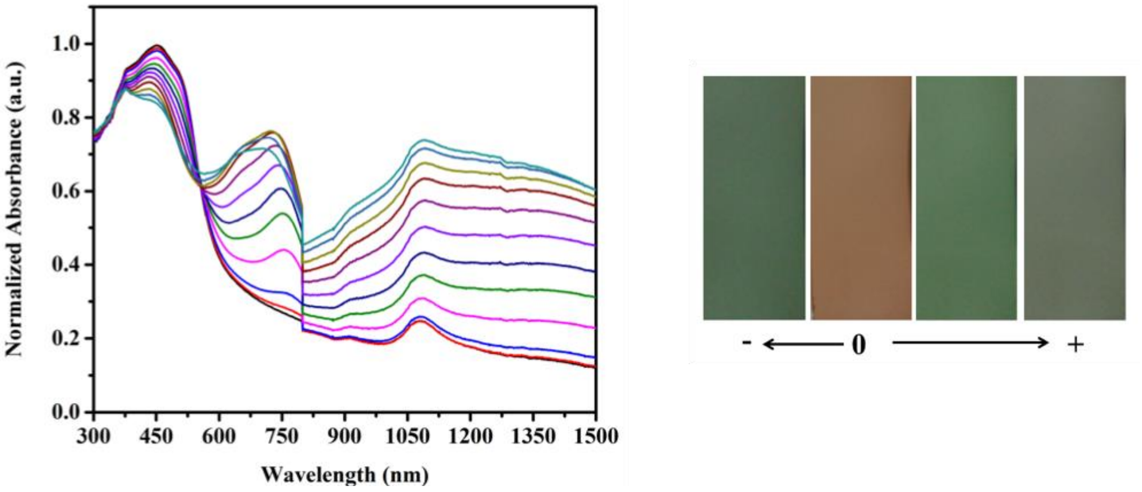

Figure 44. Change in the electronic absorption spectra at potentials between 0.0 and 1.2 V and colors of **PBDT-TFBPz** at reduced and oxidized states

The optical contrasts of the PBDT-TFBPz film was calculated to be 15% and 42% at 450 nm and 1075 nm respectively in chronoamperometry studies (Figure 45). The polymer has switching times of 2.4 seconds and 0.9 seconds at 450 nm and 1075 nm, respectively.

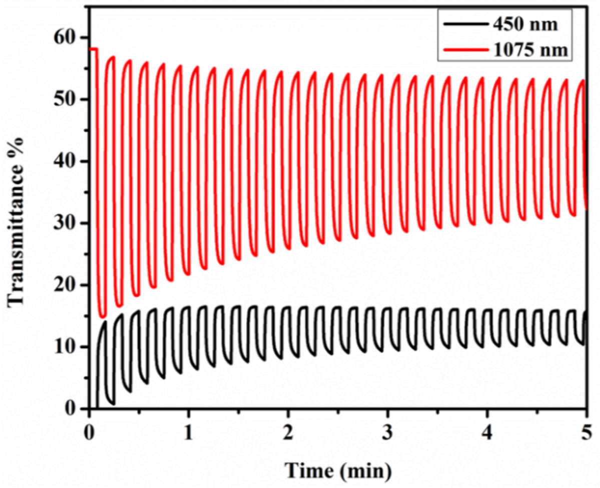

Figure 45. Electrochromic switching and percent transmittance changes of **PBDT-TFBPz** observed at 450 and 1075 nm in 0.1M TBAPF$_6$/ACN

3.2.4. Electrochemical Properties of PSi-TFBP

PSi-TFBPz showed only p-type doping ability and redox potentials were observed at 1.39 V and 0.86 V in the p-doping and p-dedoping processes, respectively (Figure 46). The HOMO and the LUMO energy levels were calculated as -5.84 eV and -3.19 eV for Psi-TFBPz. The electronic band gap could not be calculated because of only p-dobaple ability. To calculate the LUMO energy level of polymer, electronic band gap was assumed similar to optical band gap.

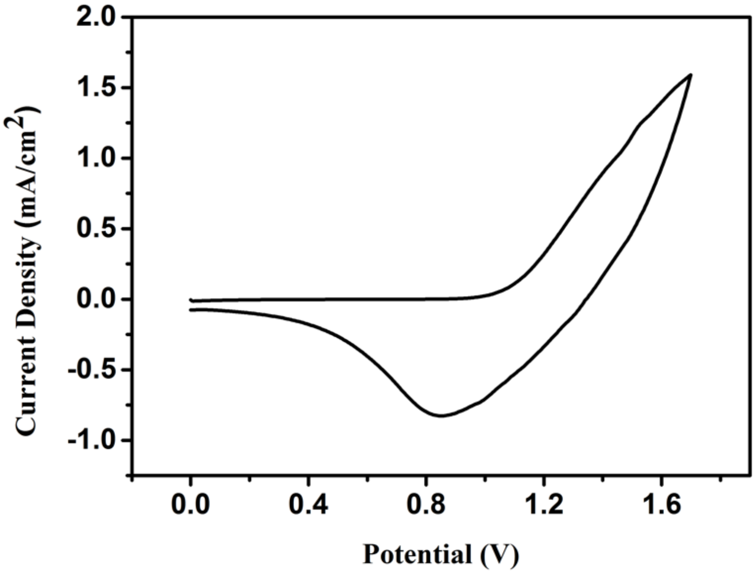

Figure 46. Single scan cyclic voltammogram of **PSi-TFBPz** on ITO between 0.0 and +1.7 V in 0.1 M TBAPF$_6$/ACN solution at a scan rate 100 mV/s

3.2.5. Spectroelectrochemical and Kinetic Properties of PSi-TFBPz

Spectroelectrochemical and kinetic properties of the PSi-TFBPz were carried out in 0.1 M TBAPF$_6$/ACN electrolyte-solvent couple. Optical changes were studied via applying potentials ranging from 0.0 V to +1.4 V for polymer. Figure 47 shows spectroelectrochemistry and related colors change of polymer at oxidized states. PBDT-TFBPz has an absorption maximum at 375 nm and the optical band gap was found from the onset of π-π* transition as 2.65 eV.

The optical contrasts of the PSi-TFBPz film was calculated to be 13%, 67% and 73% at 375 nm, 570 nm and 1710 nm respectively in chronoamperometry studies (Figure 47). The polymer has switching times of 3.9 s, 1.2 s and 1 s at 375 nm, 570 nm and 1710 nm, respectively (Table 5).

In neutral state, PSi-TFBPz was detected as yellow (L: 74, a: -8, b: 69). The colors of polymer changed when applied potential such as PSi-TFBPz was observed as dark green (L: 40, a: -6, b: 18) at 1.2 V, dark grey (L: 34 a: -4, b: -1) at 1.30 V and purple (L: 27, a: -7, b: -22) at 1.40 V (Table 6).

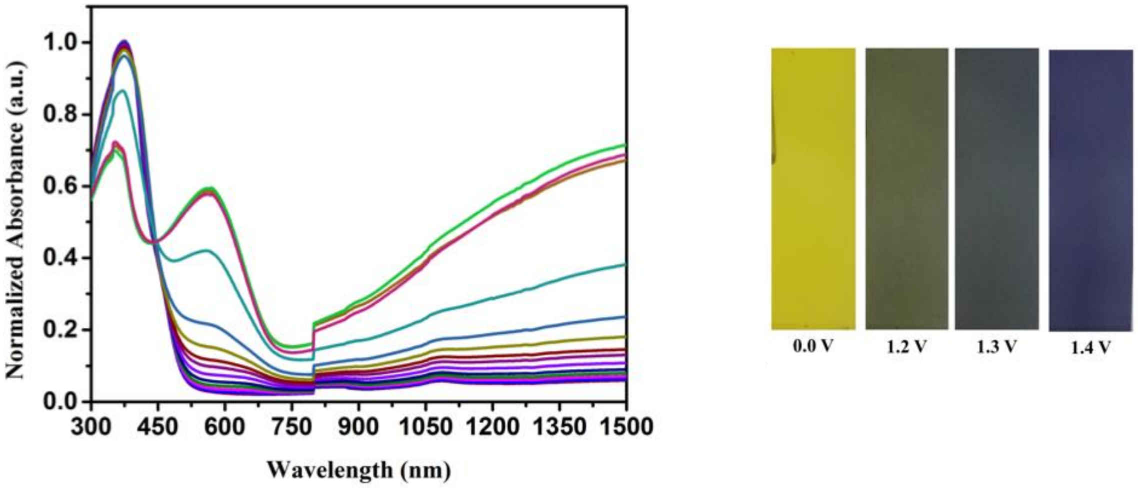

Figure 47. Change in the electronic absorption spectra at potentials between 0.0/1.4 V and colors of **PSi-TFBPz** at oxidized states

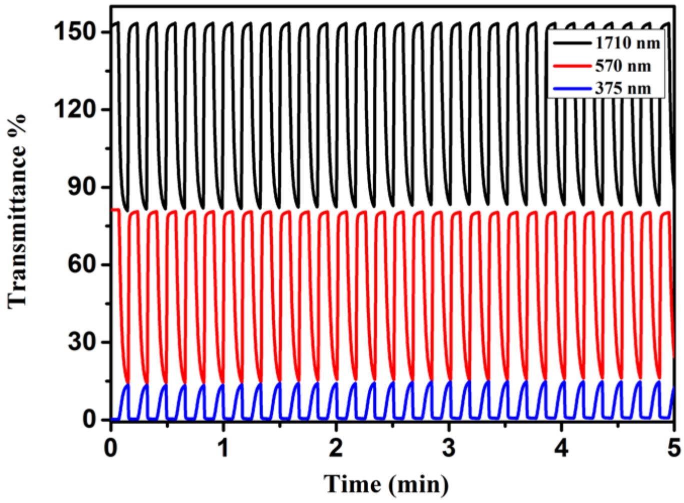

Figure 48. Electrochromic switching and percent transmittance changes of **PSi-TFBPz** observed at 375 nm, 570 nm and 1710 nm in 0.1M TBAPF$_6$/ACN

Table 4. Electronic properties of copolymers

Copolymers	**$E_{p\text{-doping}}^{p}$ (V)**	**$E_{p\text{-dedoping}}^{p}$ (V)**	**$E_{n\text{-doping}}^{p}$ (V)**	**$E_{n\text{-dedoping}}^{p}$ (V)**	**HOMO (eV)**	**LUMO (eV)**	**E_g^{el} (eV)**	**λ_{max} (nm)**	**E_g^{op} (eV)**
PBDT-FBPz	0.95	0.80	-	-	-5.41	-3.07	-	380/ 395	2.34
PBDT-TFBPz	1.04/ 1.23	0.55/ 0.83	-1.46	-1.31	-5.74	-3.94	1.80	454	1.87
PSi-TFBPz	1.39	0.86	-	-	-5.84	-3.19	-	375	2.65

Table 5. Optical contrast ratios and switching times of the copolymers at the determinate maximum wavelengths

Copolymers	**Wavelength (nm)**	**Optical Contrast (%)**	**Switching time (s)**
PBDT-TFBPz	450	15	2.4
	1075	42	0.9
PSi-TFBPz	375	13	3.9
	570	67	1.2
	1710	73	1

Table 6. Colorimetry results of the Copolymers

Copolymers	**Applied potential (V)**	**L**	**a**	**b**
PBDT-TFBPz	-2.00	68	-6	7
	0.00	71	14	28
	1.10	68	-8	11
	1.40	67	-6	6
PSi-FBPz	0.00	74	-8	69
	1.20	40	-6	18
	1.30	34	-4	-1
	1.40	27	7	-22

3.3. Photovoltaic Studies of Copolymers

Three new conducting copolymers were designed and synthesized as donor materials for organic solar cell applications. These conducting polymers have different donor units and a fluorine atom on the polymer backbone to decrease HOMO energy level of polymers for achieving high V_{oc}. Moreover, 3-hexylthiophene was used as a π-bridge and improved solubility of polymers. Normalized solution and thin film light absorbance of the polymer are demonstrated in Figure 49. PBDT-TFBPz showed more broad absorptions when compared with PBDT-DBPz. The added 3-hexylthiophene bridge leaded to obtained broader absorption. The thiophene bridges would increase the effective conjugation of the polymer chain that translate into broader and stronger absorption which contributed to the high performance of the polymer in OSCs [92][119].

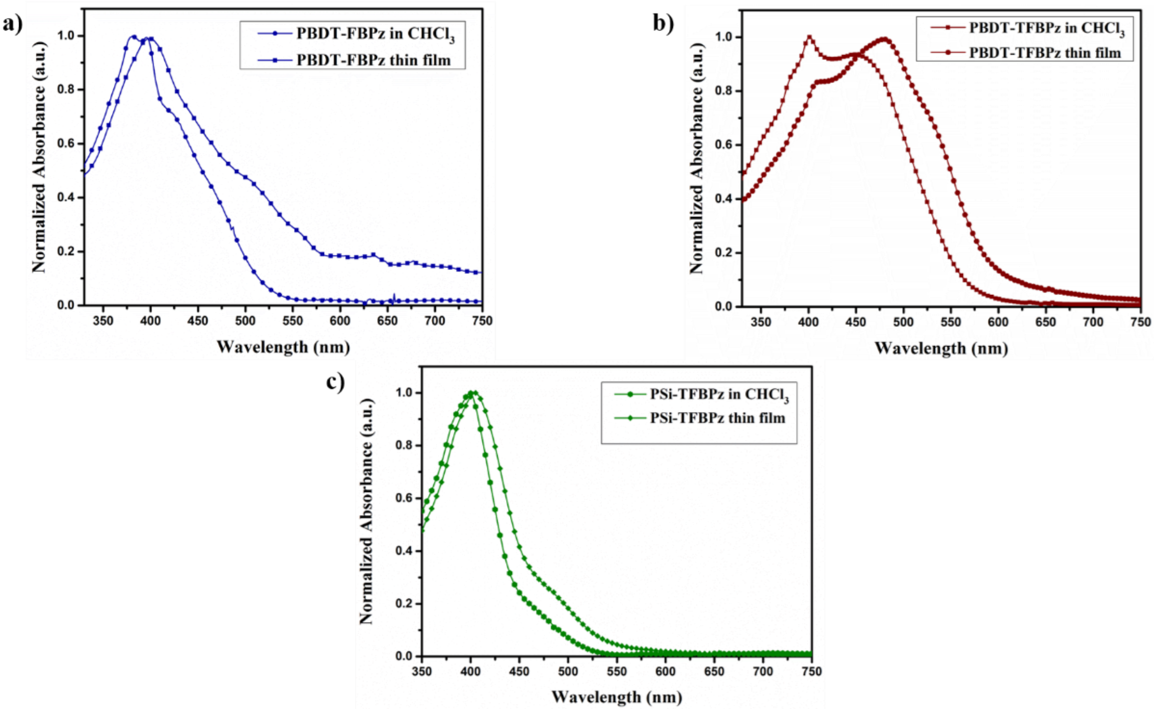

Figure 49. Normalized solution and thin film absorbance spectra of a)**PBDT-FBPz**, b)**PBDT-TFBPz**, and c)**PBDT-TFBPz**

The thin film absorbance spectra of polymer:PCBM71 ratios were determined from the maximum power conversion efficiencies of polymers as 1:1, 1:3 and 1:4 for PBDT-FBPz, PBDT-TFBPz and Psi-TFBPz, respectively and given in Figure 50. As expected, PBDT-TFBPz showed more broad absorption among three polymers. The thin film absorbance of polymer and PCBM mixtures showed additional absorbance peaks since PCBM and polymers were formed intermolecular charge transfer (ICT).

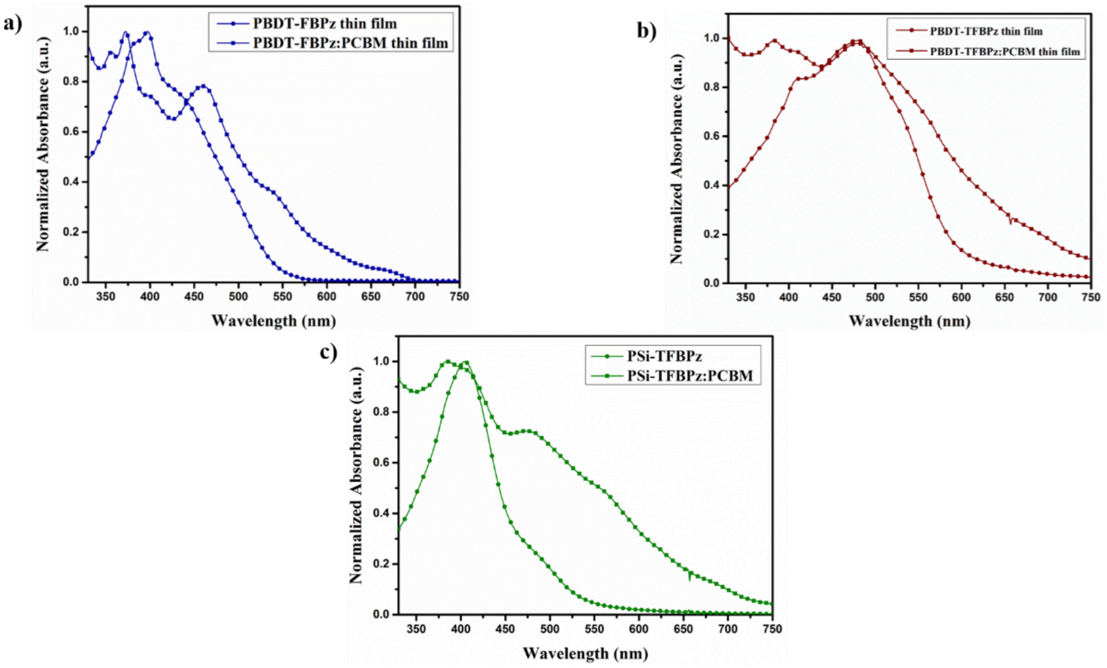

Figure 50. Normalized thin film and solution absorbance spectra of a)**PBDT-FBPz:PCBM71** (1:1), b)**PBDT-TFBPz:PCBM71** (1:2), and c)**PBDT-TFBPz:PCBM71** (1:4)

After introducing thiophene bridges in PBDT-TFBPz, its LUMO energy level decreased to -3.94 and its HOMO energy level decreased to -5.74 eV as shown in Figure 51. The increased conjugation on polymer backbone from the thiophene rings is usually expected to give a higher HOMO energy through improved delocalization of the D–A HOMO wave function. As a result of these substitutions, coplanarity can be increased along the conjugated polymer backbone, thus the electronic band gap (E_g^{ec}) of PBDT-TFBPz was observed lower than that of PBDT-FBPz [120].

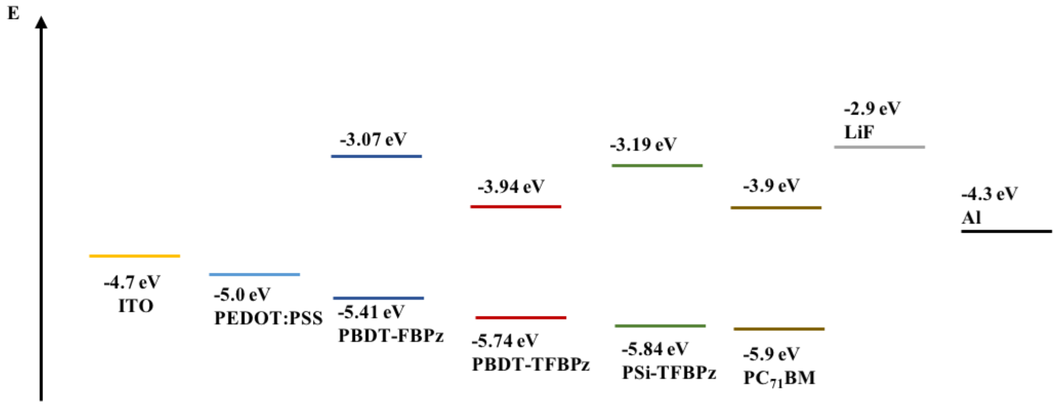

Figure 51. Energy level diagrams of copolymers and OPV materials

The current density-voltage characteristics were shown in Figure 52. During photovoltaic device optimization studies, the polymer and PCBM blend ratios were changed. Additionally, organic active layers were coated at different speeds. The highest PCE was found as 1.53 % under AM 1.5 G illumination at 100 mW/cm^2 for PBDT-TFBPz. Also, the highest PCE was found as 1.12 % and 0.58 % for PBDT-FBPz and PSi-TFBPz. The PSi-FBPz showed deepest HOMO energy level among three polymers, thus the open circuit voltage value was observed as 0.82 V since V_{oc} is dependent on the HOMO level of donor unit [62]. The results of organic photovoltaic devices were summarized in Table 7.

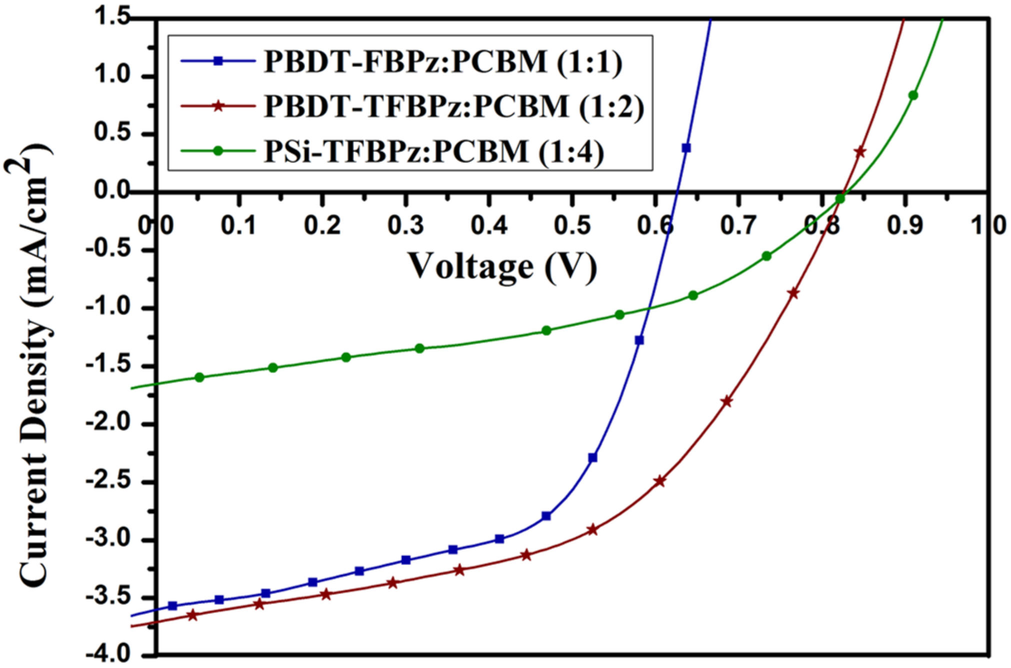

Figure 52. Current density - voltage curves of the optimized a)**PBDT-FBPz:PCBM71**, b)**PBDT-TFBPz:PCBM71**, and c)**PBDT-TFBPz:PCBM71** devices under AM 1.5 G illumination at 100 mW/cm^2

The ratios of number of charges collected by electrodes to the number of incident photons were determined by using IPCE method. The ratio of polymer and PCBM were prepared as 1:1, 1:3 and 1:4 for PBDT-FBPz, PBDT-TFBPz and PSi-TFBPz, respectively. The maximum IPCE was measured as 00% at 00 nm, 00% at 00 nm, and 00% at 00nm for PBDT-FBPz, PBDT-TFBPz and PSi-TFBPz in the range of 330-750 nm by using monochromic light. Consequently, the IPCE absorption spectrum was consistent with UV-Vis absorption spectrums of polymer:PCBM blends (Figure 53).

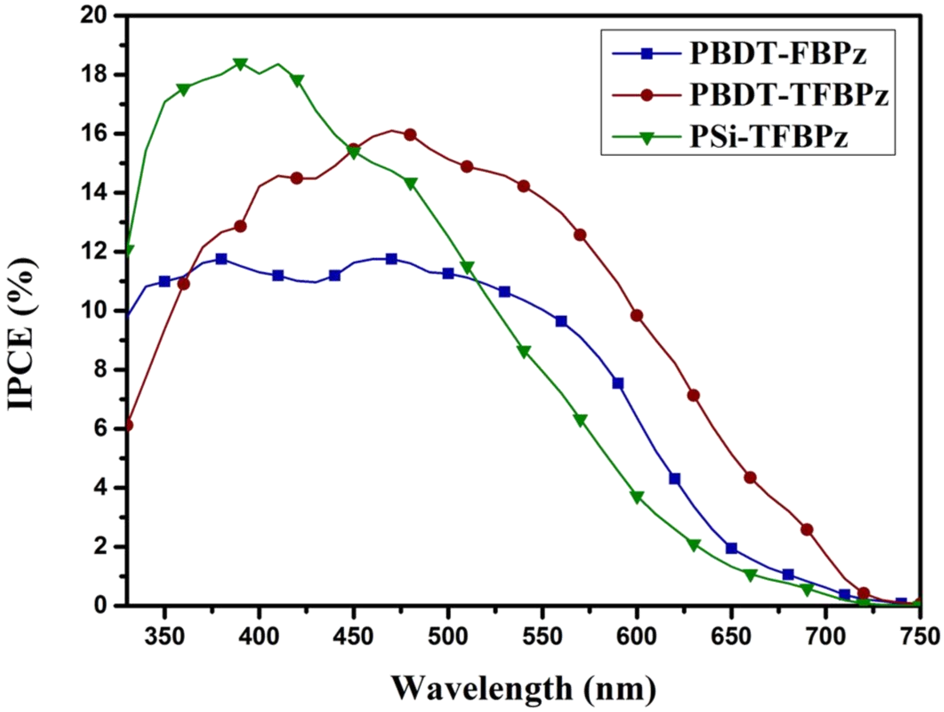

Figure 53. IPCE curves of the organic photovoltaic devices based on a)**PBDT-FBPz:PCBM71** (1:1), b)**PBDT-TFBPz:PCBM71** (1:2), and c)**PBDT-TFBPz:PCBM71** (1:4)

Table 7. Summary of the organic photovoltaic devices parameters

Polymer	**Polymer: PCBM71 ratio**	**V_{oc} (V)**	**J_{sc} (mA/cm^2)**	**V_{max} (V)**	**J_{max} (mA/cm^2)**	**FF (%)**	**η (%)**	**Polymer (rpm)**
PBDT-FBPz	1:1	0.63	3.13	0.48	2.38	57	**1.12**	500
PBDT-FBPz	1:1	0.66	1.43	0.51	1.09	58	0.54	750
PBDT-FBPz	1:2	0.65	2.37	0.48	1.81	56	0.86	750
PBDT-FBPz	1:2	0.67	2.47	0.56	1.67	56	0.92	500
PBDT-FBPz	1:3	0.67	2.38	0.52	1.75	57	0.90	750
PBDT-FBPz	1:3	0.68	2.27	0.53	1.69	58	0.89	500
PBDT-FBPz	1:1	0.67	1.87	0.53	1.40	59	0.73	750
PBDT-FBPz	1:1	0.67	1.92	0.51	1.44	57	0.73	1000
PBDT-TFBPz	1:2	0.73	2.40	0.50	1.64	46	0.80	300
PBDT-TFBPz	1:3	0.81	3.71	0.57	2.69	51	**1.53**	300
PBDT-TFBPz	1:4	0.61	2.08	0.38	1.41	42	0.51	300
PSi-TFBPz	1:2	0.83	1.84	0.54	1.03	36	0.54	300
PSi-TFBPz	1:3	0.83	1.45	0.55	0.85	38	0.45	300
PSi-TFBPz	1:4	0.82	1.65	0.61	0.96	43	**0.58**	500

CHAPTER 4

CONCLUSIONS

Two newly fluorinated dibenzo[a,c]phenazine (DBP) based monomers were synthesized by Stille coupling and characterized by NMR spectroscopy. These monomers included 3-hexylthiophene and 3,4-ethylenedioxythiophene (EDOT) as the donor units. Homopolymers were obtained with electropolymerization method on transparent ITO coated glasses. The optoelectronic properties of homopolymers were determined with cyclic voltammetry, kinetic studies and spectroelectrochemistry. In the neutral state, the color of 3-hexylthiophene containing homopolymers (PTFBPz) was observed as yellow and for 3,4-ethylenedioxythiophene containing homopolymers observed as light purple. 3,4-Ethylenedioxythiophene contained homopolymers showed lower oxidation potential (0.72 V) than other homopolymers. EDOT is an electron rich moiety it leads to decrease oxidation potential of monomer and enhance absorption properties. The band gaps of the polymers were calculated from π-π^* transitions using $E=h\nu$ equation as 2.40 eV and 1.86 eV for **PTFBPz** and **PEFBPz**, respectively. Moreover, three new conjugated polymers, PBDT-FBPz and PBDT-TFBPz were synthesized via Stille coupling and PSi-TFBPz was synthesized via Suzuki coupling reactions. The optoelectronic properties of copolymers were determined with cyclic voltammetry, kinetic studies and spectroelectrochemistry. 3-Hexylthiophene and Benzodithiophene based copolymer (PBDT-TFBPz) showed orange color in its neutral state whereas Silafluorene based copolymer (PSi-TFBPz) was yellow in its neutral state. The optical band gap of the polymers was calculated as 2.34 eV, 1.87 eV and 2.65 eV for **PBDT-FBPz**, **PBDT-TFBPz** and **PSi-TFBPz**, respectively. 3-Hexylthiophene based copolymer (PBDT-TFBPz) has the lowest optical band gap among three polymers. The polymer based organic solar cells were constructed by using three different conjugated polymers used as donor units in active layer. The best PCE was reported as 1.53 % for **PBDT-TFBPz** with high V_{oc} value of 0.81 V, a J_{sc} of 3.71 mA.cm^{-2} and a FF of 51% among three polymers. PBDT-TFBPz showed higher open circuit voltage than others due to its lower HOMO energy level. Moreover, PCE was reported as 1.12 % for **PBDT-FBPz** with a V_{oc} value of 0.63 V, a J_{sc} of 3.13 mA.cm^{-2} and a FF of 57 % with polymer:PCBM71 ratio 1:1. The blend of PSi-TFBPz and PCBM71 showed a PCE of 0.58 % with a V_{oc} value of 0.82 V, a J_{sc} of 1.65 mA.cm^{-2}, a FF of 43 %. Silafluorene based polymer showed higher open circuit voltage among three polymers due to its higher HOMO energy level. Additionally, IPCE were obtained as 12% for **PBDT-FBPz** at 379/463 nm, 16 % for **PBDT-TFBPz** at 470 nm, 18 % for **PSi-TFBPz** at 410 nm.

REFERENCES

[1] H. Shirakawa, E. J. Louis, A. G. MacDiarmid, C. K. Chiang, and A. J. Heeger, “Synthesis of electrically conducting organic polymers: halogen derivatives of polyacetylene, (CH),” *J. Chem. Soc. Chem. Commun.*, no. 16, pp. 578–580, 1977.

[2] C. K. Chiang, C. R. Fincher, Y. W. Park, A. J. Heeger, H. Shirakawa, E. J. Louis, S. C. Gau, and A. G. MacDiarmid, “Electrical conductivity in doped polyacetylene,” *Phys. Rev. Lett.*, vol. 39, no. 17, pp. 1098–1101, 1977.

[3] C. J. Brabec, N. S. Sariciftci, and J. C. Hummelen, “Plastic solar cells,” *Adv. Funtional Mater.*, vol. 11, no. 1, pp. 15–26, 2001.

[4] J. H. Burroughes, D. D. C. Bradley, A. R. Brown, R. N. Marks, K. Mackay, R. H. Friend, P. L. Burns, and A. B. Holmes, “Light-emitting diodes based on conjugated polymers,” *Nature*, vol. 347, no. 6293, pp. 539–541, 1990.

[5] G. Gunbas and L. Toppare, “Electrochromic conjugated polyheterocycles and derivatives-highlights from the last decade towards realization of long lived aspirations.,” *Chem. Commun. (Camb).*, vol. 48, no. 8, pp. 1083–101, 2012.

[6] J. Roncali, “Synthetic Principles for Bandgap Control in Linear π-Conjugated Systems,” *Chem. Rev.*, vol. 97, no. 1, pp. 173–206, 1997.

[7] S. J. Higgins, “Conjugated polymers incorporating pendant functional groups synthesis and characterisation” *Chem. Soc. Rev.*, vol. 26, no. 4, p. 247, 1997.

[8] F. Wudl, M. Kobayashi, and A. J. Heeger, “Poly(isothianaphthene)” *J. Org. Chem.*, vol. 49, no. 18, pp. 3382–3384, 1984.

[9] H. Meng and F. Wudl, “A robust low band gap processable n-type conducting polymer based on poly(isothianaphthene),” *Macromolecules*, vol. 34, no. 6, pp. 1810–1816, 2001.

[10] R. J. Waltman, J. Bargon, and a F. Diaz, “Electrochemical studies of some conducting polythiophene films,” *J. Phys. Chem.*, vol. 87, no. 8, pp. 1459–1463, 1983.

[11] C. Winder and N. S. Sariciftci, “Low bandgap polymers for photon harvesting in bulk heterojunction solar cells,” *J. Mater. Chem.*, vol. 14, no. 7, p. 1077, 2004.

[12] H. Zhou, L. Yang, and W. You, “Rational Design of High Performance Conjugated Polymers for Organic Solar Cells,” *Macromolecules*, vol. 45, pp. 607–632, 2012.

[13] E. E. Havinga, W. ten Hoeve, and H. Wynberg, “Alternate donor-acceptor small-band-gap semiconducting polymers; Polysquaraines and polycroconaines,” *Synthetic Metals*, vol. 55, no. 1. pp. 299–306, 1993.

[14] H. A. M. Van Mullekom, J. A. J. M. Vekemans, E. E. Havinga, and E. W. Meijer, "*Developments in the chemistry and band gap engineering of donor-acceptor substituted conjugated polymers*," vol. 32, no. 1. 2001.

[15] W. a Gazotti, a E. Nogueira, E. M. Girotto, L. D. P. Condutores, I. De Quimica, U. E. De, S. Paulo, L. Micaroni, D. De Quimica, U. Federal, M. Martini, L. De Cristalografia, D. D. F. Aplicada, I. De Fisica, U. D. S. Paulo, S. Paulo, S. Neves, M. De Paoli, and L. D. M. Eletroativos, "*Optical Devices Based on Conductive Polymers*," vol. 10. 2001.

[16] W. P. Su, J. R. Schrieffer, and A. J. Heeger, “Solitons in polyacetylene,” *Phys. Rev. Lett.*, vol. 42, no. 25, pp. 1698–1701, 1979.

[17] J. Bredas and G. Street, “Polarons, bipolarons, and solitons in conducting polymers,” *Acc. Chem. Res.*, vol. 1305, no. 4, pp. 309–315, 1985.

[18] G. B. Street, “Upon Doping,” vol. 30, no. 2, pp. 1023–1025, 1984.

[19] C. Deibe, T. Strobe, and V. Dyakonov, “Role of the charge transfer state in organic donor-acceptor solar cells,” *Adv. Mater.*, vol. 22, no. 37, pp. 4097–4111, 2010.

[20] D. Polyacetylene and B. D. Macinnes, “Organic Batteries : Reversible,” pp. 317–319, 1981.

[21] T. Oi, “Electrochromic Materials,” *Ann. Rev. Mater. Res.*, vol. 16, no. 1, pp. 185–201, 1986.

[22] J. Roncali, “Molecular engineering of the band gap of π-conjugated systems: Facing technological applications,” *Macromol. Rapid Commun.*, vol. 28, no. 17, pp. 1761–1775, 2007.

[23] D. Baran, A. Balan, S. Celebi, B. Meana Esteban, H. Neugebauer, N. S. Sariciftci, and L. Toppare, “Processable multipurpose conjugated polymer for electrochromic and photovoltaic applications,” *Chem. Mater.*, vol. 22, no. 9, pp. 2978–2987, 2010.

[24] R. H. Friend, “Conjugated polymers. New materials for optoelectronic devices,” *Symp. A Q. J. Mod. Foreign Lit.*, vol. 73, no. 3, pp. 425–430, 2001.

[25] A. A. Argun, P. H. Aubert, B. C. Thompson, I. Schwendeman, C. L. Gaupp, J. Hwang, N. J. Pinto, D. B. Tanner, A. G. MacDiarmid, and J. R. Reynolds, “Multicolored electrochromisin in polymers: Structures and devices,” *Chem. Mater.*, vol. 16, no. 23, pp. 4401–4412, 2004.

[26] D. D. Yao, R. A. Rani, A. P. O'Mullane, K. Kalantar-Zadeh, and J. Z. Ou, "Enhanced coloration efficiency for electrochromic devices based on anodized Nb_2O_5/electrodeposited MoO_3 binary systems," *J. Phys. Chem. C*, vol. 118, no. 20, pp. 10867–10873, 2014.

[27] P. M. Beaujuge and J. R. Reynolds, "Color control in pi-conjugated organic polymers for use in electrochromic devices.," *Chem. Rev.*, vol. 110, no. 1, pp. 268–320, 2010.

[28] L. Lu, T. Zheng, Q. Wu, A. M. Schneider, D. Zhao, and L. Yu, "Recent Advances in Bulk Heterojunction Polymer Solar Cells," *Chem. Rev.*, vol. 115, no. 23, pp. 12666–12731, 2015.

[29] J. Nelson, "The Phisics of Solar Cells," *Prop. Semicond. Mater.*, p. 384, 2003.

[30] "Volume 2: The Swiss Years: Writings, 1900-1909 (English translation supplement) Page 86 (100 of 416).pdf." .

[31] J. Moan, "Visible Light and UV Radiation," *Radiat. home, outdoors Work.*, pp. 69–85, 2001.

[32] E. Bundgaard and F. C. Krebs, "Low band gap polymers for organic photovoltaics," *Sol. Energy Mater. Sol. Cells*, vol. 91, no. 11, pp. 954–985, 2007.

[33] H. Hoppe and N. S. Sariciftci, "Organic solar cells: An overview," *J. Mater. Res.*, vol. 19, no. March, pp. 1924–1945, 2004.

[34] C. W. Tang, "Two-layer organic photovoltaic cell," *Appl. Phys. Lett.*, vol. 48, no. 2, pp. 183–185, 1986.

[35] F. Zhu, *Excitonic and Photonic Processes in Materials*, vol. 203. 2015.

[36] M. W. Rowell, M. A. Topinka, M. D. McGehee, H. J. Prall, G. Dennler, N. S. Sariciftci, L. Hu, and G. Gruner, "Organic solar cells with carbon nanotube network electrodes," *Appl. Phys. Lett.*, vol. 88, no. 23, pp. 23–25, 2006.

[37] C. J. Brabec, F. Padinger, J. C. Hummelen, R. A. J. Janssen, and N. S. Sariciftci, "Realization of large area flexible fullerene π-conjugated polymer photocells: a route to plastic solar cells," *Synth. Met.*, vol. 102, no. 1–3, pp. 861–864, 1999.

[38] H. Frohne, S. E. Shaheen, C. J. Brabec, D. C. Muller, N. S. Sariciftci, and K. Meerholz, "Influence of the anodic work function on the performance of organic solar cells," *Chemphyschem*, vol. 3, no. 9, p. 795–+, 2002.

[39] F. Wudl, "The chemical properties of buckminsterfullerene (C_{60}) and the birth and infancy of fulleroids," *Acc. Chem. Res.*, vol. 25, no. 3, pp. 157–161, 1992.

[40] B. Kippelen, "Recent Advances in Organic Photovoltaic Cells and Integrated Modules," *ASHA*, vol. 1, p. 2007, 2007.

[41] S. S. Oh, D. H. Yeo, K. H. Park, H. B. Kim, M. H. Ha, H. J. Oh, M. W. Park, J. S. Park, D. W. Park, D. G. Jung, H. Y. Chae, H. S. Kim, J. H. Boo, and E. Y. Nam, “Performance Enhancement of Organic Solar Cells with the LiF/Al Cathode Structure by the Pyromellitic Dianhydride Layer,” *Adv. Mater. Res.*, vol. 415–417, pp. 1608–1610, 2011.

[42] M. P. De Jong, R. Friedlein, W. Osikowicz, R. Salaneck, and M. Fahlman, “Molecular Crystals and Liquid Crystals Ultraviolet Photoelectron Spectroscopy of Polymers,” *Mol. Cryst. Liq. Cryst.*, vol. 1406, no. August 2012, pp. 193–203, 2006.

[43] S. G??nes, H. Neugebauer, and N. S. Sariciftci, “Conjugated polymer-based organic solar cells,” *Chem. Rev.*, vol. 107, no. 4, pp. 1324–1338, 2007.

[44] S. R. Forrest, “The Limits to Organic Photovoltaic Cell Efficiency,” *MRS Bull.*, vol. 30, no. 01, pp. 28–32, 2005.

[45] V. I. Arkhipov, P. Heremans, and H. Bässler, “Why is exciton dissociation so efficient at the interface between a conjugated polymer and an electron acceptor,” *Appl. Phys. Lett.*, vol. 82, no. 25, pp. 4605–4607, 2003.

[46] R. N. Marks, J. J. M. Halls, D. D. C. Bradley, R. H. Friend, and a B. Holmes, “The photovoltaic response in poly(p-phenylene vinylene) thin-film devices,” *J. Phys. Condens. Matter*, vol. 6, no. 7, p. 1379, 1994.

[47] M. Knupfer, “Exciton binding energies in organic semiconductors,” *Appl. Phys. A Mater. Sci. Process.*, vol. 77, no. 5, pp. 623–626, 2003.

[48] L. A. Pettersson, L. S. Roman, and O. Inganäs, “Modeling photocurrent action spectra of photovoltaic devices based on organic thin films Modeling photocurrent action spectra of photovoltaic devices based on organic thin films,” *J. Appl. Phys.*, vol. 487, no. 1999, pp. 487–496, 2011.

[49] P. Peumans, A. Yakimov, and S. R. Forrest, “Small molecular weight organic thin-film photodetectors and solar cells,” *J. Appl. Phys.*, vol. 93, no. 7, pp. 3693–3723, 2003.

[50] N. S. Sariciftci, D. Braun, C. Zhang, V. I. Srdanov, A. J. Heeger, G. Stucky, and F. Wudl, “Semiconducting polymer-buckminsterfullerene heterojunctions: Diodes, photodiodes, and photovoltaic cells,” *Appl. Phys. Lett.*, vol. 62, no. 6, pp. 585–587, 1993.

[51] J. J. M. Halls, K. Pichler, R. H. Friend, S. C. Moratti, and A. B. Holmes, “Exciton diffusion and dissociation in a poly(p-phenylenevinylene)/C60 heterojunction photovoltaic cell,” *Appl. Phys. Lett.*, vol. 68, no. 22, pp. 3120–3122, 1996.

[52] G. Li, V. Shrotriya, J. Huang, Y. Yao, T. Moriarty, K. Emery, and Y. Yang,

"High-efficiency solution processable polymer photovoltaic cells by self-organization of polymer blends," *Nat. Mater.*, vol. 4, no. 11, pp. 864–868, 2005.

[53] M. P. de Jong, L. J. van IJzendoorn, and M. J. a de Voigt, "Stability of the interface between indium-tin-oxide and poly(3,4-ethylenedioxythiophene)/poly(styrenesulfonate) in polymer light-emitting diodes," *Appl. Phys. Lett.*, vol. 77, no. 2000, pp. 2255–2257, 2000.

[54] A. W. Hains and T. J. Marks, "High-efficiency hole extraction/electron-blocking layer to replace poly(3,4-ethylenedioxythiophene):poly(styrene sulfonate) in bulk-heterojunction polymer solar cells," *Appl. Phys. Lett.*, vol. 92, no. 2, pp. 108–111, 2008.

[55] S. K. Hau, H. L. Yip, N. S. Baek, J. Zou, K. O'Malley, and A. K. Y. Jen, "Air-stable inverted flexible polymer solar cells using zinc oxide nanoparticles as an electron selective layer," *Appl. Phys. Lett.*, vol. 92, no. 25, pp. 1–4, 2008.

[56] H. L. Yip, S. K. Hau, N. S. Baek, H. Ma, and A. K. Y. Jen, "Polymer solar cells that use self-assembled-monolayer-modified ZnO/metals as cathodes," *Adv. Mater.*, vol. 20, no. 12, pp. 2376–2382, 2008.

[57] F. C. Krebs, "Air stable polymer photovoltaics based on a process free from vacuum steps and fullerenes," *Sol. Energy Mater. Sol. Cells*, vol. 92, no. 7, pp. 715–726, 2008.

[58] K. Wang, C. Liu, T. Meng, C. Yi, and X. Gong, "Inverted organic photovoltaic cells," *Chem. Soc. Rev.*, vol. 45, p. -, 2016.

[59] M. C. Scharber and N. S. Sariciftci, "Efficiency of bulk-heterojunction organic solar cells," *Prog. Polym. Sci.*, vol. 38, no. 12, pp. 1929–1940, 2013.

[60] J. Rn Rostalski and D. Meissner, "Monochromatic versus solar efficiencies of organic solar cells," *Sol. Energy Mater. Sol. Cells*, vol. 61, pp. 87–95, 2000.

[61] M. C. Scharber, D. Mühlbacher, M. Koppe, P. Denk, C. Waldauf, A. J. Heeger, and C. J. Brabec, "Design rules for donors in bulk-heterojunction solar cells - Towards 10 % energy-conversion efficiency," *Adv. Mater.*, vol. 18, no. 6, pp. 789–794, 2006.

[62] C. J. Brabec, a Cravino, D. Meissner, N. S. Sariciftci, T. Fromherz, M. T. Rispens, L. Sanchez, and J. C. Hummelen, "Origin of the open circuit voltage of plastic solar cells, Adv," *Funct. Mater.*, vol. 11, no. 5, pp. 374–380, 2001.

[63] J. Liu, J. Liu, Y. Shi, Y. Shi, Y. Yang, and Y. Yang, "Solvation Induced Morphology Effects on the Performance of Polymer Based Photovoltaic Devices," *Adv. Funct. Mater.*, vol. 11, no. 6, p. 420, 2001.

[64] J. K. J. van Duren, J. Loos, F. Morrissey, C. M. Leewis, K. P. H. Kivits, L. J. van IJzendoorn, M. T. Rispens, J. C. Hummelen, and R. A. J. Janssen, "In-Situ

Compositional and Structural Analysis of Plastic Solar Cells," *Adv. Funct. Mater.*, vol. 12, no. 10, pp. 665–669, 2002.

[65] C. J. Brabec, S. E. Shaheen, C. Winder, N. S. Sariciftci, and P. Denk, "Effect of LiF/metal electrodes on the performance of plastic solar cells," *Appl. Phys. Lett.*, vol. 80, no. 7, pp. 1288–1290, 2002.

[66] K. Sugiyama, H. Ishii, Y. Ouchi, and K. Seki, "Dependence of indium tin oxide work function on surface cleaning method as studied by ultraviolet and x-ray photoemission spectroscopies.pdf," *J. Appl. Phys.*, vol. 87, no. 1, pp. 295–298, 2000.

[67] E. P. Woo, R. Stevenson, J. J. M. Halls, A. C. Arias, J. D. MacKenzie, R. H. Friend, D. Richards, and M. Inbasekaran, "Photovoltaic Performance and Morphology of Polyfluorene Blends: A Combined Microscopic and Photovoltaic Investigation," *Macromolecules*, vol. 34, no. 17, pp. 6005–6013, 2001.

[68] D. Gupta, S. Mukhopadhyay, and K. S. Narayan, "Fill factor in organic solar cells," *Sol. Energy Mater. Sol. Cells*, vol. 94, no. 8, pp. 1309–1313, 2010.

[69] P. Cheng and X. Zhan, "Stability of organic solar cells: challenges and strategies," *Chem. Soc. Rev.*, vol. 45, pp. 2544–2582, 2016.

[70] M. Glatthaar, M. Riede, N. Keegan, K. Sylvester-Hvid, B. Zimmermann, M. Niggemann, A. Hinsch, and A. Gombert, "Efficiency limiting factors of organic bulk heterojunction solar cells identified by electrical impedance spectroscopy," *Sol. Energy Mater. Sol. Cells*, vol. 91, no. 5, pp. 390–393, 2007.

[71] A. Seemann, T. Sauermann, C. Lungenschmied, O. Armbruster, S. Bauer, H.-J. Egelhaaf, and J. Hauch, "Reversible and irreversible degradation of organic solar cell performance by oxygen," *Sol. Energy*, vol. 85, no. 6, pp. 1238–1249, Jun. 2011.

[72] A. J. Parnell, A. J. Cadby, A. D. F. Dunbar, G. L. Roberts, A. Plumridge, R. M. Dalgliesh, M. W. a. Skoda, and R. a. L. Jones, "Physical mechanisms responsible for the water-induced degradation of PC $_{61}$ BM P3HT photovoltaic thin films," *J. Polym. Sci. Part B Polym. Phys.*, p. n/a–n/a, 2015.

[73] J. A. Hauch, P. Schilinsky, S. A. Choulis, S. Rajoelson, and C. J. Brabec, "The impact of water vapor transmission rate on the lifetime of flexible polymer solar cells," *Appl. Phys. Lett.*, vol. 93, no. 10, 2008.

[74] S. Hameed and P. Predeep, "Polymer Light Emitting Diodes - a Review on," *Rev. Adv. Mater. Sci.*, vol. 26, pp. 30–42, 2010.

[75] N. Thejo Kalyani and S. J. Dhoble, "Organic light emitting diodes: Energy saving lighting technology - A review," *Renew. Sustain. Energy Rev.*, vol. 16,

no. 5, pp. 2696–2723, 2012.

[76] U. Mitschke and P. Bäuerle, “The electroluminescence of organic materials,” *J. Mater. Chem.*, vol. 10, no. 7, pp. 1471–1507, 2000.

[77] S. Reineke, M. Thomschke, B. Lüssem, and K. Leo, “White organic light-emitting diodes: Status and perspective,” *Rev. Mod. Phys.*, vol. 85, no. 3, pp. 1245–1293, 2013.

[78] H. Frohne, S. E. Shaheen, C. J. Brabec, D. C. Müller, N. S. Sariciftci, and K. Meerholz, “Influence of the anodic work function on the performance of organic solar cells.,” *Chemphyschem*, vol. 3, no. 9, pp. 795–799, 2002.

[79] N. Miyaura and A. Suzuki, “Palladium-Catalyzed Cross-Coupling Reactions of Organoboron Compounds,” *Chem. Rev.*, vol. 95, no. 7, pp. 2457–2483, 1995.

[80] D. R. Rutherford, J. K. Stille, M. C. Elliott, and V. R. Reichert, “Poly(2,5-ethynylenethiophenediylethynylenes), Related Heteroaromatic Analogues, and Poly(thieno[3,2-b]thiophenes). Synthesis and Thermal and Electrical Properties,” *Macromolecules*, vol. 25, pp. 2294–2306, 1992.

[81] K. Sonogashira, “Development of Pd-Cu catalyzed cross-coupling of terminal acetylenes with sp_2-carbon halides,” *J. Organomet. Chem.*, vol. 653, no. 1–2, pp. 46–49, 2002.

[82] J. Louie, J. F. Hartwig, and A. F. Fry, “Discrete high molecular weight triarylamine dendrimers prepared by palladium-catalyzed amination,” *J. Am. Chem. Soc.*, vol. 119, no. 48, pp. 11695–11696, 1997.

[83] A. Guram and S. Buchwald, “Palladium-catalyzed aromatic aminations with in situ generated aminostannanes,” *J. Am. Chem. Soc.*, vol. 116, no. 10, pp. 7901–7902, 1994.

[84] T. Gibtner, F. Hampel, J. P. Gisselbrecht, and A. Hirsch, “End-cap stabilized oligoynes: Model compounds for the linear sp carbon allotrope carbyne,” *Chem. - A Eur. J.*, vol. 8, no. 2, pp. 408–432, 2002.

[85] T.H.E.U. Synthesis, “The ullmann synthesis,” no. 192, pp. 1945–1963, 1964.

[86] E. Negishi, “Novel and selective α-substitution of ketones and other carbonyl compounds based on Pd-catalyzed cross coupling of α,β-unsaturated carbonyl derivatives containing α-halogen or α-metal groups,” *J. Organomet. Chem.*, vol. 576, no. 1–2, pp. 179–194, 1999.

[87] T. Yamamoto, A. Morita, Y. Miyazaki, T. Maruyama, H. Wakayama, Z.-H. Zhou, Y. Nakamura, T. Kanbara, S. Sasaki, and K. Kubota, “Preparation of .Ir-Conjugated Poly(thiophene-2,5-diyl), Poly(*p*-phenylene),and Related Polymers Using Zerovalent Nickel Complexes. Linear Structure and Properties of the 7-Conjugated Polymers,” *Macromolecules*, vol. 25, pp. 1214–1223, 1214.

[88] D. Milstein and J. K. Stille, “A general, selective, and facile method for ketone synthesis from acid chlorides and organotin compounds catalyzed by palladium,” *J. Am. Chem. Soc.*, vol. 100, no. 11, pp. 3636–3638, 1978.

[89] D. Milstein and J. K. Stille, “Palladium-catalyzed coupling of tetraorganotin compounds with aryl and benzyl halides. Synthetic utility and mechanism,” *J. Am. Chem. Soc.*, vol. 101, no. 1, pp. 4992–4998, 1979.

[90] J. H. Kim, C. E. Song, H. U. Kim, I. N. Kang, W. S. Shin, M. J. Park, and D. H. Hwang, “New quinoxaline derivatives as accepting units in donor-acceptor type low-band gap polymers for organic photovoltaic cells,” *J. Polym. Sci. Part A Polym. Chem.*, vol. 51, no. 19, pp. 4136–4149, 2013.

[91] Y. Zhang, J. Zou, H. Yip, K.-S. Chen, D. F. Zeigler, Y. Sun, and A. K.-Y. Jen, “Development of Indacenodithiophene and Quinoxaline-Based Conjugated Polymers for Efficient Polymer Solar Cells,” *Chem. Mater.*, vol. 23, no. 9, pp. 2289–2291, 2011.

[92] J. Zhang, W. Cai, F. Huang, E. Wang, C. Zhong, S. Liu, M. Wang, C. Duan, T. Yang, and Y. Cao, “Synthesis of quinoxaline-based donor-acceptor narrow-band-gap polymers and their cyclized derivatives for bulk-heterojunction polymer solar cell applications,” *Macromolecules*, vol. 44, no. 4, pp. 894–901, 2011.

[93] M. Zhang, X. Guo, X. Wang, H. Wang, and Y. Li, “Synthesis and Photovoltaic Properties of D-A Copolymers Based on Alkyl-Substituted Indacenodithiophene Donor Unit,” *Chem. Mater.*, vol. 23, pp. 4264–4270, 2011.

[94] H. Pan, Y. Li, Y. Wu, P. Liu, B. S. Ong, S. Zhu, and G. Xu, “Synthesis and Thin-Film Transistor Performance of Poly(4,8-didodecylbenzo[1,2-b:4,5-b‘]dithiophene),” *Chem. Mater.*, vol. 18, no. 14, pp. 3237–3241, 2006.

[95] H. Pan, Y. Wu, Y. Li, P. Liu, B. S. Ong, S. Zhu, and G. Xu, “Benzodithiophene copolymer A low-temperature, solution-processed high-performance semiconductor for thin-film transistors,” *Adv. Funct. Mater.*, vol. 17, no. 17, pp. 3574–3579, 2007.

[96] Y. Liang, Y. Wu, D. Feng, S.-T. Tsai, H.-J. Son, G. Li, and L. Yu, “Development of new semiconducting polymers for high performance solar cells.,” *J. Am. Chem. Soc.*, vol. 131, no. 1, pp. 56–57, 2009.

[97] Y. Liang, Z. Xu, J. Xia, S. T. Tsai, Y. Wu, G. Li, C. Ray, and L. Yu, “For the bright future-bulk heterojunction polymer solar cells with power conversion efficiency of 7.4%,” *Adv. Mater.*, vol. 22, no. 20, pp. 135–138, 2010.

[98] G. Li, X. Gong, J. Zhang, Y. Liu, S. Feng, C. Li, and Z. Bo, “4-Alkyl-3,5-

difluorophenyl-Substituted Benzodithiophene-Based Wide Band Gap Polymers for High-Efficiency Polymer Solar Cells," *ACS Appl. Mater. Interfaces*, vol. 8, no. 6, pp. 3686–3692, 2016.

[99] L. Dou, J. Gao, E. Richard, J. You, C. C. Chen, K. C. Cha, Y. He, G. Li, and Y. Yang, "Systematic investigation of benzodithiophene- and diketopyrrolopyrrole- based low-bandgap polymers designed for single junction and tandem polymer solar cells," *J. Am. Chem. Soc.*, vol. 134, no. 24, pp. 10071–10079, 2012.

[100] M. Zhang, Y. Gu, X. Guo, F. Liu, S. Zhang, L. Huo, T. P. Russell, and J. Hou, "Efficient polymer solar cells based on benzothiadiazole and alkylphenyl substituted benzodithiophene with a power conversion efficiency over 8%," *Adv. Mater.*, vol. 25, no. 35, pp. 4944–4949, 2013.

[101] D. Liu, W. Zhao, S. Zhang, L. Ye, Z. Zheng, Y. Cui, Y. Chen, and J. Hou, "Highly Efficient Photovoltaic Polymers Based on Benzodithiophene and Quinoxaline with Deeper HOMO Levels," *Macromolecules*, vol. 48, no. 15, pp. 5172–5178, 2015.

[102] G. Lu, H. Usta, C. Risko, L. Wang, A. Facchetti, M. A. Ratner, and T. J. Marks, "Synthesis, characterization, and transistor response of semiconducting silole polymers with substantial hole mobility and air stability. Experiment and theory," *J. Am. Chem. Soc.*, vol. 130, no. 24, pp. 7670–7685, 2008.

[103] G. Li, C. Kang, X. Gong, J. Zhang, C. Li, Y. Chen, H. Dong, W. Hu, F. Li, and Z. Bo, "5‑Alkyloxy-6-fluorobenzo[c][1,2,5]thiadiazole- and SilafluoreneBased D−A Alternating Conjugated Polymers: Synthesis and Application in Polymer Photovoltaic Cells," 2014.

[104] X. C. Wang, Y. P. Sun, S. Chen, X. Guo, M. J. Zhang, X. Y. Li, Y. F. Li, and H. Q. Wang, "Effects of pi-Conjugated Bridges on Photovoltaic Properties of Donor-pi-Acceptor Conjugated Copolymers," *Macromolecules*, vol. 45, pp. 1208–1216, 2012.

[105] R. Kroon, M. Lenes, J. C. Hummelen, P. W. M. Blom, and B. de Boer, *Small Bandgap Polymers for Organic Solar Cells (Polymer Material Development in the Last 5 Years)*, vol. 48, no. 3. 2008.

[106] S. Li, B. Zhao, Z. He, S. Chen, J. Yu, A. Zhong, R. Tang, H. Wu, Q. Li, J. Qin, and Z. Li, "Synthesis, characterization and photovoltaic performances of D–A copolymers based on BDT and DBPz: the largely improved performance caused by additional thiophene blocks," *J. Mater. Chem. A*, vol. 1, no. 14, p. 4508, 2013.

[107] Y. Sun, C. Zhang, B. Dai, B. Lin, H. Yang, X. Zhang, L. Guo, and Y. Liu, "Side chain engineering and conjugation enhancement of benzodithiophene and

phenanthrenequnioxaline based conjugated polymers for photovoltaic devices," *J. Polym. Sci. Part A Polym. Chem.*, vol. 53, no. 16, pp. 1915–1926, 2015.

[108] H.-Y. Chen, S.-C. Yeh, C.-T. Chen, and C.-T. Chen, "Comparison of thiophene- and selenophene-bridged donor–acceptor low band-gap copolymers used in bulk-heterojunction organic photovoltaics," *J. Mater. Chem.*, vol. 22, p. 21549, 2012.

[109] J. Bersier, P. M. Bersier, L. Carlsson, T. Fuchigami, E. Steckhan, and J. Yoshida, *Electrochemistry V*. 1994.

[110] H.-Y. Y. Chen, J. H. Hou, S. Q. Zhang, Y. Y. Liang, G. W. Yang, Y. Yang, L. P. Yu, Y. Wu, and G. Li, "Polymer solar cells with enhanced open-circuit voltage and efficiency," *Nat. Photonics*, vol. 3, no. 11, pp. 649–653, 2009.

[111] S. C. Price, A. C. Stuart, L. Yang, H. Zhou, and W. You, "Fluorine substituted conjugated polymer of medium band gap yields 7% efficiency in polymer-fullerene solar cells," *J. Am. Chem. Soc.*, vol. 133, no. 12, pp. 4625–4631, 2011.

[112] X. C. Wang, Z. G. Zhang, H. Luo, S. Chen, S. Q. Yu, H. Q. Wang, X. Y. Li, G. Yu, and Y. F. Li, "Effects of fluorination on the properties of thieno 3,2-b thiophene-bridged donor-pi-acceptor polymer semiconductors," *Polym. Chem.*, vol. 5, pp. 502–511, 2014.

[113] A. C. Stuart, J. R. Tumbleston, H. Zhou, W. Li, S. Liu, H. Ade, and W. You, "Fluorine substituents reduce charge recombination and drive structure and morphology development in polymer solar cells," *J. Am. Chem. Soc.*, vol. 135, no. 5, pp. 1806–1815, 2013.

[114] S. S. Zhu and T. M. Swager, "Conducting polymetallorotaxanes: Metal ion mediated enhancements in conductivity and charge localization," *J. Am. Chem. Soc.*, vol. 119, no. 51, pp. 12568–12577, 1997.

[115] Y. Qin, "Alginate fibers: an overwiew of the production processes and applications in wound management," *Polym. Int.*, vol. 57, no. April, pp. 171–180, 2008.

[116] E. K. Unver, S. Tarkuc, Y. A. Udum, C. Tanyeli, and L. Toppare, "Effect of conjugated core building block dibenzo[a,c]phenazine unit on π-conjugated electrochromic polymers: Red-shifted absorption," *J. Polym. Sci. Part A Polym. Chem.*, vol. 48, no. 8, pp. 1714–1720, 2010.

[117] A. J. H. J. L. Bredas, "Influence of donor and acceptor substituents on the electronic characteistics of poly(paraphenylene vinylene) and poly(paraphenylene)," *Chemical Physics Letters*, vol. 217, no. January. pp. 507–512, 1994.

[118] H. Yao, L. Ye, H. Zhang, S. Li, S. Zhang, and J. Hou, "Molecular Design of

Benzodithiophene-Based Organic Photovoltaic Materials," *Chem. Rev.*, p. acs.chemrev.6b00176, 2016.

[119] X. Wang, P. Jiang, Y. Chen, H. Luo, Z. Zhang, H. Wang, X. Li, G. Yu, and Y. Li, "Thieno[3,2-b]thiophene-Bridged D-π-A Polymer Semiconductor Based on Benzo[1,2-b:4,5-b']dithiophene and Benzoxadiazole," *Macromol. (Washington, DC, U. S.)*, vol. 46, no. Copyright (C) 2014 American Chemical Society (ACS). All Rights Reserved., pp. 4805–4812, 2013.

[120] L. Pandey, C. Risko, J. E. Norton, and J.-L. Brédas, "Donor − Acceptor Copolymers of Relevance for Organic Photovoltaics : A Theoretical Investigation of the Impact of Chemical Structure Modifications on the Electronic and Optical Properties," *Macromolecules*, vol. 45, pp. 6405–6414, 2012.

APPENDIX A

NMR DATA

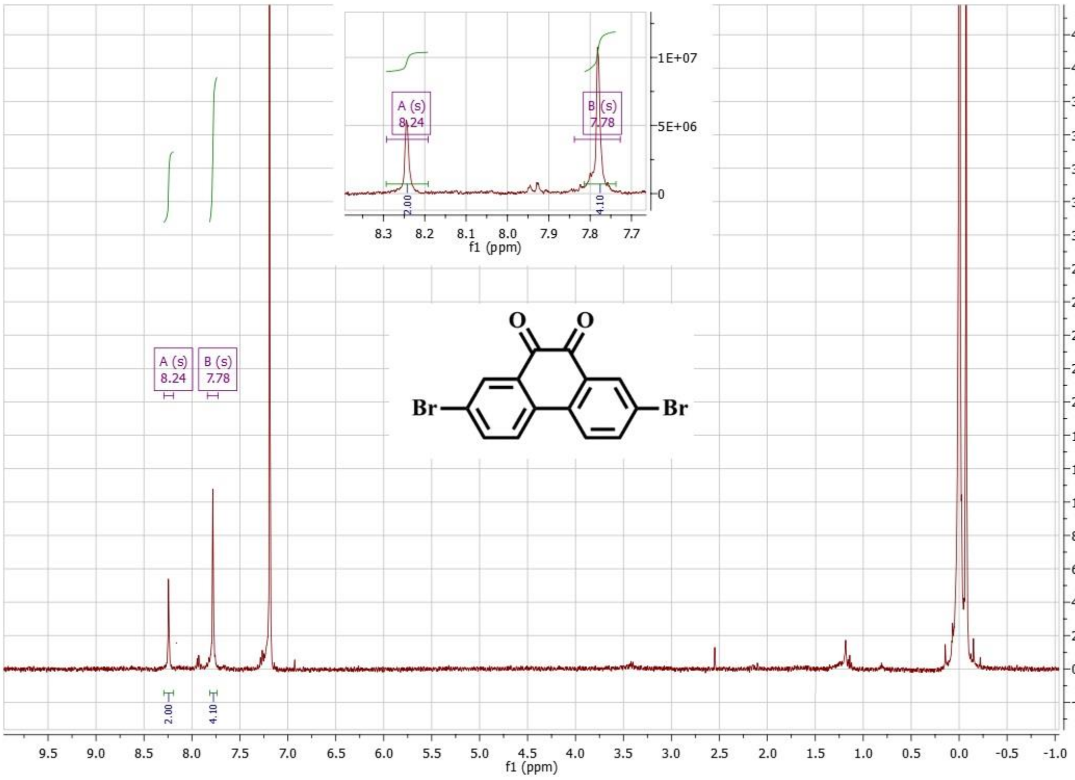

Figure 54. ^{1}H-NMR data of 2,7-dibromophenanthrene-9,10-dione

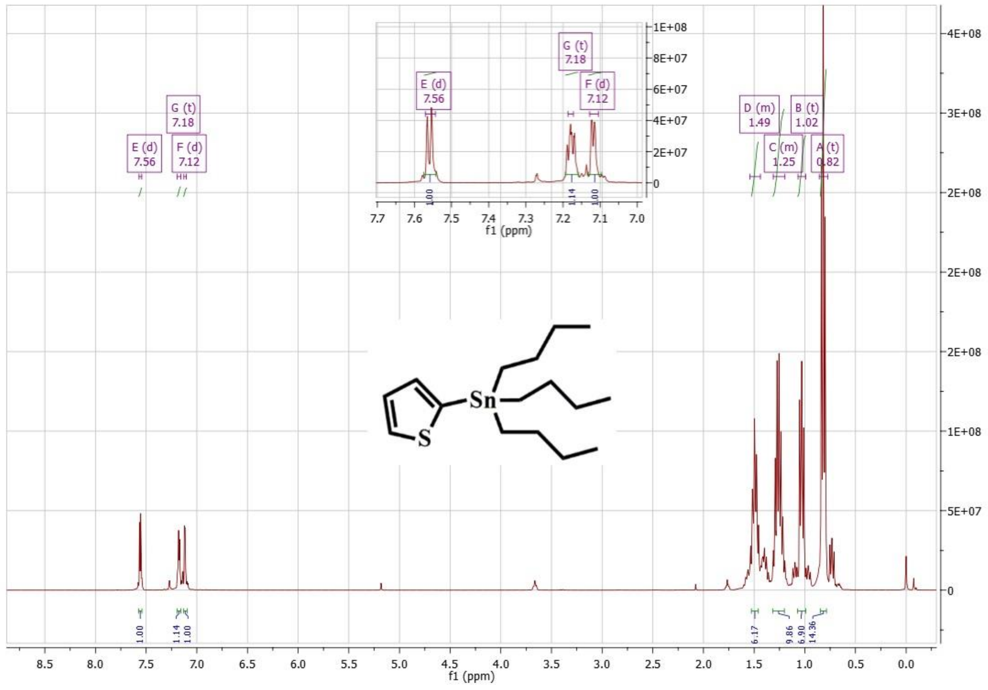

Figure 55. ^{1}H-NMR data of tributyl(thiophen-2-yl)stannane

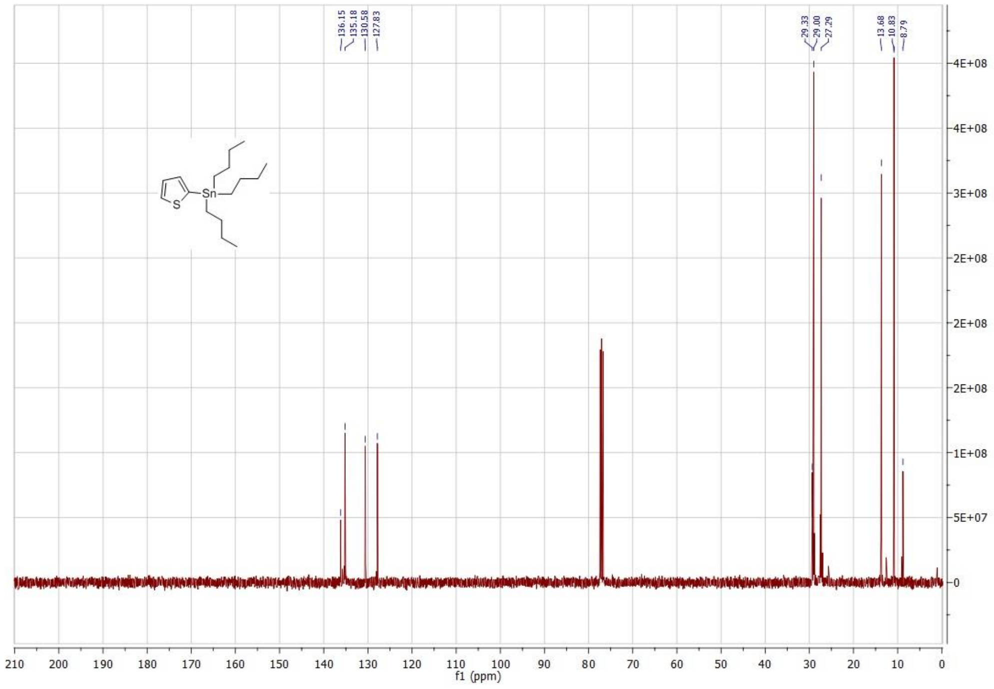

Figure 56. ^{13}C-NMR data of tributyl(thiophen-2-yl)stannane

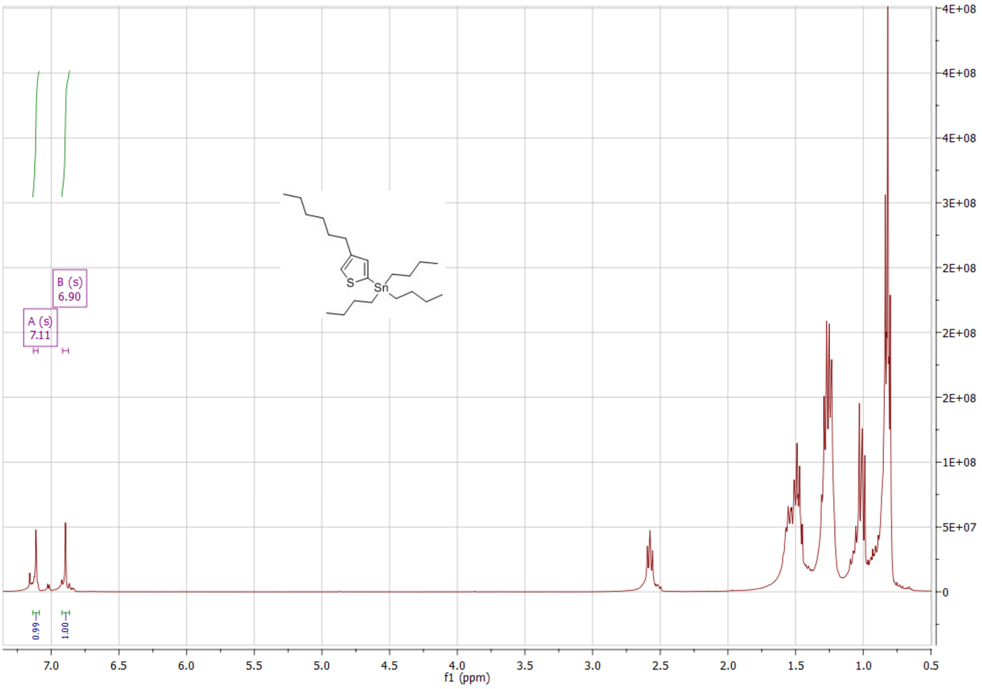

Figure 57. ^{1}H-NMR data of tributyl(4-hexylthiophen-2-yl)stannane

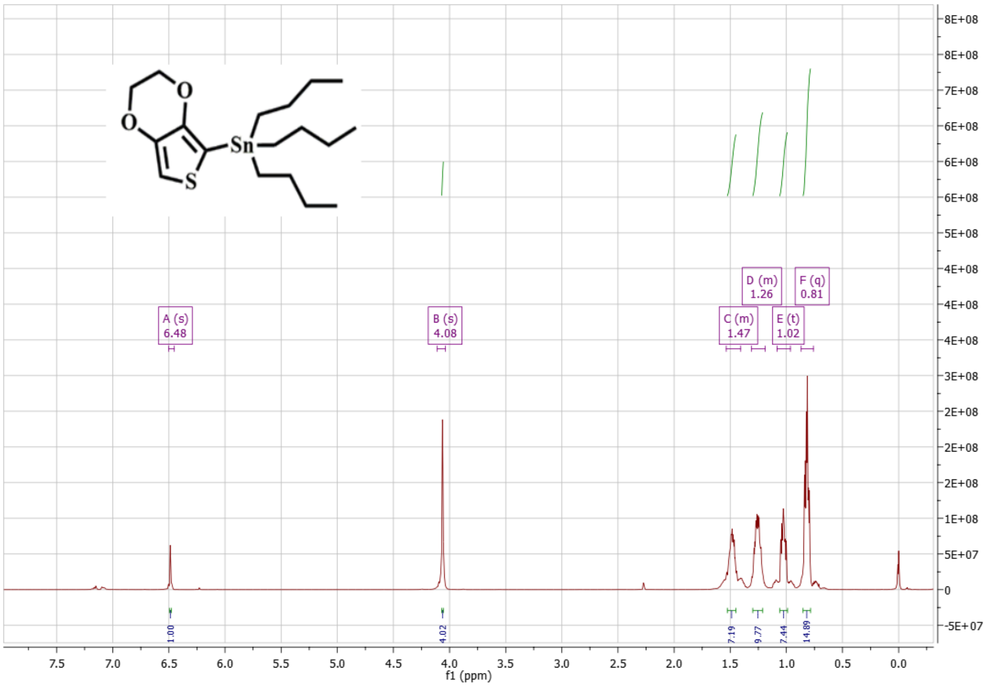

Figure 58. ^{1}H-NMR data of tributyl(2,3-dihydrothieno[3,4-b][1,4]dioxin-7-yl)stannane

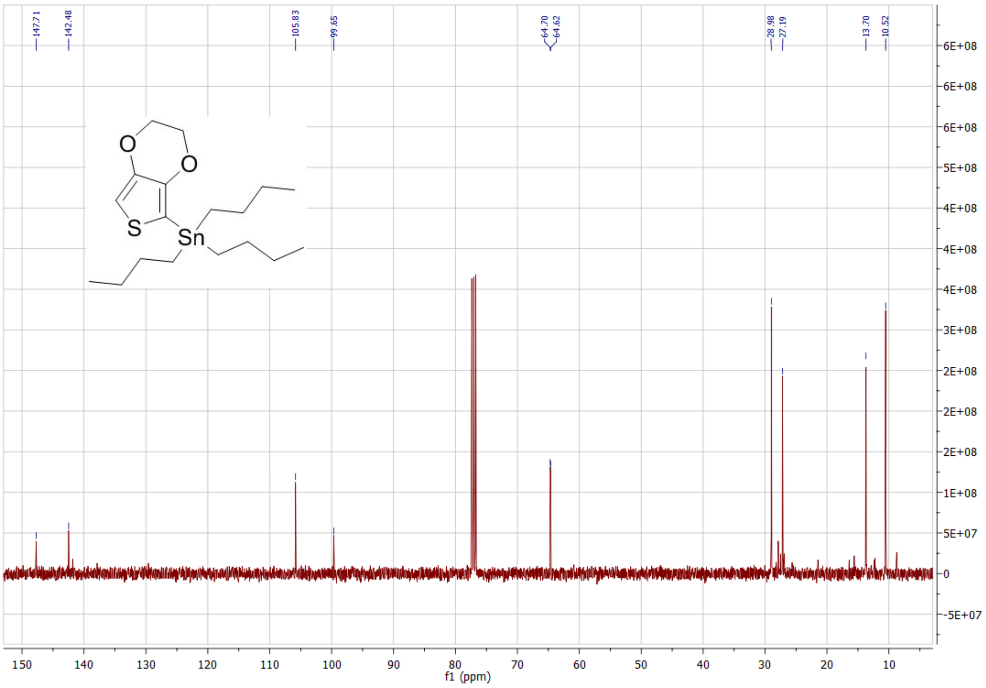

Figure 59. ^{13}C-NMR data of tributyl(2,3-dihydrothieno[3,4-b][1,4]dioxin-7-yl)stannane

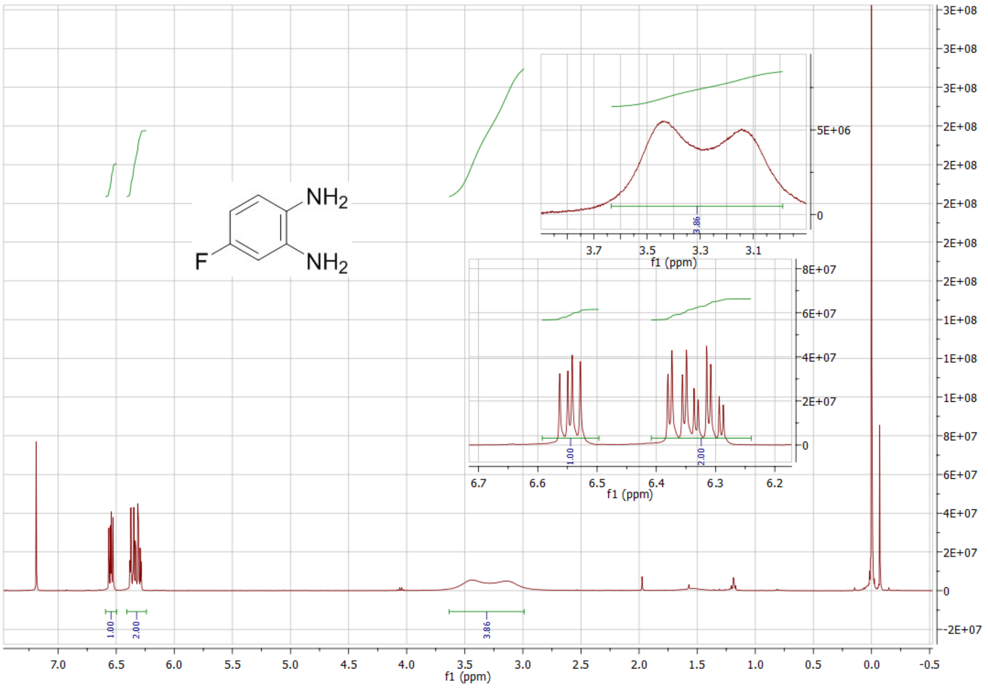

Figure 60. ^{1}H-NMR data of 4-fluorobenzene-1,2-diamine

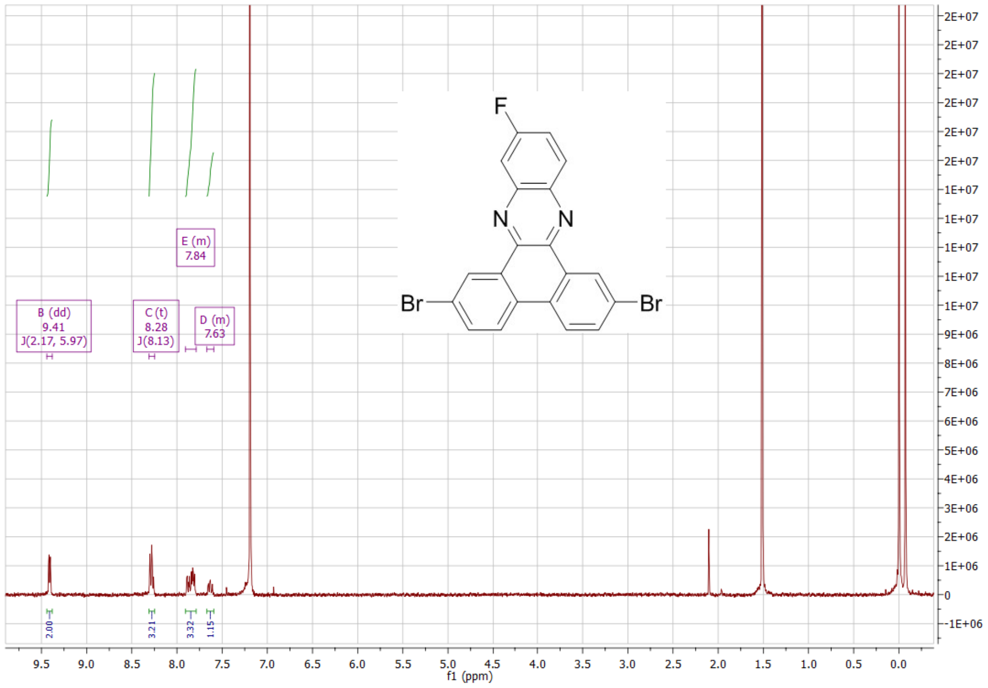

Figure 61. ^{1}H-NMR data of 2,7-dibromo-11-fluorodibenzo[a,c]phenazine

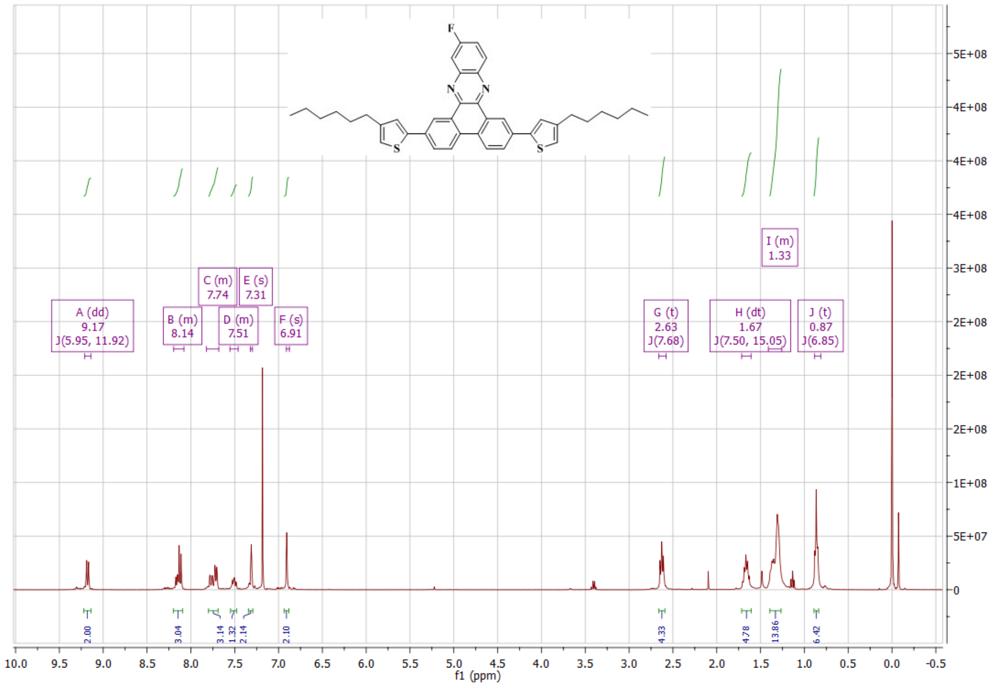

Figure 62. ^{1}H-NMR data of 11-fluoro-2,7-bis(4-hexylthiophen-2-yl)dibenzo[a,c]phenazine

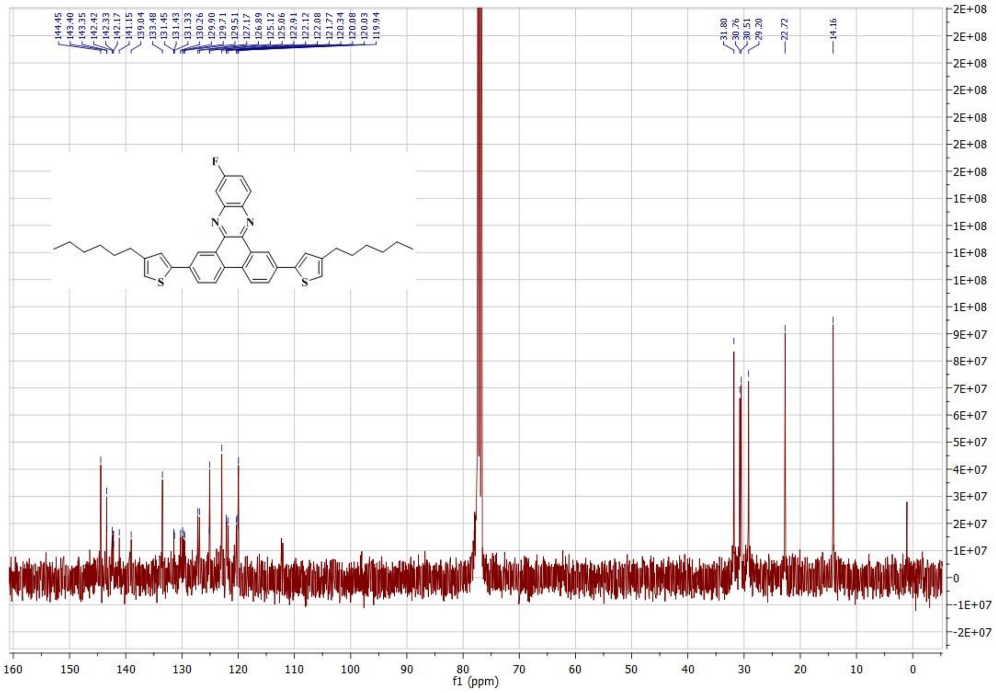

Figure 63. ^{13}C-NMR data of 11-fluoro-2,7-bis(4-hexylthiophen-2-yl)dibenzo[a,c]phenazine

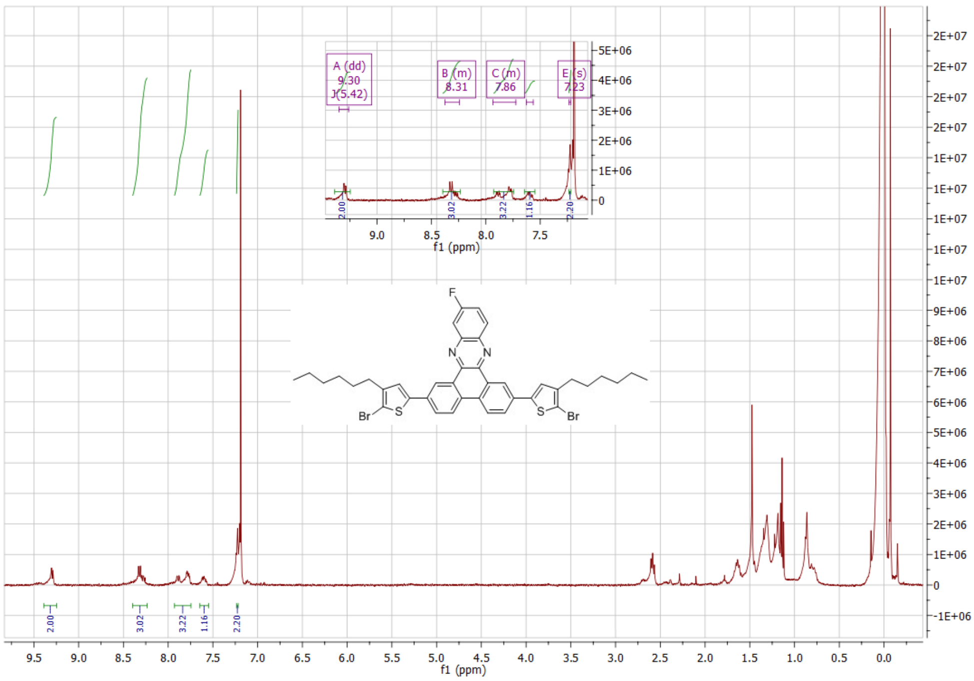

Figure 64. ^{1}H-NMR data of 2,7-bis(5-bromo-4-hexylthiophen-2-yl)-11-fluorodibenzo[a,c]phenazine

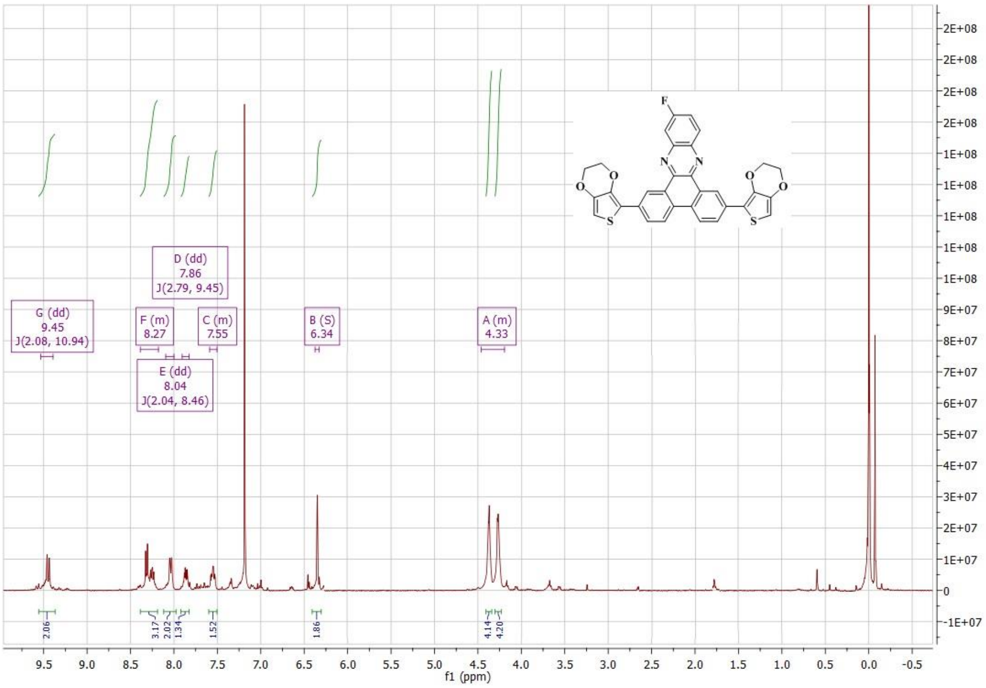

Figure 65. ^{1}H-NMR data of 2,7-bis(2,3-dihydrothieno[3,4-b][1,4]dioxin-5-yl)-11-fluorodibenzo[a,c]phenazine

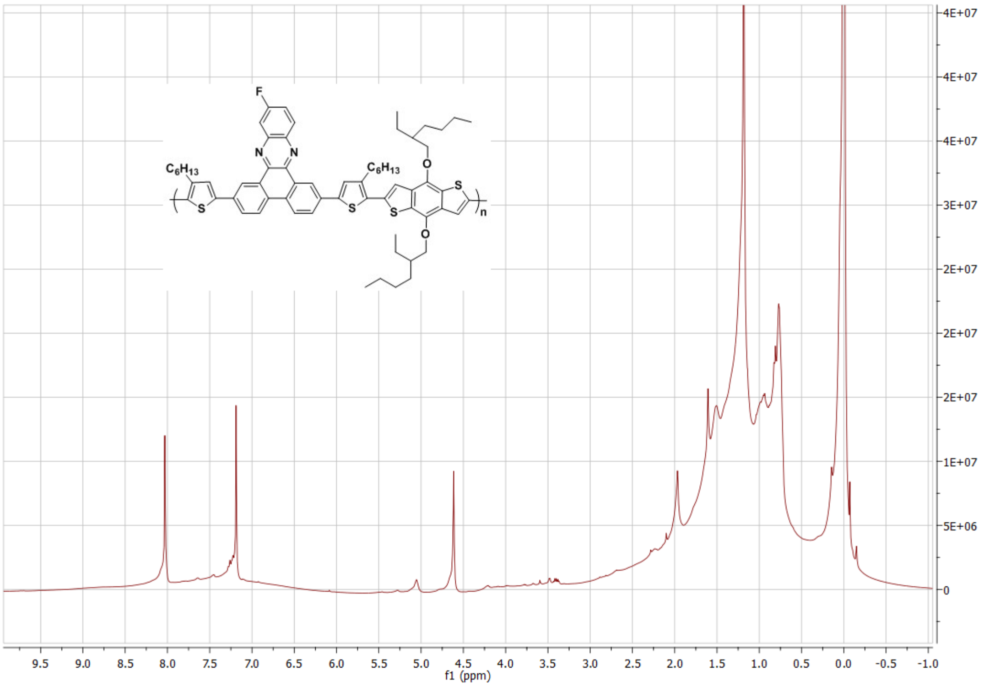

Figure 66. ^{1}H-NMR data of PBDT-TFBPz

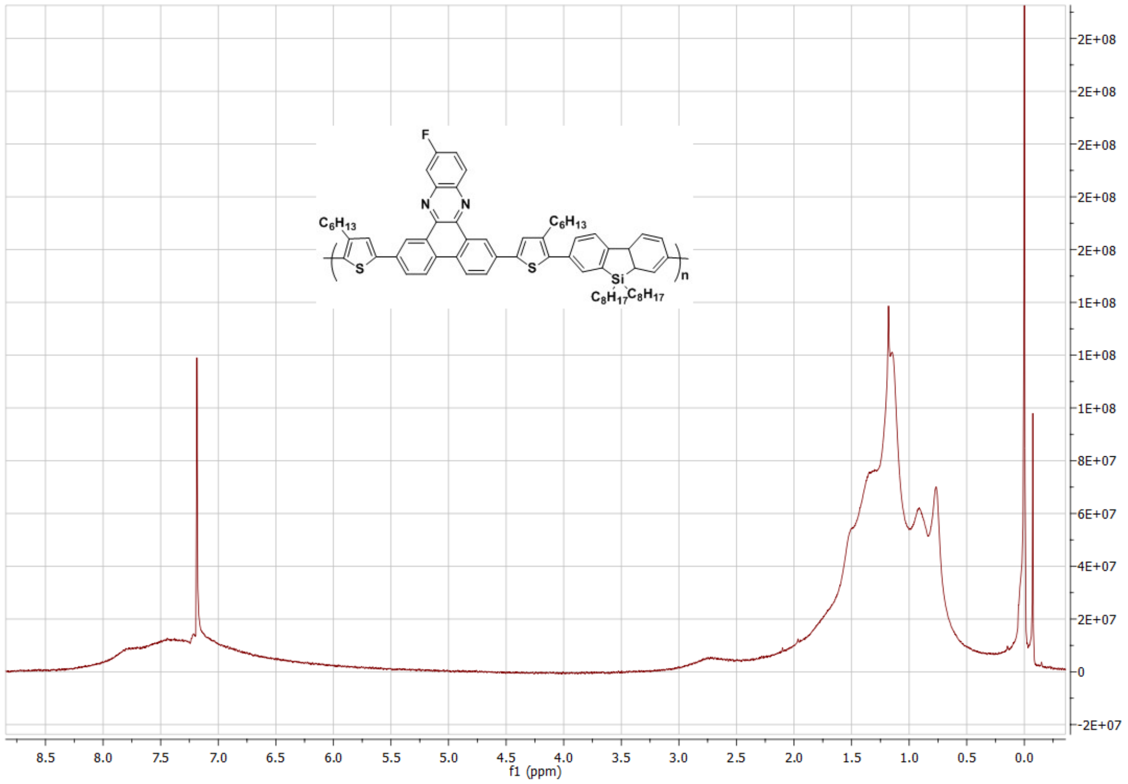

Figure 67. ^{1}H-NMR data of PSi-TFBPz